TURUN
YLIOPISTO
UNIVERSITY
OF TURKU

HIGH-SPEED JETS DOWNSTREAM OF THE EARTH'S BOW SHOCK

Laura Vuorinen

TURUN YLIOPISTON JULKAISUJA – ANNALES UNIVERSITATIS TURKUENSIS
SARJA – SER. AI OSA – TOM. 716 | ASTRONOMICA – CHEMICA – PHYSICA – MATHEMATICA | TURKU 2024

TURUN
YLIOPISTO
UNIVERSITY
OF TURKU

HIGH-SPEED JETS DOWNSTREAM OF THE EARTH'S BOW SHOCK

Laura Vuorinen

TURUN YLIOPISTON JULKAISUJA – ANNALES UNIVERSITATIS TURKUENSIS
SARJA – SER. AI OSA – TOM. 716 | ASTRONOMICA – CHEMICA – PHYSICA – MATHEMATICA | TURKU 2024

University of Turku

Faculty of Science
Department of Physics and Astronomy
Physics
Doctoral Programme in Exact Sciences

Supervised by

Dr. Heli Hietala
Department of Physics and Astronomy
Queen Mary University of London
London, UK

Prof. Rami Vainio
Department of Physics and Astronomy
University of Turku
Turku, Finland

Reviewed by

Assoc. Prof. Brian M. Walsh
Center for Space Physics
Boston University
Boston, Massachusetts, USA

Dr. Imogen Gingell
School of Physics and Astronomy
University of Southampton
Southampton, UK

Opponent

Dr. Christian Mazelle
Institut de Recherche en Astrophysique et Planétologie (IRAP)
CNRS - University of Toulouse - CNES
Toulouse, France

ISBN 978-951-29-9777-0 (PRINT)
ISBN 978-951-29-9778-7 (PDF)
ISSN 0082-7002 (PRINT)
ISSN 2343-3175 (ONLINE)
Painosalama, Turku, Finland, 2024

UNIVERSITY OF TURKU
Faculty of Science
Department of Physics and Astronomy
Physics
VUORINEN, LAURA: High-Speed Jets Downstream of the Earth's Bow Shock
Doctoral dissertation, 140 pp.
Doctoral Programme in Exact Sciences
June 2024

ABSTRACT

The solar wind is decelerated at the Earth's bow shock, after which it flows around the magnetosphere in the magnetosheath. Amidst the shocked plasma, faster flows can be often observed. These dynamic pressure enhancements, called magnetosheath jets, form as part of shock dynamics, and some of them can ultimately collide into the boundary of the magnetosphere, launching disturbances inside the magnetosphere. In this thesis, we study various aspects of magnetosheath jets to improve our understanding of their contribution to solar wind–magnetosphere interaction.

We use subsolar magnetosheath observations of the Time History of Events and Macroscale Interactions during Substorms (THEMIS) spacecraft and OMNI solar wind data to study where and under which solar wind conditions jets occur. The orientation of the interplanetary magnetic field (IMF) strongly controls jet occurrence and we find that jets are nine times more common downstream of the quasi-parallel shock than the quasi-perpendicular shock. Further analysis reveals that low IMF magnitude, high Alfvénic Mach number, and high plasma beta increase their occurrence in the quasi-perpendicular regime. We create a statistical model of jet occurrence to reconstruct their yearly occurrence throughout solar cycles 23 and 24. Our results suggest that there is no substantial variation across the solar cycle.

We also investigate acceleration of electrons at bow waves/shocks ahead of the fastest jets. We use a one-dimensional Monte Carlo model, where electrons are energized by shock drift acceleration at the jet-driven bow wave/shock amplified by a collapsing trap that forms between the bow wave and the magnetopause. We find that the simulated energy flux increases of suprathermal electrons are comparable to previous observational results, indicating that such a process could explain the observed energization. Transient structures both upstream and downstream of the Earth's bow shock contribute to the total acceleration in the system.

Finally, we study whether jets can be expected to alter conditions for magnetopause reconnection. Our analysis of THEMIS data shows that magnetic field is more variable inside jets than typically in the magnetosheath. Most jets contain periods of polarity opposite to the prevailing IMF, suggesting that jets may potentially modulate local conditions for reconnection. Magnetopause reconnection is a significant process in solar wind–magnetosphere interaction and our results motivate future studies where direct and indirect signatures of jets influencing reconnection should be investigated. Their total contribution on the system must arise from their numbers.

KEYWORDS: space physics, solar wind, magnetosheath jets, magnetosphere

TURUN YLIOPISTO
Matemaattis-luonnontieteellinen tiedekunta
Fysiikan ja tähtitieteen laitos
Fysiikka
VUORINEN, LAURA: High-Speed Jets Downstream of the Earth's Bow Shock
Väitöskirja, 140 s.
Eksaktien tieteiden tohtoriohjelma
Kesäkuu 2024

TIIVISTELMÄ

Aurinkotuuli hidastuu Maan keulashokilla ja virtaa Maan magnetosfäärin ohi turbulentissa välivyöhykkeessä. Siellä havaitaan usein myös nopeita suihkuvirtauksia, joilla on ympäröivää plasmaa korkeampi dynaaminen paine. Nämä suihkuvirtaukset muodostuvat osana keulashokin dynamiikkaa ja puskevat ympäröivän plasman läpi kohti magnetosfäärin ulkoreunaa, johon iskeytyessään ne voivat aiheuttaa häiriötä magnetosfäärissä. Tässä tutkielmassa tutkimme välivyöhykkeen suihkuvirtauksien esiintyvyyttä ja vaikutuksia osana aurinkotuulen ja magnetosfäärin vuorovaikutusta.

Hyödynsimme Time History of Events and Macroscale Interactions during Substorms -satelliittien (THEMIS) havaintoja ja OMNI-aurinkotuulidataa tutkiessamme missä ja millaisissa aurinkotuulen olosuhteissa suihkuvirtauksia esiintyy. Planeettainvälisen magneettikentän (IMF) suunta on tärkein esiintyvyyttä kontrolloiva parametri, ja tulostemme mukaan virtaukset ovat yhdeksän kertaa yleisempiä pitkittäisen kuin poikittaisen shokin alavirrassa. Tarkempi analyysimme paljasti, että poikittaisella shokilla esiintyvyyttä kasvattaa alhainen IMF:n voimakkuus ja korkeat Alfvénin Mach-luku ja plasman beeta. Kehitimme tilastollisen mallin muodostaaksemme suihkuvirtausten vuosittaisen esiintyvyyden aurinkosykleille 23 ja 24. Tulostemme mukaan esiintyvyydessä ei ole merkittäviä muutoksia aurinkosyklin aikana.

Tutkimme myös nopeimpien suihkuvirtausten ajamien keula-aaltojen/-shokkien elektronikiihdytystä. Oleellisimmat fysikaaliset elementit sisältävässä yksiulotteisessa Monte Carlo -mallissamme elektronit kiihtyvät shokin ajautumakiihdytysprosessissa ja shokin ja magnetopausin muodostamassa magneettisessa loukussa. Mallinnettu supratermisten elektronien energiavuon kasvu on verrattavissa aikaisempiin satelliittihavaintoihin, eli vastaavanlainen prosessi voisi selittää havaittua elektronikiihdytystä suihkuvirtausten keula-aalloilla. Sekä ylä- että alavirran lokaalit rakenteet vahvistavat hiukkaskiihdytystä Maan keulashokin ympäristössä.

Lopuksi tutkimme suihkuvirtausten mahdollista kykyä vaikuttaa magnetopausin rekonnektioon. THEMIS-datan analyysimme perusteella suurin osa suihkuvirtauksista sisältää IMF:n suunnalle vastakkaista magneettikenttää, eli ne voivat mahdollisesti aiheuttavaa paikallisia muutoksia rekonnektion olosuhteisiin magnetopausilla. Magnetopausin rekonnektio on tärkeä prosessi, jossa aurinkotuulen energiaa siirtyy magnetosfääriin. Tuloksemme motivoivat tulevia tutkimuksia, joissa suihkuvirtausten vaikutusta rekonnektioon tulisi mitata suorilla ja epäsuorilla havainnoilla. Suihkuvirtausten kokonaisvaikutus syntyy niiden yleisyydestä läpi aurinkosyklin.

ASIASANAT: avaruusfysiikka, aurinkotuuli, suihkuvirtaukset, magnetosfääri

Acknowledgements

Looking back on the years leading up to the completion of this PhD project, I feel incredibly fortunate to have had the opportunity to pursue this work as my job. I would like to thank the University of Turku Graduate School and the Vilho, Yrjö and Kalle Väisälä Fund for their financial support. I can only begin to thank the people who have contributed to this journey and supported me along the way.

My deepest gratitude goes to my main supervisor, Heli. I am truly indebted to you for introducing me to the field of space physics during my summer internship in 2018 and for guiding me ever since. You have been an excellent supervisor and taken care to continuously challenge me and foster my independence while always being available and supporting me during difficult times. Working with you has been an absolute pleasure, and I am proud to have you as my mentor. Next, I would like to extend my gratitude to my second supervisor, Rami. Thank you for welcoming me into your group and offering invaluable guidance and various opportunities to expand my expertise. It has been truly inspiring to learn from you over these years.

I extend my thanks to all the co-authors of the work included in this thesis: Adrian, Ferdinand, Florian, and Terry. I would like to give special recognition to Adrian for his peer-support that became invaluable to me during the pandemic. Thank you for your continued support, for sharing ideas, and for your friendship. Along with Adrian and Florian, I want to thank the rest of our magnetosheath jet network (Adrian P., Eva, Jonas, Luis, Nikol, and Savvas). It has been a pleasure getting to know and work with you, and I hope our collaborations will continue in the future.

To all the people at the University of Turku Space Research Laboratory, I express my gratitude for making me feel at home and for being a wonderful group of people. I have learned so much from you and have thoroughly enjoyed your company. I am confident that our collaborations will continue in the future. Special thanks go to Christian and Seve for accompanying me on this PhD journey and making it fun, to Nina, Jan, Sasha, and Annamaria for the great climbing sessions, and to Immanuel for being an excellent office mate.

I would like to thank my friends and family for supporting me and believing in me throughout all these years. Finally, to Erika, thank you for your love, support, encouragement, and patience.

Espoo, June 2024
Laura Vuorinen

Table of Contents

Abbreviations

1D/2D/3D	one/two/three-dimensional
ARTEMIS	Acceleration, Reconnection, Turbulence and Electrodynamics of the Moon's Interaction with the Sun
AU	astronomical unit
BS	bow shock
BW	bow wave
CIR	co-rotating interaction region
CME	coronal mass ejection
DSA	diffusive shock acceleration
ESA	Electrostatic Analyzer / European Space Agency
FAB	field-aligned beam
FGM	FluxGate Magnetometer
GSE	Geocentric Solar Ecliptic (coordinate system)
GSM	Geocentric Solar Magnetospheric (coordinate system)
GIPM	Geocentric Interplanetary Medium (coordinate system)
HSS	high-speed stream
HT	de Hoffmann–Teller (frame)
IMF	interplanetary magnetic field
L1	Lagrange point 1
MHD	magnetohydrodynamics
MMS	Magnetospheric Multiscale (mission)
MP	magnetopause
MSH	magnetosheath
NASA	National Aeronautics and Space Administration
PIC	particle-in-cell (simulation)
SDA	shock drift acceleration
SIR	stream interaction region
SLAMS	short large-amplitude magnetic structure
SW	solar wind
THEMIS	Time History of Events and Macroscale Interactions during Substorms (mission)
ULF	ultra-low frequency
UT	universal time
VDF	velocity distribution function

List of Original Publications

This dissertation is based on the following original publications, which are referred to in the text by their Roman numerals:

I L. Vuorinen, H. Hietala, and F. Plaschke.
Jets in the magnetosheath: IMF control of where they occur.
Annales Geophysicae, 2019; 37: 689–697.

II L. Vuorinen, H. Hietala, A. T. LaMoury and F. Plaschke.
Solar wind parameters influencing magnetosheath jet formation: low and high IMF cone angle regimes.
Journal of Geophysical Research: Space Physics, 2023; 128, e2023JA031494.

III L. Vuorinen, A. T. LaMoury, H. Hietala and F. Koller.
Magnetosheath jets over solar cycle 24: An empirical model.
Journal of Geophysical Research: Space Physics, 2023; 128, e2023JA031493.

IV L. Vuorinen, R. Vainio, H. Hietala, and T. Z. Liu.
Monte Carlo Simulations of Electron Acceleration at Bow Waves Driven by Fast Jets in the Earth's Magnetosheath.
The Astrophysical Journal, 2022; 934: 165.

V L. Vuorinen, H. Hietala, F. Plaschke, and A. T. LaMoury.
Magnetic field in magnetosheath jets: A statistical study of B_Z near the magnetopause.
Journal of Geophysical Research: Space Physics, 2021; 126: e2021JA029188.

Author's contribution to the publications

In Paper I and Paper V, the author conducted the data analysis and wrote the manuscripts with comments from the co-authors. In Paper II, the author conceived the study, conducted the data analysis, and wrote the manuscript with comments from the co-authors. In Paper III, the author conceived the study, developed the statistical model,

conducted most of the data analysis, and wrote the manuscript with comments from the co-authors. In Paper IV, the author developed the simulation code in Python, conducted the analysis of simulation data, and wrote the manuscript with comments from the co-authors.

List of publications not included in the thesis

I F. Plaschke, M. Jernej, H. Hietala, and L. Vuorinen.
On the alignment of velocity and magnetic fields within magnetosheath jets.
Annales Geophysicae, 2020; 38, 287–296.

II A. T. LaMoury, H. Hietala, F. Plaschke, L. Vuorinen, and J. P. Eastwood.
Solar wind control of magnetosheath jet formation and propagation to the magnetopause.
Journal of Geophysical Research: Space Physics, 2021; 126, e2021JA029592.

III D. Trotta, L. Vuorinen, H. Hietala, T. Horbury, N. Dresing, J. Gieseler, A. Kouloumvakos, D. Price, F. Valentini, E. Kilpua, and R. Vainio.
Single-spacecraft techniques for shock parameters estimation: A systematic approach.
Frontiers in Astronomy and Space Sciences, 2022; 9:1005672.

IV M. Owens, M. Lockwood, L. A. Barnard, S. L. Yardley, H. Hietala, A. T. LaMoury, and L. Vuorinen.
Annual Variations in the Near-Earth Solar Wind.
Solar Physics, 2023; 289, 111.

V L. Annie John, S. Nyberg, L. Vuorinen, R. Vainio, A. Afanasiev, S. Poedts, and N. Wijsen.
Effects of adiabatic focusing and free-escape boundaries in coronal shock acceleration.
Journal of Space Weather and Space Climate, 2024; 14, 15.

VI H. Hietala, D. Trotta, A. Fedeli, L. B. Wilson III, L. Vuorinen, and J. T. Coburn.
Candidates for downstream jets at interplanetary shocks.
Monthly Notices of the Royal Astronomical Society, 2024; 531, 2, 2415–2421.

VII I. C. Jebaraj, O. V. Agapitov, V. V. Krasnoselskikh, L. Vuorinen, M. Gedalin, K. E. Choi, E. Palmerio, N. Wijsen, N. Dresing, A. Afanasiev, R. Vainio, E. K. J. Kilpua, A. Kouloumvakos, D. Trotta, M. Balikhin, J. Verniero, J. G. Mitchell, C. Cohen, M. Hill, N. Raouafi, and S. D. Bale.
Acceleration of electrons and ions by an “almost” astrophysical shock in the heliosphere.
The Astrophysical Journal Letters, 2024; 968, L8.

VIII G. U. Farwa, N. Dresing, J. Gieseler, L. Vuorinen, I. G. Richardson, C. Palmroos, S. Valkila, B. Heber, S. Jensen, P. Kühl, L. Rodríguez-García,

and R. Vainio.
Electron and proton peak intensities in solar energetic particle events.
Astronomy & Astrophysics; in review.

IX M. Jarry, N. Dresing, A. P. Rouillard, I. Plotnikov, R. Vainio, C. Palmroos, A. Kouloumvakos, and L. Vuorinen.
The evolution of coronal shock wave properties and their relation with solar energetic particles.
Astronomy & Astrophysics; submitted.

1 Introduction

The interplanetary space is not completely empty. Our planet is immersed in a flow of plasma coming from the Sun — the *solar wind*. As it leaves from the Sun, the solar wind carries the solar magnetic field with it, which forms the *interplanetary magnetic field* (IMF). Upon arriving at the Earth, the solar wind plasma and magnetic field interact with the Earth's *magnetosphere*, a protective bubble formed by our planet's intrinsic magnetic field. The properties of the solar wind vary in relation to different source regions on the Sun, and the distribution of these source regions varies across the solar cycle. Near the solar maximum, the solar wind is also frequently embedded with large-scale solar wind structures, e.g., coronal mass ejections (CMEs), which introduce large variations and extreme conditions upon reaching the Earth. The solar wind conditions at the Earth control how much solar wind energy and mass can enter the magnetosphere (Bothmer and Zhukov, 2007). Sometimes the wind blows harder, sometimes gentler, and the magnetosphere responds by becoming compressed, or by expanding. The orientation of the IMF is of particular significance for this interaction. When it is oppositely aligned to the Earth's magnetic field, these two fields can merge in a process called *magnetic reconnection*, essentially creating an opening for solar wind plasma and energy to access the magnetosphere.

Solar wind–magnetosphere interaction leads to a plethora of effects in the near-Earth space, of which part can be called *space weather*. This term encompasses variable phenomena in space that can have adverse effects on human technology, infrastructure, and life in space and here on the ground (Bothmer and Daglis, 2007). Humans and satellites in space are vulnerable to particle radiation, while severe space storms cause magnetic disturbances on the ground that can induce hazardous currents into pipelines and power grids. Space physics studies phenomena in space and their relation to space weather, which is becoming ever more important as our civilization relies on these technological systems that can be vulnerable to space weather effects. Space physics is also adjacent to the field of astrophysics, but distinguished by the availability of a wide range of *in-situ* spacecraft measurements.

In this thesis, we investigate in-situ observations of the Earth's *bow shock* and its downstream region, the *magnetosheath*. The bow shock forms when the solar wind first meets the Earth's magnetosphere. Due to the supersonic nature of the solar wind, the flow cannot simply divert around the obstacle, but a shock wave forms, where the solar wind is abruptly slowed down, compressed, and heated. In

the region downstream of the shock, the flow is subsonic and can divert around the magnetosphere. Thus, it is actually the shocked solar wind in the magnetosheath that ultimately interacts with the magnetosphere. The Earth's bow shock is our best laboratory for *collisionless shocks*, which exist in plasmas throughout the Universe, e.g., ahead of other planetary bodies, driven by fast CMEs, and around supernova remnants. Shocks are important sites for particle acceleration in the heliosphere, and shocks at supernovae remnants are believed to accelerate cosmic rays. Studying the Earth's bow shock with all available in-situ measurement techniques allows us to make fundamental discoveries that help us understand shock waves also in other environments.

The strongest disturbances in the magnetosphere and the ionosphere can be attributed to variations in the upstream solar wind. However, the Earth's magnetosphere and the bow shock system are highly dynamical systems in and of themselves, too. Studying the Earth's magnetosheath, we find that even during steady solar wind conditions faster flows occasionally emerge from the shock and travel deeper in the magnetosheath (Plaschke et al., 2018, and the references within). These flows are called *magnetosheath jets*, and they are defined by their higher anti-sunward dynamic pressure compared to the surrounding ambient magnetosheath plasma. Jets can propagate through the magnetosheath and push against the boundary of the Earth's magnetosphere, the *magnetopause*, perturbing the magnetosphere and the ionosphere. Magnetosheath jets are very common during certain solar wind conditions, but the significance of their contribution to solar wind–magnetosphere interaction is still not well understood.

In this thesis, we answer the following research questions:

1. Where and during which solar wind conditions do magnetosheath jets occur?
2. How does the jet occurrence vary across the solar cycle?
3. How do bow waves driven by the fastest jets accelerate electrons in the magnetosheath?
4. Can jets introduce magnetic field variations at the magnetopause which could influence conditions for magnetopause reconnection?

Studying where, when, and how often jets form is the first step towards understanding their relevance for the solar wind–magnetosphere interaction. Understanding the conditions in which jets emerge also allows us to make predictions on the existence of jets in other shock environments of different parameter regimes, elucidating the potential universality of these transient structures. We also focus on two potential effects of magnetosheath jets at different points of their lifetime as they move from the bow shock towards the magnetopause. First, during their propagation some jets can accelerate particles as they drive their own bow waves ahead of them. Magnetosheath

jets can thus provide additional energization of particles within a shock environment. We study the mechanism of this acceleration process, focusing on electrons. Some jets survive all the way through the magnetosheath and eventually collide into the magnetopause. We investigate their magnetic properties to understand whether jets can alter the magnetic conditions for magnetopause reconnection, which is the most important process by which solar wind energy enters the magnetosphere. We aim to understand whether jets can modulate it upon their impact, either by triggering reconnection during unfavorable conditions or suppressing it during favorable conditions. While the scale and energy of magnetosheath jets is small compared to structures in the solar wind, their importance arises from their numbers. The role of jets on the dayside magnetosphere dynamics may be especially significant during times of high jet occurrence and steady solar wind conditions.

This thesis is organized as follows. In Chapter 2, we introduce the basic theory of plasma, collisionless shocks in space, and magnetic reconnection relevant for this thesis. Chapter 3 presents a further introduction to the Earth's environment in the *heliosphere*, that is the area under the influence of the Sun, and a description of the structure of the Earth's bow shock environment. Having set the scene, Chapter 4 focuses on magnetosheath jets that play the leading role in this work. We provide a brief review on the occurrence and formation of jets, how they propagate and influence the surrounding magnetosheath plasma, and how they can influence the magnetosphere and the ionosphere. We pay special attention to the topics relevant to the research conducted as a part of this thesis. In Chapter 5, we present the data and methods employed, and Chapter 6 presents a summary of the results of this thesis. Finally, in Chapter 7, we provide the conclusions of this thesis and further discuss the implications of our results and their relevance for the study of magnetosheath jets and the solar wind–magnetosphere interaction. We also offer an outlook for further research on this topic.

2 Theory

In this chapter, we provide an introduction to the theoretical background of plasma physics. We briefly cover the nature of plasma, the fourth and most common state of matter in the Universe, before moving to two fundamental plasma phenomena: collisionless shocks and magnetic reconnection.

2.1 Plasma

Over 99 % of the ordinary matter in the Universe is in the form of plasma — ionized, but quasi-neutral, gas consisting of a large number of charged particles (electrons and positive ions). Electromagnetic fields are important for the dynamics of plasma, by definition. These dynamics can studied with multiple levels of description, ranging from microscopic to macroscopic. One can follow exactly the motion of individual particles using laws of electrodynamics. The opposite end is to study plasma as a single fluid by combining the Navier-Stokes equations of hydrodynamics with Maxwell's equations of electromagnetism into *magnetohydrodynamics* (MHD). In between lies, e.g., the Vlasov theory, which follows the evolution of distribution functions, i.e., particle number densities in phase space.

Depending on the phenomenon under investigation and its relevant length and time scales, the different levels of description are required to understand the physics of plasma. In this thesis, we will be mostly applying a fluid picture by using bulk quantities such as ion bulk speed and ion number density calculated as moments of the ion distribution function. However, this picture falls short when the distribution consists of multiple populations, e.g., a core and a beam population. We visit the levels of individual particles and distribution functions when necessary. Kinetic effects are paramount for understanding the physics of, e.g., collisionless shocks in space. Crucially, these effects manifest themselves on all scales, even on the global level.

An important concept in space plasmas is that of magnetic field being *frozen-in* into the plasma flow. Considering resistive MHD with Ohm's law

$$\mathbf{E} = -\mathbf{V} \times \mathbf{B} + \frac{\mathbf{J}}{\sigma}, \tag{1}$$

the so-called MHD *induction equation* can be written as (e.g., Koskinen, 2011a)

$$\frac{\partial \mathbf{B}}{\partial t} = \nabla \times (\mathbf{V} \times \mathbf{B}) + \frac{1}{\mu_0 \sigma} \nabla^2 \mathbf{B}. \tag{2}$$

Here $\mathbf{E}$ is the electric field, $\mathbf{V}$ is the bulk flow velocity of the plasma, $\mathbf{B}$ is the magnetic field, $\mathbf{J}$ is the current density, σ is the electrical conductivity of the plasma, t is time, and μ_0 is the vacuum permeability. The first term on the right-hand side of Equation 2 is the convection (or rather the *advection*) term that describes how the magnetic field follows the movement of the plasma. The second term is the diffusion term. In space plasmas, the convection term typically dominates due to very high conductivity. In the so-called *ideal MHD* limit where $\sigma \to \infty$, the magnetic field follows the motion of the plasma as if it was frozen-in to the plasma. A corollary to this is the statement that plasma elements initially on the same magnetic field line remain on the same field line. However, diffusion of the magnetic field becomes important in regions where electrical resistivity $1/\sigma$ increases, local magnetic field gradients become large, and/or the plasma is at rest ($\mathbf{V} = 0$). In these circumstances, the frozen-in condition breaks down, changing the magnetic field configuration.

2.2 Collisionless shocks

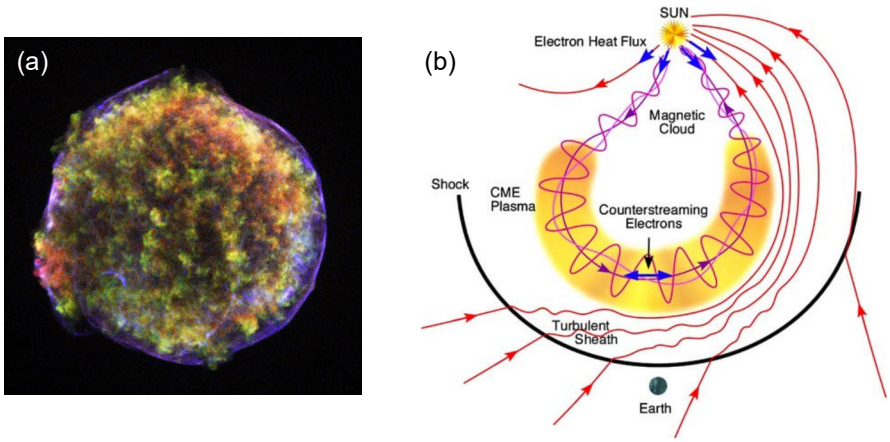

Figure 1. (a) A false-color image of Tycho's supernova remnant with a shell-like shock wave surrounding it, as observed by the Chandra X-ray Observatory (Credit: NASA/CXC/Rutgers/J. Warren & J. Hughes et al., http://chandra.harvard.edu/photo/2005/tycho/). (b) A cartoon of an interplanetary CME driving a shock wave (Zurbuchen and Richardson, 2006, reproduced with permission from SNCSC).

In space, we often encounter shock waves. They are observed, e.g., around supernova remnants (Figure 1a) and ahead of planets and CMEs (Figure 1b). The basic principle of these shock waves is essentially the same as for hydrodynamic shocks observed here on Earth, e.g., ahead of a supersonic aircraft that moves through air faster than the local information speed, the sound speed $V_\mathrm{s} = \sqrt{\gamma P/\rho}$. Here, γ is the polytropic index, P is the gas pressure, and ρ is the mass density. In ordinary fluids, when a supersonic flow meets an obstacle, *sound waves* cannot transmit infor-

mation of the existence of the obstacle and the incoming flow cannot deflect around it. A shock wave forms, at which the flow is decelerated, compressed, and heated, becoming subsonic.

A magnetized plasma supports many additional types of waves, and the propagation angle θ of waves with respect to the background magnetic field is important. In the MHD single-fluid picture (e.g., Koskinen, 2011a), there is a second characteristic speed called the Alfvén speed $V_\mathrm{A} = B/\sqrt{\mu_0 \rho}$. Both the *Alfvén waves*, that travel at this speed, and the previously considered sound waves can propagate in a magnetized plasma along the magnetic field ($\theta = 0°$). A *magnetosonic wave* can travel perpendicular ($\theta = 90°$) to the magnetic field with a characteristic speed called the magnetosonic speed $V_\mathrm{ms} = \sqrt{V_\mathrm{s}^2 + V_\mathrm{A}^2}$. When considering oblique propagation at an arbitrary angle θ with respect to the magnetic field, the Alfvén wave has a phase speed $V_\mathrm{A} \cos\theta$ and there are two additional wave modes: the *fast* ($+$) and *slow* ($-$) MHD waves with phase speeds

$$\left\{ \frac{1}{2} \left[\left(V_\mathrm{s}^2 + V_\mathrm{A}^2\right) \pm \sqrt{\left(V_\mathrm{s}^2 + V_\mathrm{A}^2\right)^2 - 4 V_\mathrm{s}^2 V_\mathrm{A}^2 \cos^2\theta} \right] \right\}^{1/2} . \tag{3}$$

The highest information speed in MHD is that of the fast MHD wave. Shock waves are associated with either two of the compressive wave modes: the fast or slow MHD wave, which are often also referred to as the fast and slow magnetosonic wave, respectively.

In addition to the different wave modes, there is a fundamental difference in shock waves observed in space compared to those observed in ordinary fluids. In hydrodynamic shock waves, the kinetic energy of the incoming supersonic flow is converted to heat via particle collisions. Space plasmas are so tenuous that the collisional mean free path is too high for collisions to play a role. Instead, at these *collisionless shocks*, wave–particle interactions replace the role of collisions (e.g., Burgess and Scholer, 2015). Plasma instabilities lead to the generation of waves, and particles scatter off of irregularities in the electromagnetic field, emulating the scattering due to collisions and providing dissipation. Shock waves transform kinetic energy of the incoming flow into heat. This is an irreversible, entropy-increasing process, in which the upstream flow that exceeds the local information speed turns into the downstream flow that is below the local information speed.

2.2.1 MHD jump conditions

Shock waves can be described by the so-called MHD Rankine-Hugoniot jump conditions, which are conservation relations that uniquely relate the state of plasma upstream and downstream of the shock. These equations are derived under the assumption of ideal MHD, in which the magnetic field is frozen-in into the flow of the plasma. The Rankine-Hugoniot conditions then arise from conservation laws of

mass, momentum, and energy through the shock layer together with Faraday's law in the steady state and Gauss' law for magnetism. They describe the changes in macroscopic plasma properties in a dynamic equilibrium across a planar discontinuity between homogeneous plasma regions upstream and downstream of the shock. Assuming a polytropic equation of state, the jump conditions can be written as (e.g., Burgess and Scholer, 2015):

$$[\rho V_n] = 0 \tag{4}$$

$$\left[\rho \mathbf{V} V_n + \left(P + \frac{B^2}{2\mu_0}\right)\hat{\mathbf{n}} - \frac{B_n \mathbf{B}}{\mu_0}\right] = 0 \tag{5}$$

$$\left[\left(\frac{1}{2}\rho V^2 + \frac{\gamma P}{\gamma - 1} + \frac{B^2}{\mu_0}\right) V_n - \frac{B_n \mathbf{B}\cdot\mathbf{V}}{\mu_0}\right] = 0 \tag{6}$$

$$[\mathbf{B}_n] = 0 \tag{7}$$

$$[V_n \mathbf{B}_t - B_n \mathbf{V}_t] = 0 \tag{8}$$

in a frame where the shock is at rest. $[a] = a_2 - a_1$ denotes the change of quantity a from the upstream value (subscript 1) to the downstream value (subscript 2). Here, ρ is the mass density, $\mathbf{V}$ is the bulk flow velocity, P is the plasma pressure, $\mathbf{B}$ is the magnetic field, μ_0 is the vacuum permeability, and γ is the polytropic index of the plasma. The vector components parallel to the normal of the discontinuity plane are denoted with the subscript n, while the components tangential to the discontinuity plane are denoted with the subscript t.

These equations apply to other types of discontinuities as well, but shocks are the solutions for which there is mass flow across the discontinuity ($\rho V_n \neq 0$) and there is compression from upstream to downstream (the compression ratio $r = \rho_2/\rho_1 = V_{n1}/V_{n2} > 1$). It is important to note that these jump conditions do not describe any of the kinetic processes near the shock transition, but they describe the large-scale changes in bulk quantities across a shock. A shock wave transforms kinetic energy of the incoming flow into thermal energy of the plasma. The strength of a shock is typically characterized by its Mach number, which is the ratio of the upstream flow speed parallel to shock normal in the shock rest frame and a characteristic speed. For example, the Alfvénic Mach number is written as $M_\mathrm{A} = V_n/V_\mathrm{A}$. The larger the Mach number, the stronger the shock: the more energy needs to be dissipated at the shock and the larger the changes from upstream to downstream. By definition, the Mach number of a shock has to exceed unity. Hydrodynamic shocks have sonic Mach numbers $M_\mathrm{s} = V_n/V_\mathrm{s} > 1$, while fast-mode (slow-mode) shocks are defined by the fast (slow) magnetosonic Mach number $M_\mathrm{ms,f} = V_n/V_\mathrm{ms,f} > 1$ ($M_\mathrm{ms,s} = V_n/V_\mathrm{ms,s} > 1$). The MHD jump conditions also permit a third shock solution: an intermediate shock associated with the Alfvén wave. We will not consider this solution further, but only note that a perturbation analysis shows that this solution is non-evolutionary in the MHD framework (Burgess and Scholer, 2015). A

clear observational difference between a fast-mode and a slow-mode shock is that in a fast-mode shock the magnetic field magnitude increases from the upstream to the downstream, while in a slow-mode shock it decreases. Fast-mode shocks are much more common in the heliosphere, and we will focus on them in this thesis. The Earth's bow shock is an example of a fast-mode shock.

Another important parameter that is used to characterize a shock is the acute angle θ_{Bn1} (denoted just as θ_{Bn} from here onwards) between the local shock normal and the upstream magnetic field. This is a measure of shock obliquity, which is important in the MHD jump conditions. Equation 7 shows that the normal component of the magnetic field does not change across the discontinuity. Thus, for a *parallel* shock with $\theta_{Bn} = 0°$, there is no compression of the magnetic field, and these ideal MHD jump conditions reduce to those of a hydrodynamic shock.

2.2.2 Quasi-parallel and quasi-perpendicular shock regimes

The single-fluid MHD picture of a shock does not model all important features of collisionless shock waves. The particle dynamics at the shock can become very important for the energy dissipation and the structure of the shock. If the Mach number of the shock is sufficiently high (as is often the case in the heliosphere; Burgess and Scholer, 2015), the shock becomes *supercritical* and starts reflecting ions due to the cross-shock potential that develops across the shock layer. This potential is a result of charge separation, owing to the difference in inertia for ions and electrons. Incoming ions penetrate deeper, and thus an upstream-directed electric field forms. The cross-shock potential thus slows down and reflects ions and accelerates electrons incident from the upstream. In addition to this, magnetic mirroring contributes to the reflection of particles at fast-mode shocks, where the magnetic field is stronger on the downstream side of the shock.

What happens to the shock-reflected particles greatly depends on the obliquity of the shock. Shocks are traditionally categorized in two regimes: *quasi-parallel* shocks with $\theta_{Bn} < 45°$ and *quasi-perpendicular* shocks with $\theta_{Bn} > 45°$. When θ_{Bn} is high, reflected particles are swiftly convected downstream because they cannot travel far upstream in the direction transverse to the magnetic field. In contrast, when θ_{Bn} is low, the particles can easily travel far back upstream along the magnetic field lines. Reflected particles upstream of the quasi-parallel shock region lead to the formation of a *foreshock*, which is a region full of intense electromagnetic waves that form due to the interaction between the backstreaming particles and the incoming upstream plasma via plasma instabilities. The steepening of these waves can lead to non-linear structures which play a role in decelerating the incoming plasma. Quasi-perpendicular and quasi-parallel shock crossings look drastically different in spacecraft data, especially in the case of the Earth's bow shock, which we will return to in Section 3.2.1.

2.2.3 Shock-acceleration mechanisms

Shocks are important particle accelerators in the Universe. Shocks at supernova remnants are believed to accelerate cosmic rays (e.g., Reynolds, 2011). CME-driven shocks are believed to explain wide-spread and gradual solar energetic particle events in the heliosphere (e.g., Desai and Giacalone, 2016). The two main forms of Fermi shock acceleration considered here are *shock drift acceleration* (SDA) and *diffusive shock acceleration* (DSA).

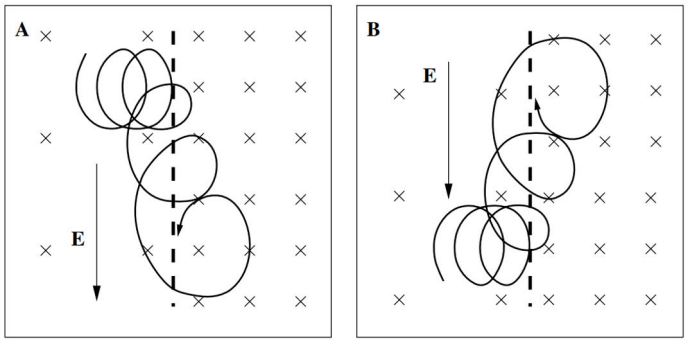

Figure 2. A sketch of shock drift mechanism that takes place at quasi-perpendicular shocks. The magnetic field is into the page, and the upstream side is on the left-hand side of the shock. Panel A shows ions drifting parallel to the electric field and panel B shows electron drifting anti-parallel to it. Figure by courtesy of R. Vainio.

Shock drift acceleration takes place at fast-mode quasi-perpendicular shocks, where there is a substantial magnetic field increase from the upstream to the downstream and the particles can be magnetically mirrored. The particles are accelerated by the upstream convective electric field $\mathbf{E}_1 = -\mathbf{V}_1 \times \mathbf{B}_1$ (Webb et al., 1983). Particles incident on the shock feel the stronger downstream magnetic field which turns the guiding center drift of ions (electrons) parallel (anti-parallel) to the convective electric field. This causes the particles to gain energy from the electric field (see Figure 2). The interaction of the particle with the shock can be easily treated by moving to the so-called de Hoffmann–Teller frame (HT-frame). In this shock rest frame, the velocity and magnetic field vectors align on both the upstream and the downstream side of the shock, and thus the convective electric field disappears. Now, if we ignore the effect of cross-shock potential, the total momentum p of the particle is conserved in this frame. We also assume that its first adiabatic invariant $p_\perp^2/B$ (where $p_\perp$ is the momentum perpendicular to the magnetic field) is conserved.

Particles moving toward the shock with pitch-angle cosine μ in the loss-cone $|\mu| > \sqrt{1-1/r_B}$ (where $r_B = B_2/B_1$ is the magnetic compression ratio) get transmitted downstream, while the other particles get reflected back upstream with the parallel momentum changing $|\Delta p_\parallel| = 2|p_\parallel|$. In the upstream rest frame, this

corresponds to

$$|\Delta p'_{\parallel}| = \frac{|\Delta p_{\parallel}|}{\sqrt{1 - \left(V_{1n}/\cos\theta_{Bn}\right)^2/c^2}} \tag{9}$$

(c is the speed of light) and an increase in total momentum of the particle (e.g., Koskinen, 2011c). The fundamental limitation in the energy gain of pure SDA is that the particles interact with the shock only once. In reality, the effect of cross-shock electric field, which increases ion reflection and decreases electron reflection, should also be considered. In fact, specular reflection via the cross-shock electric field alone can similarly facilitate ion drift acceleration. This process is called shock surfing acceleration (Shapiro and Üçer, 2003).

Diffusive shock acceleration (DSA) is a mechanism where particles are able to interact with the shock multiple times due to scattering off of magnetic irregularities that are present both upstream and downstream of the shock wave (Drury, 1983). This mechanism is most efficient at quasi-parallel shocks where energetic particles can more easily return to the shock. When a particle is scattered, its energy is conserved in the frame of the scattering center but its pitch-angle, and thus propagation direction, changes, allowing an energetic particle to cross the shock multiple times. The scattering centers are often assumed to be frozen-in into the local plasma flow. As the downstream flow is slower than the upstream flow ($V_2 < V_1$) in the frame of the shock, the flow converges at the shock and particles are accelerated via the Fermi mechanism. Numerous crossings of the shock lead to a systematic increase in the energy of the particle. For particle speeds greatly exceeding the plasma flow speed, DSA produces a power-law spectrum

$$\frac{\mathrm{d}N}{\mathrm{d}p} = \frac{3N_0}{r-1}\left(\frac{p_0}{p}\right)^{(r+2)/(r-1)}, \tag{10}$$

where N is the number of particles, p_0 is the injection momentum, and r is the compression ratio of the shock (Vainio and Afanasiev, 2018). The spectral index $\sigma = (r+2)/(r-1)$ is thus a function of r only. DSA is believed to be responsible for accelerating charged particles to the highest energies. In the heliosphere, DSA has been established as an important mechanism accelerating high-energy ions, but its role for electrons, for which the scales of relevant magnetic fluctuations are smaller, is still unclear.

In **Paper IV**, we model electron acceleration at an MHD shock wave to study acceleration at magnetosheath jet-driven shocks in the magnetosheath. In this model, SDA is the dominant shock acceleration mechanism. However, multiple interactions with the shock and further energization are facilitated by a collapsing magnetic trap, which allows particles to return to the shock from the upstream.

2.3 Magnetic reconnection

The frozen-in condition in a plasma breaks down when the resistivity becomes high enough and/or the spatial scale of a boundary between two magnetic domains becomes small (Koskinen, 2011b). A shear in magnetic field leads to a current sheet following Ampère's law

$$\nabla \times \mathbf{B} = \mu_0 \mathbf{J}, \tag{11}$$

and diffusion can happen very fast in the form of *magnetic reconnection* across thin current sheets where plasma regions of different magnetic field orientations are pushed together, either by external driving or by a tearing instability of the current sheet itself (Biskamp, 2000). Magnetic reconnection merges the magnetic fields of these two domains, rearranging the field configuration (see Figure 3) and transforming energy stored in the magnetic field into heat and kinetic energy of plasma outflows. Importantly, this new magnetic connection allows plasma of the two previously separate domains to mix. Magnetic reconnection is a fundamental plasma process responsible, e.g., for explosive energy release in solar flares and for space weather processes at Earth due to the transfer of mass and energy by magnetic reconnection at the dayside magnetopause and in the magnetotail. Most important for this thesis is how magnetic reconnection at the dayside magnetopause between the magnetic field in the shocked solar wind (in the magnetosheath) and the Earth's magnetic field allows solar wind energy to enter the magnetosphere. This process will be further discussed in Section 3.2.3.

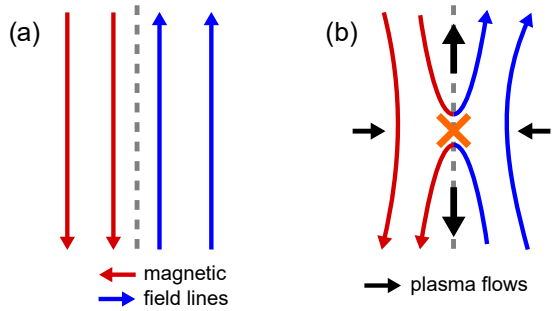

Figure 3. A cartoon illustrating how anti-parallel field lines (panel a) undergo magnetic reconnection (panel b).

In collisionless plasmas, wave–particle interactions and turbulence take on the role of particle collisions and produce effective resistivity. The generalized Ohm's law also contains other terms in addition to the resistive term that can be responsible for the breaking the frozen-in condition in the reconnection process (e.g., Cassak and Fuselier, 2016). Magnetic reconnection is a complex phenomenon of which details and microphysical mechanisms are out of the scope of this thesis (see, e.g., a recent review by Wang et al., 2023).

Macroscopically the most important parameter for reconnection is the magnetic shear angle, i.e., the angle between the magnetic field vectors on both sides of the current sheet: reconnection is most likely when the fields are exactly anti-parallel. Figure 3a shows a cartoon of this simplified geometry and Figure 3b illustrates the reconfiguration of the magnetic field topology in reconnected field lines along with reconnection plasma outflows from the so-called X-line (or X-point in this 2D case), where the field lines merge. In **Paper V**, we study the magnetic field within magnetosheath jets to understand if jets can modulate this magnetic shear at the magnetopause.

The magnetic fields need not be strictly anti-parallel for reconnection to happen. If a so-called guide field exists (out of the reconnection plane), component reconnection can still take place. Asymmetries between the plasma and magnetic field conditions on the two sides of the current sheet further influence the onset, efficiency, and geometry of magnetic reconnection (see, e.g., Cassak and Fuselier, 2016, and the references within). Most notably, when a guide-field exists, plasma β (the ratio of plasma pressure and magnetic pressure) asymmetry can suppress reconnection when the diamagnetic drift of the X-line, caused by the plasma pressure gradient, exceeds the reconnection outflow speed of the order of Alfvén speed (Swisdak et al., 2003). Swisdak et al. (2010) wrote the $\Delta\beta$-shear condition for this suppression as

$$\Delta\beta > \frac{2L_p}{d_\mathrm{i}} \tan(\Theta/2), \tag{12}$$

where d_i is the ion inertial length, L_p is the pressure scale length ($L_p/d_\mathrm{i} \sim 1$), and Θ is the magnetic shear angle. For low $\Delta\beta$ reconnection can occur over a wide range of magnetic shear angles, while for high $\Delta\beta$ it only occurs when the magnetic shear is high.

3 Earth in the Heliosphere

In this chapter, we describe the Earth's place in the *heliosphere* — the region that is permeated by plasma and magnetic field originating from the Sun. We then move closer to the Earth's magnetosphere — the magnetic bubble that protects the Earth from this environment. We only cover its dayside boundaries where the solar wind first meets the magnetosphere: the bow shock and the magnetopause. We also introduce the magnetosheath region in between, where the shocked solar wind flows around the magnetosphere and faster magnetosheath jets are frequently observed.

3.1 Solar wind and interplanetary magnetic field

Plasma is constantly flowing out from the Sun, filling the interplanetary space. Parker (1958) first theorized that the Sun's hot upper atmosphere, the solar corona, is in a dynamic equilibrium expanding outwards in the form of *solar wind* and it turns from subsonic to supersonic close to the Sun. At planetary distances, the solar wind is in fact super-fast-magnetosonic. Parker (1958) also correctly predicted that this flow of plasma drags the Sun's magnetic field into the interplanetary space, as the magnetic flux is "frozen-in" to the plasma flow. Near the solar surface, magnetic flux is also frozen-in to the plasma co-rotating with the Sun. As a consequence of the field both co-rotating with the Sun and following the solar wind that moves radially outwards from the Sun, the *interplanetary magnetic field* (IMF) forms a spiral geometry, called the Parker spiral. How tight the Parker spiral wounds is controlled by the solar wind speed, and thus IMF field lines tend to become less curved for higher solar wind speeds. At the Earth's orbital distance (1 AU $= 1.5 \times 10^8$ km), the magnetic field is tilted on average by $\sim 45^\circ$ with respect to the Sun-Earth line in the ecliptic plane. In reality, this nominal spiral geometry is disturbed because the solar wind flowing out from the Sun is not uniform and its properties vary in both space and time, often in a turbulent manner.

Solar wind consists mostly of protons and electrons and it can be observationally divided into two categories: *fast* (400–800 km/s) solar wind that is tenuous and *slow* (250–400 km/s) solar wind that is denser (Kallenrode, 1998). These two types originate from different regions on the Sun. The fast wind comes from coronal holes that are regions where magnetic field lines extend far out into space. In contrast, the slow wind comes from regions of closed field lines. During a solar minimum of the

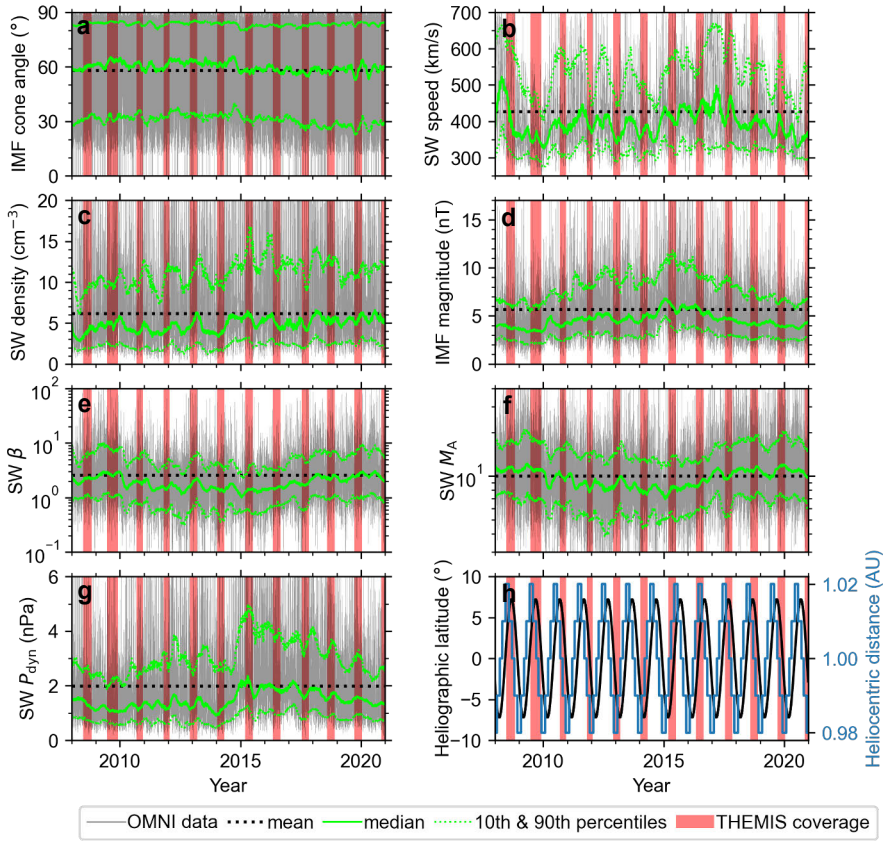

Figure 4. OMNI solar wind observations for the years 2008–2020 spanning solar cycle 24: the means (black dotted line), hourly observations (gray line), and the running 90-day median (green solid line) and the 10th and 90th percentiles (green dotted lines). P_{dyn} denotes dynamic pressure. THEMIS (see Section 5.1.1) observation intervals in the subsolar magnetosheath are highlighted in red (using the data set by Koller et al., 2022). The figure is from **Paper III** (Vuorinen et al., 2023b) and licensed under CC BY.

Sun's 11-year activity cycle (famously followed by the evolution of the number of sunspots), the regions of closed field lines, the source regions for slow solar wind, are distributed close to the solar equator, while the coronal holes are observed at the Sun's polar regions. However, at the solar maximum, the structure of the Sun's magnetic field has become complex with source regions for the slow solar wind distributed over all latitudes (Hansteen, 2009). In Figure 4, we present time series of OMNI solar wind observations (see Section 5.1.3; Papitashvili and King, 2020) from years 2008–2020. OMNI data is interspersed from measurements of multiple spacecraft at the Earth's Lagrange point L1 (at a distance of 0.01 AU $= 1.5 \times 10^6$ km from the Earth), so these measurements correspond to the solar wind conditions at the Earth. We can see the conditions vary on a wide range of time scales.

In addition to the variable nature of the solar wind source regions, the solar wind is also disturbed by large-scale structures embedded into the flow. These include interplanetary CMEs (Kilpua et al., 2017) and stream/co-rotating interaction regions (SIRs/CIRs; Richardson, 2018). SIRs and CIRs form when faster solar wind streams catch up slower solar wind streams ahead of them. The occurrence rate of these structures is also highly linked to the Sun's activity cycle. CMEs are most prevalent during solar maxima, while SIRs and CIRs are most common at the declining phase of the solar cycle. At their peak prevalence, these structures can both constitute roughly half of the solar wind that arrives at the Earth (Richardson and Cane, 2012). From the point of view of the Earth and its magnetosphere, these structures are enormous in size, so they are sensed as variations in the solar wind and IMF conditions. CME magnetic clouds (the ejecta) exhibit very low plasma β and M_{A} conditions with slow, but large, variations in magnetic field orientation, and sheath regions downstream of CME-driven shocks contain strong fluctuations both in plasma quantities and in the magnetic field. SIRs and CIRs exhibit a transition from slow to high solar wind with a compression region in between. The edges of the compression region can steepen into shock waves at the Earth's orbital distance: a forward shock at the leading edge and a reverse shock at the trailing edge (e.g., Richardson, 2018).

Solar wind and IMF variations influence the dynamics of the Earth's magnetosphere. In particular, the IMF orientation is important for the structure and dynamics of the Earth's bow shock and for conditions of magnetic reconnection at the dayside boundary of the Earth's magnetosphere. In **Papers I–III**, we investigate how solar wind conditions and the solar cycle influence the occurrence rates of magnetosheath jets. While the IMF is typically inclined with respect to the Sun-Earth line, during *radial IMF* they are almost aligned. This substantial deviation from the nominal Parker spiral is noteworthy from the perspective of magnetosheath jets, as we will discuss in Chapter 4. Prolonged radial IMF intervals can be observed at the trailing end of CMEs, or more generally at rarefaction regions where slower solar wind follows a faster solar wind stream (e.g., Orlove et al., 2013).

3.2 Dayside boundaries of Earth's magnetosphere

In this section, we describe the structure of the Earth's dayside magnetosphere. We focus on topics relevant to this thesis that considers magnetosheath jets that form at the Earth's bow shock and can propagate all the way through the magnetosheath, eventually impacting the magnetopause. Thus, we cover dayside magnetospheric boundaries, the bow shock and the magnetopause, where the solar wind first meets the Earth's magnetosphere (see Figure 5), and the turbulent magnetosheath region in between.

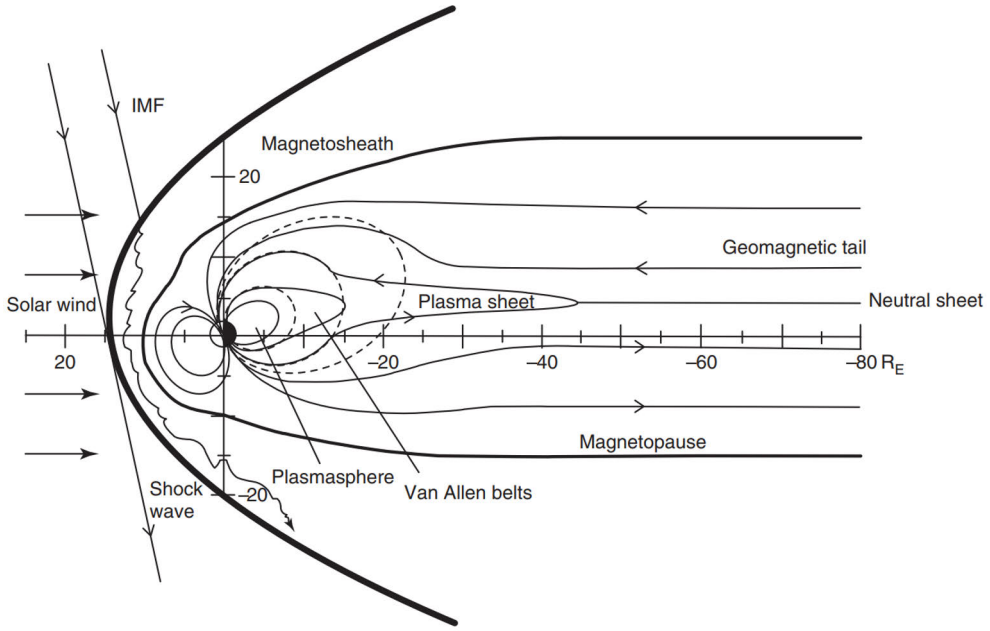

Figure 5. A cartoon of the structure of the Earth's magnetosphere and the impinging solar wind with its magnetic field, the IMF. Reprinted from Parks (2015), with permission from Elsevier.

3.2.1 Bow shock and foreshock

The Earth has a standing bow shock ahead of it, where the super-fast-magnetosonic solar wind is decelerated to sub-fast-magnetosonic speeds in the direction normal to the shock. The bow shock is curved around the Earth's magnetosphere that has a dipole-like configuration on the dayside (see Figure 5). The location of the bow shock can vary by multiple Earth radii ($R_{\mathrm{E}} = 6,371\,\mathrm{km}$) in response to variations in solar wind conditions, but its subsolar standoff distance is typically around 14 R_{E} from the center of the Earth (Farris et al., 1991). During high solar wind dynamic pressure conditions, the magnetosphere is compressed and the bow shock stands closer to the Earth. As can be seen in Figure 6, the curved shape combined with variations in the obliquity of the IMF means that some parts of the bow shock are quasi-parallel and others quasi-perpendicular at any given time (Burgess and Scholer, 2015). For the nominal Parker spiral geometry, the dawnside is quasi-parallel and the duskside is quasi-perpendicular. A parameter of particular interest in this thesis is the IMF *cone angle*

$$\alpha = \arccos\left(\frac{|B_X|}{B}\right) \in [0^\circ, 90^\circ], \tag{13}$$

which is the acute angle between the Sun-Earth line and the IMF vector. At the subsolar region of the Earth's bow shock, where the nominal shock normal is almost

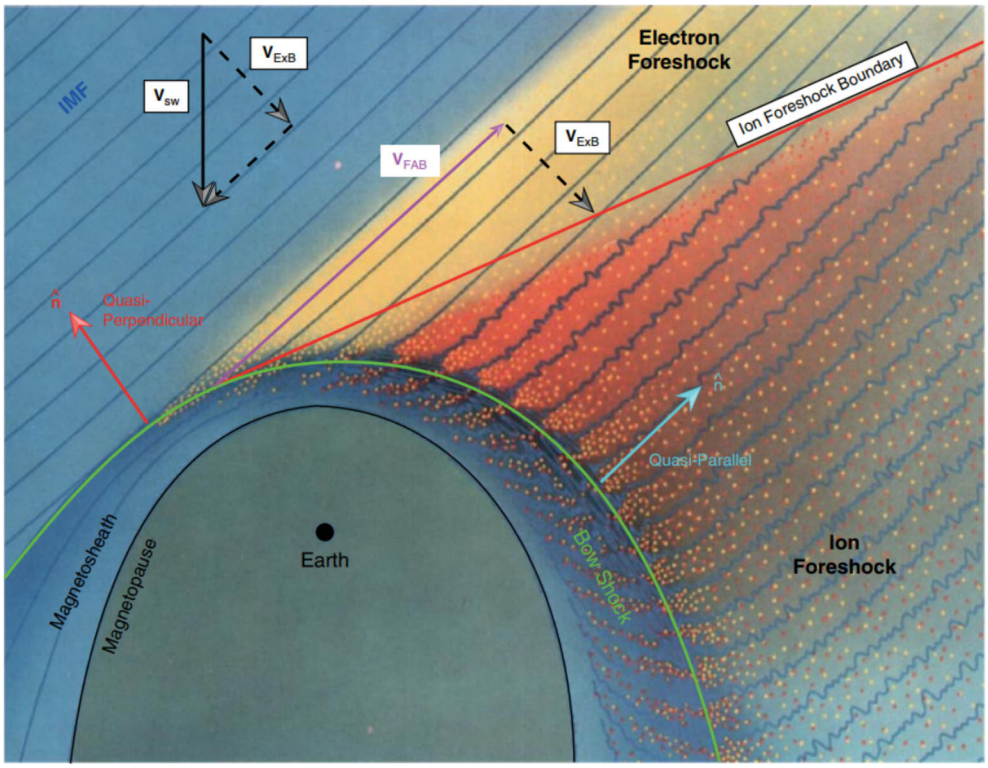

Figure 6. A sketch of the foreshock region that is magnetically connected to the quasi-parallel shock region. Figure obtained from Wilson III (2016), who adapted it from the original figure by Tsurutani and Rodriguez (1981), reproduced with the permission of American Geophysical Union.

aligned with the Sun-Earth line, the IMF cone angle closely approximates the shock obliquity angle θ_{Bn}. Importantly, when the IMF cone angle is low, the whole subsolar region of the Earth's bow shock has a quasi-parallel geometry. Such conditions of *quasi-radial IMF* ($\alpha < 30°$) are observed around 16 % of the time (Suvorova et al., 2010).

The Earth's bow shock is supercritical and thus reflects a fraction of incoming particles. As discussed in Sections 2.2.2 and 2.2.3, the shock obliquity θ_{Bn} controls how these reflected particles are transported and energized near the shock (see, e.g., Burgess et al., 2012). At the quasi-perpendicular shock, while most particles are convected downstream, a small fraction of energetic ions and electrons are observed upstream of the shock as field-aligned beams (FABs). These are likely energized by a mechanism akin to shock-drift acceleration (Oka et al., 2005; Burgess et al., 2012). At the quasi-parallel shock, ions can undergo diffusive shock acceleration, and a diffuse ion population is observed upstream of the shock (see, e.g., recent results by Johlander et al., 2021). The energetic backstreaming particles make up the *foreshock* region, where different types of ion distributions are observed at different locations.

This is a consequence of shock obliquity varying quickly on a field line that sweeps across the bow shock and of an anti-sunward $\mathbf{E} \times \mathbf{B}$ particle drift caused by the solar wind convectional electric field ($\mathbf{E} = -\mathbf{V} \times \mathbf{B}$). The edge of the electron foreshock is located near the point of first, tangential, connection between the IMF and the bow shock (as shown in Figure 6). In contrast, the edge of the ion foreshock is located closer to the Earth, as ions are slower and the effect of the earthward drift is relatively larger.

The extended foreshock region is spatially located where upstream magnetic field lines are connected to the quasi-parallel shock, as illustrated in Figure 6. As reviewed by Eastwood et al. (2005), the backstreaming particles interact with the incoming solar wind, generating waves via plasma instabilities. The waves then interact with the plasma, e.g., facilitating particle acceleration. The foreshock is thus a highly complex region consisting of multiple types of waves and particle populations. The dominant wave mode in the Earth's foreshock is the so-called 30-second ULF (ultra-low frequency) wave, which is observed in association with the diffuse ions deeper in the foreshock, but is believed to be excited by ion beams originating from the quasi-perpendicular shock and to grow upon convecting to the quasi-parallel region (Eastwood et al., 2005). This wave is of fast-mode nature, i.e., the perturbations in magnetic field magnitude and density are correlated. In addition to ULF waves, coherent localized enhancements of magnetic field are also frequently observed. These have been named *short large-amplitude magnetic structures* (SLAMSs; Schwartz, 1991), which propagate sunward in the frame of the upstream bulk flow but are advected towards the shock. SLAMSs are believed to form as ULF waves steepen upon convecting toward the shock, due to a gradient in suprathermal ion pressure (Giacalone et al., 1993) or via the gyroresonant interaction between solar wind ions and ULF waves as more recently suggested and supported by MMS observations (Chen et al., 2021b).

The foreshock modulates the quasi-parallel shock. Schwartz (1991) suggested that the quasi-parallel shock itself consists of layers of SLAMSs. This picture fits the observed corrugation of the quasi-parallel shock (Lucek et al., 2008). As a consequence, time series data of a spacecraft crossing a quasi-parallel shock shows a complex transition from upstream to downstream (e.g., Burgess et al., 2005). Figure 7a shows an example of THEMIS E crossing the quasi-parallel bow shock from the magnetosheath to the upstream solar wind. The presence of the foreshock region can be identified from the enhanced fluxes of 10 keV ions (panel i) and the magnetic field fluctuations (panel ii) on the upstream side. Magnetosheath jets are also significantly more common downstream of the quasi-parallel shock, and thus their occurrence follows the location of the quasi-parallel shock, as will be discussed in Chapter 4 and in **Paper I**. The anti-sunward dynamic pressure $P_{\mathrm{dyn},X}$ enhancement at $\sim$19:17 UT (in panel vi; highlighted with a black arrow) is an example of a magnetosheath jet.

For the quasi-perpendicular shock, the general shock structure is more well-

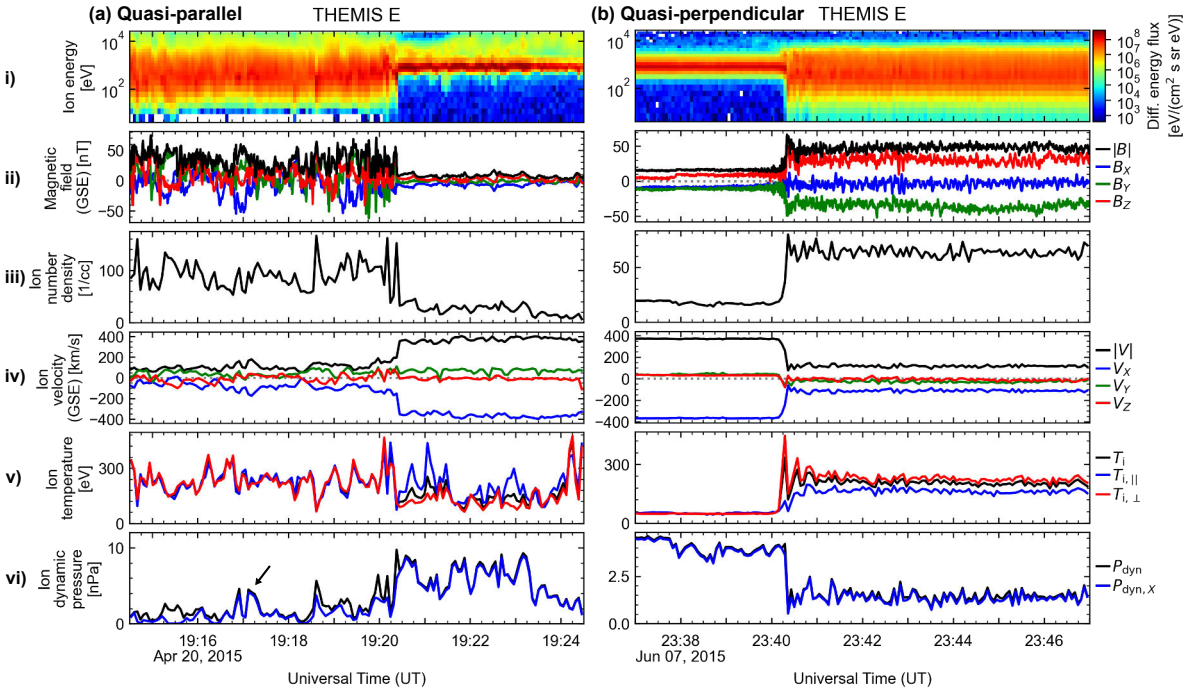

Figure 7. THEMIS E observations of (a) an outbound (from downstream to upstream) quasi-parallel bow shock crossing on April 20, 2015, and (b) an inbound (from upstream to downstream) quasi-perpendicular bow shock crossing on June 07, 2015. A magnetosheath jet is highlighted downstream of the quasi-parallel shock in panel vi.

defined (e.g., Bale et al., 2005). The foreshock caused by reflected particles is spatially limited to a small region near the shock, called *the foot*, where the reflected ions gyrate back to the shock. It manifests as a magnetic field increase ahead of the shock, caused by the current carried by the ions (Treumann, 2009). The shock ramp is a sharp transition (a "jump") often followed by an overshoot, where the magnetic field reaches its peak before decreasing to the downstream value. These different parts of the shock structure are typically relatively easy to identify in a quasi-perpendicular shock crossing (with the appropriate time resolution), where both the upstream and downstream regions are less turbulent and the shock itself exhibits less non-stationarity than in the case of a quasi-parallel shock crossing. Figure 7b shows an example of an inbound (upstream to downstream) crossing of the quasi-perpendicular bow shock as observed by THEMIS E. However, we note that for high M_{A} non-stationarity of the quasi-perpendicular shock becomes evident and shock transition becomes complex (Sundberg et al., 2017; Madanian et al., 2021). In **Paper II**, we investigate jet-like structures downstream of a quasi-perpendicular high-M_{A} shock and find that in such conditions gyrating ion populations near the shock can lead to jet-like enhancements in dynamic pressure.

3.2.2 Magnetosheath

The downstream region of the Earth's bow shock is called the magnetosheath, which is the primary region of focus of this thesis. In the subsolar region, the magnetosheath has a width of 2–4 R_{E} along the Sun-Earth line. Here the shocked sub-fast-magnetosonic solar wind can flow past the magnetosphere. Notably, it is the magnetosheath flow that interacts with the boundary of the Earth's magnetosphere. As expected for a fast-mode shock, the downstream magnetosheath flow is slower, denser, hotter, and exhibits a stronger magnetic field (see, e.g., Figure 7). Deeper in the magnetosheath the flow deviates more and more from the Sun-Earth line. Spreiter et al. (1966) already showed using gasdynamic flow models that the interplanetary magnetic field is advected into the magnetosheath and the magnetic field drapes around the magnetopause. Utilizing IMP 1 and IMP 2 (Interplanetary Monitoring Platform) spacecraft observations, Fairfield (1967) found that IMF conditions determine the magnetic field properties in the magnetosheath and that structures present in the IMF can be later detected in the magnetosheath.

The plasma properties in the downstream magnetosheath vary depending on whether the shock region is quasi-parallel or quasi-perpendicular (e.g., Lucek et al., 2005). The so-called quasi-parallel magnetosheath (downstream of the quasi-parallel shock), is typically more turbulent than that downstream of a quasi-perpendicular shock due to fluctuations originating from the foreshock region. Recently Turc et al. (2023) provided evidence that rather than directly transmitting, the dominant 30-second ULF foreshock fluctuations cause downstream fluctuations in three ways: 1) they modulate the shock generating fast-mode fluctuations downstream of the shock, 2) mode-convert to Alfvén waves at the shock, and 3) influence the cyclical shock reformation process. On the other hand, the quasi-perpendicular magnetosheath typically exhibits a high ion temperature anisotropy $T_{\perp} > T_{\parallel}$, which can be favorable for either the Alfvén ion cyclotron or the mirror-mode instability (e.g., Lucek et al., 2005).

Although the magnetosheath plasma has been processed by the shock, upstream transients can often be observed within the magnetosheath, including both solar wind and foreshock structures. Additionally, the shock dynamics themselves can produce transient magnetosheath structures. All these three scenarios are proposed mechanisms for magnetosheath jet generation, which we will return to in Chapter 4.

3.2.3 Magnetopause

The outer boundary of the Earth's magnetosphere is called the magnetopause. It is a current layer that separates the plasma populations and magnetic fields of the magnetosheath and the magnetosphere. The nominal magnetopause essentially stands in pressure balance between the incoming solar wind dynamic pressure and the magnetic pressure in the magnetosphere, typically with a subsolar standoff distance of around $10\,R_{\mathrm{E}}$ (Farris et al., 1991). Sometimes the wind blows with larger dynamic pressure and the magnetosphere responds by being compressed, moving the magnetopause boundary earthward. The magnetopause is not an impenetrable barrier (e.g., Eastwood et al., 2015, and the references within). Magnetic reconnection at the magnetopause can connect the interplanetary magnetic field draped into the magnetosheath to the Earth's magnetic field and enable transfer of mass and energy from the solar wind into the magnetosphere. Additionally, the Kelvin-Helmholtz instability at the flanks of the magnetopause (Nykyri and Otto, 2001; Hasegawa et al., 2004), where there are significant velocity shears across the boundary, and cross-field diffusion (Johnson and Cheng, 1997) enable mass transfer into the magnetosphere.

At the subsolar magnetopause, the conditions on the Earth's side of the magnetopause are typically relatively steady, and thus whether reconnection occurs depends largely on the conditions on the magnetosheath side (Cassak and Fuselier, 2016). In this region, the Earth's magnetic field points northward. Therefore, magnetic reconnection is very favorable when in the magnetosheath the magnetic field is directed southward, which naturally occurs when the IMF orientation is southward. During southward IMF, energy transfer from the solar wind into the magnetosphere is significantly enhanced due to subsolar magnetopause reconnection (e.g., Palmroth et al., 2006). This process drives the famous Dungey cycle by transporting energy and magnetic flux into the magnetotail. The magnetopause standoff distance also decreases (e.g., Shue et al., 2001; Wiltberger et al., 2003, and the references within). Magnetopause reconnection also occurs during northward IMF, but in this geometry it is efficiently driven at higher latitude regions on the anti-sunward sides of the cusps, where the magnetic fields are anti-parallel. This type of reconnection is not as efficient in terms of energy transfer into the magnetosphere, but can allow for a large amount of solar wind mass to enter the dayside magnetosphere.

While the magnetic shear angle between the two domains is the inherent parameter controlling reconnection onset, where, when, and how efficiently reconnection occurs at the dayside magnetopause depends on a multitude of parameters and physical effects (Cassak and Fuselier, 2016), as discussed in Section 2.3. Asymmetries are inherently present between the magnetosheath and magnetospheric plasma at the magnetopause. Observational evidence for the validity of the $\Delta\beta$-shear condition (Equation 12) at the Earth's magnetopause has been provided, e.g., by the statistical study of THEMIS magnetopause crossings by Phan et al. (2013). Because the

plasma beta on the magnetospheric side of the magnetopause is typically small, this suppression of reconnection can happen when magnetosheath plasma exhibits a high plasma beta.

Although the upstream solar wind conditions strongly control the conditions of plasma in the magnetosheath, and thus the occurrence of magnetopause reconnection, magnetosheath fluctuations are known to also influence magnetopause reconnection. These fluctuations can suppress reconnection during otherwise favorable conditions and trigger reconnection during otherwise unfavorable conditions. For example, mirror-mode waves commonly observed in the quasi-perpendicular magnetosheath have been shown to alter steady reconnection or make reconnection bursty both in observations (Laitinen et al., 2010) and in simulations (Hoilijoki et al., 2017). It has also been proposed that disturbances related to the foreshock region could similarly alter conditions for dayside magnetopause reconnection (Zhang et al., 1997). This has been recently observed in simulations by Chen et al. (2021a). In **Paper V**, we investigate the magnetic field within magnetosheath jets to determine whether jets could similarly influence reconnection by modulating the magnetic shear at the magnetopause. The topic of jets influencing magnetopause reconnection is further discussed in Section 4.3.3.

4 Magnetosheath Jets

In this chapter, we introduce the main topic of this thesis — magnetosheath jets, i.e., transient dynamic pressure enhancements observed within the shocked magnetosheath flow. A review on jets was published by Plaschke et al. (2018). We focus on the topics most closely related to this thesis: jet occurrence during different solar wind and IMF conditions, particle acceleration at bow shocks driven by supermagnetosonic jets, and jets affecting magnetopause reconnection.

4.1 History and definitions

The term *magnetosheath jet* is today relatively well-established for a localized enhancement of dynamic pressure $P_{\mathrm{dyn}} = \rho V^2$ in the magnetosheath. Before arriving here, many types of nomenclature and different quantities have been applied for similar localized transient bulk flows in the magnetosheath. The first observations were reported by Němeček et al. (1998), who observed enhancements of ion flux ρV in Interball-1 and Magion-4 data and called them "transient flux enhancements". Later studies by Savin et al. (2008) and Amata et al. (2011) used a kinetic energy density $\frac{1}{2}\rho V^2$ threshold for "high kinetic energy (density plasma) jets" in Cluster data. Hietala et al. (2012) found "supermagnetosonic jets", enhancements of dynamic pressure and velocity, in Cluster data. After the launch of THEMIS spacecraft (see Section 5.1.1; Angelopoulos, 2008), many studies have looked into dynamic pressure enhancements in the dayside magnetosheath: e.g., "dynamic pressure enhancements/pulses" by Archer et al. (2012) & Archer and Horbury (2013) and "anti-sunward high-speed jets" by Plaschke et al. (2013).

Localized magnetosheath structures that overlap with the enhancements of ion flux or dynamic pressure are enhancements of the constituents: density and velocity. Density enhancements have been studied by Karlsson et al. (2012, 2015), who called them "plasmoids", and by Gutynska et al. (2015). Karlsson et al. (2012, 2015) separated "fast" plasmoids that exhibit an anti-sunward velocity increase and "embedded" plasmoids that travel with the magnetosheath bulk flow. They also characterized these plasmoids from the perspective of their magnetic field: paramagnetic/diamagnetic plasmoids with an increase/a decrease in magnetic field magnitude relative to their surroundings. Velocity enhancements have been studied by Hietala et al. (2009, 2012) and Gunell et al. (2014). Finally, Dmitriev and Suvorova (2015)

investigated THEMIS data for total pressure (dynamic, thermal, and magnetic pressures combined) enhancements, calling these "large scale jets".

At the present time, the term magnetosheath jet is in wide use for dynamic pressure enhancements, but different thresholds are still applied for them. Results obtained with different thresholds should be treated with some care, as they do not necessarily apply to jets obtained with other criteria. Plaschke et al. (2018) investigated the overlap between different criteria and found surprisingly low overlap between the Plaschke et al. (2013) and Archer and Horbury (2013) criteria. In Plaschke et al. (2013) criteria, the focus is on anti-sunward dynamic pressure only and the threshold is set by upstream solar wind dynamic pressure observations. Conversely, Archer and Horbury (2013) definition does not limit the direction of the flow but considers the total dynamic pressure and compares to a local magnetosheath running average. Recently, Koller et al. (2022) formed a jet definition that uses the Plaschke et al. (2013) criteria of anti-sunward jets but the thresholds are with respect to local magnetosheath averages. Ultimately different jet criteria also select for jets formed by different physical mechanisms. Flow enhancements in the magnetosheath arise as part of shock dynamics, but they can also arise from magnetopause reconnection. Local generation mechanisms in the magnetosheath are also possible. As we will find out later, the jets in the focus of this thesis are most likely generated at the Earth's bow shock.

In this thesis, we focus on magnetosheath jets as anti-sunward dynamic pressure enhancements, as this is arguably the quantity that makes them capable of perturbing the pressure balance at the magnetopause. In the subsolar magnetosheath, which is our region of interest, we also loosely refer to these as earthward jets. More precisely, we apply the jet definition introduced by Plaschke et al. (2013) in their statistical study of jets using THEMIS 2008–2011 data from the subsolar magnetosheath. Two example jets are shown in Figure 8 (shaded in magenta), where THEMIS D observations from the subsolar magnetosheath are presented. The primary criterion for a jet is that the anti-sunward dynamic pressure (in the GSE $-X$ direction; see Section 5.2) in the magnetosheath has to be over half of the dynamic pressure in the solar wind:

$$P_{\mathrm{dyn,MSH},X} = \rho_{\mathrm{MSH}} V_{\mathrm{MSH},X}^2 > \frac{1}{2} P_{\mathrm{dyn,SW}} = \frac{1}{2} \rho_{\mathrm{SW}} V_{\mathrm{SW}}^2. \tag{14}$$

The jet interval is then defined as the time period when

$$P_{\mathrm{dyn,MSH},X} > \frac{1}{4} \rho_{\mathrm{SW}} V_{\mathrm{SW}}^2. \tag{15}$$

The mass densities are computed assuming protons only, and the solar wind dynamic pressure is taken as a running average of the preceding five minutes. The moment in time within the jet when the ratio of these magnetosheath and solar wind dynamic pressures reaches its peak is denoted as t_0. An additional criterion requires

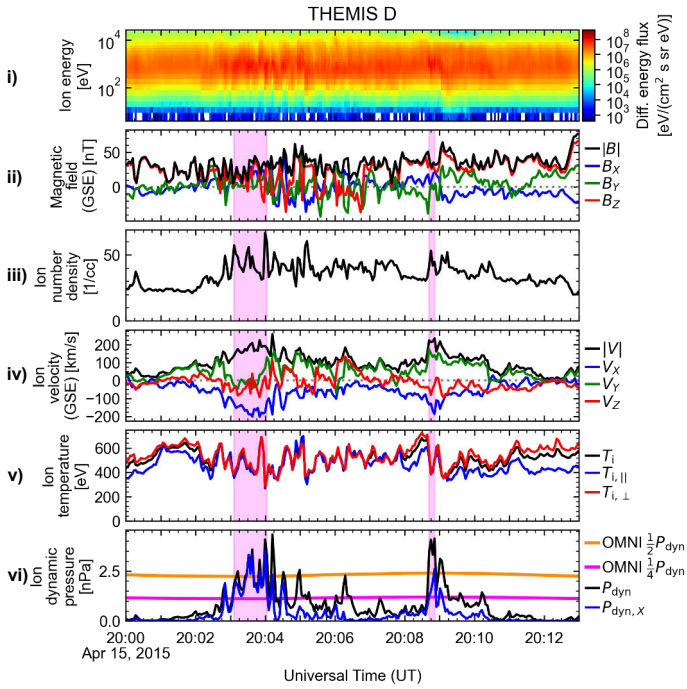

Figure 8. THEMIS D observations from the subsolar magnetosheath on April 15, 2015. Two magnetosheath jets fulfilling the Plaschke et al. (2013) criteria are highlighted in magenta shading.

that within 1-minute intervals preceding and succeeding the jet interval, V_X in the magnetosheath has to go above $V_X(t_0)/2$. This ensures that magnetosheath jets are enhancements in anti-sunward flow velocity, and not simply density fluctuations in the magnetosheath. This criterion also excludes step changes in the magnetosheath flow. As Plaschke et al. (2013) criteria are designed for jets in the subsolar region of the magnetosheath, they are not suitable for jets in the flanks of the magnetosheath. This is because the criterion is based on the upstream solar wind conditions, and at the flanks the anti-sunward velocity of the solar wind is not decelerated as effectively due to the curvature of the bow shock. This means that we are focusing on jets that travel towards the Earth and have the potential to impact the subsolar magnetopause.

The launch of the MMS mission (see Section 5.1.2; Burch et al., 2016) marked another important turning point in the study of magnetosheath jets. In addition to providing valuable statistical data, the high spatial and temporal resolution of this multi-spacecraft mission has enabled the study of the kinetic structure of jets (e.g., Raptis et al., 2022b) and the direct multi-point observation of a jet forming as a result of cyclic reformation of the quasi-parallel shock (Raptis et al., 2022a).

4.2 Occurrence

Early observations of jets were mostly made in the magnetosheath downstream of the quasi-parallel shock (Němeček et al., 1998; Savin et al., 2008; Hietala et al., 2009; Shue et al., 2009; Hietala et al., 2012), both near the bow shock and close to the magnetopause. Archer et al. (2012) utilized multi-spacecraft observations to study jets during an observational interval and reported that dynamic pressure pulses can be formed when when solar wind discontinuities interact with the Earth's bow shock. The first large statistical studies of jets were published by Plaschke et al. (2013) and Archer and Horbury (2013). These studies utilized THEMIS dayside observations and they greatly enhanced the understanding of jets as a phenomenon. In the following, we briefly compare the methodology and results of these two studies.

Archer and Horbury (2013) studied total dynamic pressure enhancements with respect to a 20 min magnetosheath running average. Plaschke et al. (2013) studied anti-sunward dynamic pressure enhancements with respect to an upstream solar wind dynamic pressure threshold. Both studies computed the shock obliquity corresponding to each observation. Plaschke et al. (2013) considered the IMF cone angle as a proxy for the shock obliquity at the subsolar bow shock region, where the curvature of the bow shock can be assumed to be low. Archer and Horbury (2013), on the other hand, used a stream-line model to trace each observation back to a point at the bow shock model, where they calculated the shock obliquity θ_{Bn} using the model bow shock normal at that particular point and the IMF vector. Both studies found that jets are indeed most often observed downstream of the quasi-parallel shock. The shock obliquity θ_{Bn}, and therefore the IMF cone angle, was found to be the only parameter strongly controlling jet occurrence. Contrary to findings by Archer et al. (2012), these statistical studies found that most jets are observed during steady IMF and solar wind conditions, which implies that a steady foreshock region is important for the generation of jets. This is an important conclusion, as it indicates that jets form even when the upstream solar wind is non-varying — that is jets are a feature of the bow shock dynamics itself.

Both studies also used empirical bow shock and magnetopause models (see Section 5.4.1) to assign a relative radial position in the magnetosheath for each measurement. Archer and Horbury (2013) found no apparent preference for where jets occur in the quasi-parallel magnetosheath, but found jets to be more common close to the magnetopause in the quasi-perpendicular magnetosheath. This is in stark contrast to findings by Plaschke et al. (2013), who concluded that jets are most common near the bow shock and their occurrence decreases towards the magnetopause. This points to a simple picture: jets are formed at the bow shock and they propagate towards the magnetopause dissipating along the way. The difference between the results of these two studies is related to the jet criteria, which capture different types of transients. The Plaschke et al. (2013) definition catches jets that form at the bow shock and

travel earthward towards the magnetopause. The Archer and Horbury (2013) criteria also capture other types of dynamic pressure enhancements, such as flux transfer events (FTEs), related to reconnection at the magnetopause. In **Paper I**, we use the data set of Plaschke et al. (2013) to further investigate where in the magnetosheath jets occur during different IMF orientations.

Since then statistical studies have been performed on ever-increasing THEMIS data sets and also on new MMS data sets, providing us more insight into jet occurrence. Raptis et al. (2020) presented a statistical study of dynamic pressure enhancements using MMS data from 2015–2019. They classified jets to quasi-parallel and quasi-perpendicular jets, referring to jets downstream of quasi-parallel and quasi-perpendicular shock regions, respectively. Additionally, jets between the two regimes were classified as boundary jets. A subset of quasi-perpendicular jets, referred to as encapsulated jets, showed a switch from quasi-perpendicular to quasi-parallel and back. The authors argued that these jets originated from the quasi-parallel shock but had travelled to the quasi-perpendicular magnetosheath.

LaMoury et al. (2021) used an extension of the Plaschke et al. (2013) data set to years 2008–2018 and studied the jets observed near the model bow shock and the jets observed near the model magnetopause, separately. They used the former subset to study how the solar wind conditions influence jet formation, and compared these results to those of the latter subset which is influenced not only by formation but also by propagation. They found that IMF cone angle was not the only parameter controlling jet occurrence. Favorable conditions for jet formation at the bow shock are low IMF magnitude, high β, high M_{A}, low P_{dyn}, and low density. This complicated the previous picture in which the IMF cone angle was the only important solar wind parameter controlling jet occurrence. In **Paper II**, we expand on this study by looking separately at the solar wind influence on jet formation in the two different shock regimes: the quasi-parallel and the quasi-perpendicular shock. We find that under low IMF cone angle conditions, that is downstream of the quasi-parallel shock, other parameters are not important for jet occurrence, but the parameters found by LaMoury et al. (2021) influence jet formation in the quasi-perpendicular regime.

Large-scale solar wind structures, such as high-speed streams (HSSs), CMEs, and SIRs, influence the solar wind conditions at Earth. Previously, jet occurrence has only been studied in the solar wind parameter space without considering the relation to different types of solar wind structures. Koller et al. (2022) performed a statistical study on how the number of observed jets varies during these large-scale solar wind structures. According to their results, jet occurrence decreases during CME sheath regions and magnetic ejecta. They speculated that the highly-varying magnetic field in CME sheaths could prevent a stable foreshock from forming, and thus make jet occurrence less likely. This is also consistent with the expectation that draping of the magnetic field in the sheath could potentially manifest as high IMF cone angle conditions, which are unfavorable for jet occurrence. Koller et al.

(2022) also added that strong magnetic field conditions inside magnetic ejecta may be unfavorable for jet generation, which matches the results of LaMoury et al. (2021). On the other hand, they found that jet occurrence rates are increased during HSSs and SIRs. Koller et al. (2023) continued this research and reported that jet occurrence decreases during high IMF cone angle and low Alfvénic Mach number conditions, and thus CME magnetic clouds represent unfavorable conditions for jet formation. On the contrary, high-speed streams were found to be very favorable for jets as they typically exhibit low IMF cone angle, IMF magnitude, and solar wind density. These results are in line with our findings presented in **Paper II**.

Since the prevalence of large-scale solar wind structures and the properties of the inflowing solar wind at the Earth vary throughout the solar cycle, an interesting question concerns the solar cycle variation of jet occurrence. In **Paper III**, we investigate the yearly averages of jet observation during the solar cycle 24. Our results suggest that jet occurrence does not vary strongly across a solar cycle on a yearly level, although there may be a 10–20 % decrease in during solar maxima when specifically CMEs are the most prevalent.

4.3 Lifespan from bow shock to magnetopause

4.3.1 Formation mechanisms

How magnetosheath jets form has been a long-standing question, because it is difficult to directly observe a jet forming in spacecraft observations. The knowledge of their connection to the quasi-parallel shock, and thus the foreshock region, has motivated many suggested jet formation mechanisms. Simulations have provided critical insight for this understanding, as the evolution of jets emerging within simulations can be more easily observed. Some jets can be attributed to solar wind discontinuities (Archer et al., 2012), but importantly, most magnetosheath jets are believed to form as part of the shock dynamics itself even during steady solar wind conditions (Archer and Horbury, 2013). The Earth's bow shock and foreshock are highly complex regions which exhibit non-linear physics that are important for the solar wind–magnetosphere interaction.

Hietala et al. (2009) and Hietala and Plaschke (2013) suggested that jets may form as the solar wind flows through a rippled shock surface, motivated by the observations of the corrugated quasi-parallel shock (Lucek et al., 2008). Using MHD jump conditions, they showed that flow through a concave ripple is less efficiently decelerated than the surrounding flow (see Figure 9). As the local inclination of the shock surface changes, this affects how much the solar wind flow is decelerated, as the shock is most efficient at decelerating flow that is aligned with the shock normal direction. Evidence for this mechanism has been found in simulations: within a 2D global hybrid simulation of the Earth's bow shock by Karimabadi et al. (2014) and a

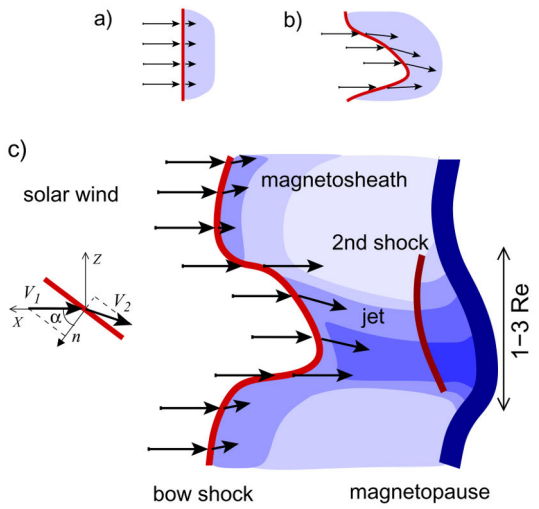

Figure 9. An illustration of the ripple jet generation mechanism. (a) Upstream flow is decelerated as it crosses the shock. (b) Flow through an inclined shock surface, a shock ripple, is less decelerated. (c) An overview showing a fast jet forming as the plasma flows through the rippled bow shock. The jet is also shown to indent the magnetopause, which launches a sunward shock wave in the magnetosheath as the magnetopause oscillates. The figure is from Hietala et al. (2012) and licensed under CC BY.

local 2D hybrid shock simulations by Hao et al. (2016a,b).

In contrast to the ripple mechanism, where jets form due to local variations in shock parameters and the consequent effect on how solar wind is processed at the shock, jets have been proposed to be structures that already form in the foreshock and later transmit into the magnetosheath. Karlsson et al. (2015) suggested that SLAMSs ($\delta B/B > 2$; Schwartz, 1991) may cross the shock and be observed as magnetosheath jets. This scenario was observed in a Vlasiator 2D hybrid-Vlasov simulation by Palmroth et al. (2018). Notably, in a more recent Vlasiator study, Suni et al. (2021) were able to link up to 75 % of jets to foreshock compressive structures (FCS) with a more relaxed $\delta B/B$ requirement than that of SLAMSs. The concurrent density enhancement in FCS contributes to enhanced dynamic pressure, but how these structures maintain a higher speed compared to the surrounding plasma is unclear. SLAMSs are known to be moving sunward in the upstream plasma frame, albeit their propagation speed decreases with increasing amplitude (Schwartz et al., 1992). Karlsson et al. (2015) proposed that SLAMSs crossing a locally inclined part in the corrugated shock surface could allow them to maintain a higher earthward speed.

Recently, Raptis et al. (2022b) reported observations of a jet forming as part of the cyclic reformation of the quasi-parallel shock. In this process, the shock is periodically reforming at a new position upstream of the old shock front, as ULF

waves steepen while approaching the old shock front. Using measurements from a fortuitous MMS string-of-pearls configuration, they observed solar wind plasma trapped between the old and the new shock front evolving into a downstream jet.

While jets are much more prevalent downstream of the quasi-parallel shock, they are also observed downstream of the quasi-perpendicular shock. The nose of the Earth's bow shock is actually more commonly in a quasi-perpendicular configuration, and thus jets downstream of the quasi-perpendicular shock add up to a sizable fraction of all jets observed at Earth. In other even more commonly quasi-perpendicular shock environments, such as planetary bow shocks beyond 1 AU, the proportion of these jets is expected to be larger still. How these jets form is poorly understood. Kajdič et al. (2021) studied such dynamic pressure enhancements and found that these jets were associated with reconnection exhausts, flux tubes connected to the quasi-parallel part of the shock, non-reconnecting current sheets, and mirror-mode waves.

To conclude, it is likely that all the aforementioned formation mechanisms are at play and jets are indeed produced via multiple different processes. The definition for a jet as a simple dynamic pressure enhancement is not very limiting, and thus this definition can include many types of transient structures. Simulations and spacecraft observations from suitable configurations allow us to observe different jet formation mechanisms. To understand which mechanism is the most prevalent, we need observational constraints on the occurrence and properties of jets resulting from each formation mechanism. Statistical studies of jets can then help us answer this question.

4.3.2 Propagation in the magnetosheath

After jets are formed, they travel in the magnetosheath and interact with the surrounding plasma. High-speed jets plough through the slower background plasma, e.g., causing vortical flows and aligning the magnetic field with their flow (Plaschke et al., 2017; Plaschke and Hietala, 2018; Plaschke et al., 2020b). Jets can compress the plasma ahead of it, forming a bow wave in front of the jet (Liu et al., 2019). Some jets can even be supermagnetosonic relative to the surrounding magnetosheath flow (Hietala et al., 2009, 2012; Liu et al., 2019), which leads to the bow wave steepening into a bow shock. In a statistical study by Liu et al. (2020a), 13 % of jets were identified as driving bow waves or shocks.

Observational studies by Liu et al. (2019, 2020a,b) have shown that jet-driven bow waves/shocks can accelerate both ions and electrons. Liu et al. (2020a) reported that for jets with bow waves the average energy flux of electrons with energies above $\sim$ 100 eV up to the instrumental limit of 25 keV was twice the value in the background magnetosheath. Liu et al. (2020b) presented three events, where the energy fluxes of electrons of a few hundred eV up to $\sim$ 10 keV (up to a few hundred keV in

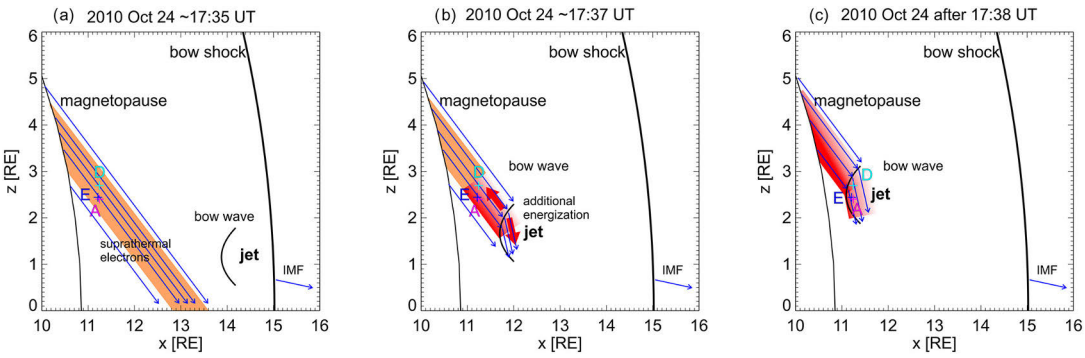

Figure 10. An illustration of an event (on October 24, 2010, around 17:30–17:40 UT) studied by Liu et al. (2020b), where THEMIS A, D, and E spacecraft observed acceleration of suprathermal electrons during the passage of a jet-driven bow wave. The figure is from Liu et al. (2020b), reproduced with the permission of American Geophysical Union.

one of the events) were enhanced ahead of a jet-driven bow wave. Figure 10 shows an illustration of the Event 3 of this study. These results show that magnetosheath jets can contribute to further acceleration of suprathermal particles downstream of the shock. In **Paper IV**, we study electron acceleration at jet-driven bow waves with test-particle Monte Carlo simulations, to gain insight on the possible acceleration mechanism at play. The results of our simplified model suggest that enhanced energy fluxes of suprathermal electrons of the order observed by Liu et al. (2020a,b) may be produced by a collapsing trap that forms between the jet-driven bow wave and the magnetopause (or some other mirror in the magnetosheath), along with shock drift acceleration at the bow wave.

4.3.3 Impacts on magnetosphere and ionosphere

While jets are most prevalent near the bow shock, jets can also be observed close to the magnetopause. This indicates that some jets can propagate all the way from the bow shock to the magnetopause, while others dissipate or disintegrate before reaching the magnetopause. LaMoury et al. (2021) found that solar wind conditions affect the formation of jets at the bow shock and their ability to propagate deep into the magnetosheath differently. According to their results, jets are more likely to propagate far into the magnetosheath when the IMF cone angle is low and the solar wind speed is high.

Plaschke et al. (2016) and later Plaschke et al. (2020a) used the data set of Plaschke et al. (2013) to study the sizes of jets and estimated how often they impact the magnetopause. This empirical model of jet impact rates is described in Section 5.4.2, and we also apply it in **Paper I**. The sizes of observed jets range from a fraction of the Earth's radius to a few Earth radii. Plaschke et al. (2020a) estimated that

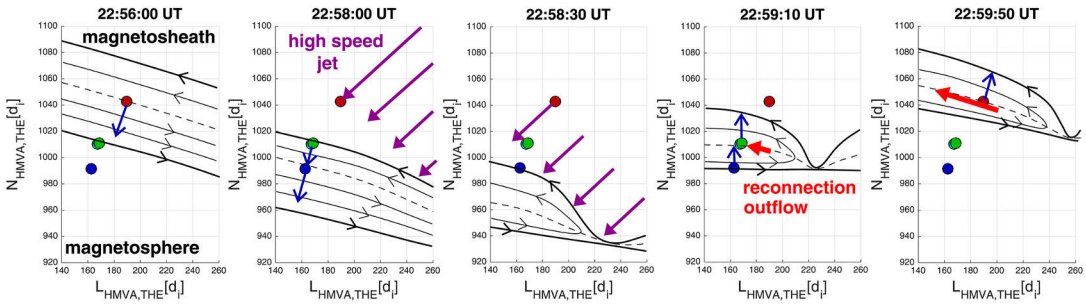

Figure 11. A sketch illustrating the proposed time evolution for the event observed by Hietala et al. (2018), where THEMIS spacecraft (the colored dots) first observed no signatures of reconnection at the magnetopause, but after a magnetosheath jet impact a reconnection outflow was observed. The figure is from Hietala et al. (2018), reproduced with the permission of American Geophysical Union.

jets with diameters $> 2\,R_{\mathrm{E}}$ (transverse to their propagation) impact a reference area of around $100\,R_{\mathrm{E}}^2$ on the subsolar magnetopause (see Section 5.4.2 for the details) on average 2.4 times per hour overall and 7.9 times per hour during low ($< 30°$) IMF cone angle conditions. Small jets are intrinsically harder to detect, but the authors estimated that the median size of jets would be of the order of $0.1\,R_{\mathrm{E}}$ and thousands of such jets could hit the magnetopause in an hour. Therefore, jets are constantly impacting the magnetopause. Larger jets naturally have more substantial individual effects, but the additive effect of continuous bombardment of smaller jets on the magnetopause may also be important.

As jets impinge on the magnetopause with their enhanced dynamic pressure, they can deform the magnetopause on scales comparable to the Earth radius (Hietala et al., 2009; Amata et al., 2011; Hietala et al., 2012; Archer et al., 2012; Escoubet et al., 2020) and launch surface waves along the magnetopause (Archer et al., 2019). These magnetopause indentations can rebound, leading to sunward flows near the magnetopause (Shue et al., 2009; Dmitriev and Suvorova, 2012). These perturbations can also launch ULF waves into the magnetosphere (Archer et al., 2013).

Jets have been proposed to potentially affect the conditions for magnetopause reconnection. Hietala et al. (2018) reported the first direct observations of this. Utilizing multi-spacecraft THEMIS measurements, they first observed no signatures of reconnection at the magnetopause. After observing an incoming magnetosheath jet, a reconnection outflow was observed (see Figure 11 for an illustration). They concluded that while the magnetic shear and β conditions were favorable for reconnection, the magnetopause was unusually thick and most likely inhibited reconnection before the jet compressed the magnetopause allowing reconnection to start. As jets are by definition enhancements of dynamic pressure, they can be expected to locally compress the magnetopause current sheet and influence reconnection in this way. Nykyri et al. (2019) presented a multi-spacecraft event, where they observed mag-

netosheath jets with southward magnetic field during weakly northward IMF. They used timing analysis to propose that these jets triggered magnetopause reconnection, which transported magnetic flux to the magnetotail, acting as the final trigger before an observed substorm onset. The authors suggested that these strong pulses of southward B_Z (in GSM coordinates; see Section 5.2) observed inside these jets provided favorable conditions for magnetopause reconnection. In **Paper V**, we statistically investigate the magnetic field within jets, in particular their north-south component B_Z (GSM), as the first step to understand whether jets can be statistically expected to alter the local conditions for magnetic reconnection, making conditions for reconnection more or less favorable. We find that the magnetic field within jets is more varying than in the surrounding magnetosheath. Most jets contain B_Z opposite to the prevailing IMF B_Z, thus potentially being able to change the local conditions for reconnection at the magnetopause.

Since the publication of our paper, our results have already motivated further research on the topic. In a recently published PhD thesis, LaMoury (2023) considered the additional effect of plasma β in the $\Delta\beta$-shear condition (Equation 12). Studying THEMIS 2008–2018 observations near the magnetopause, they found that the plasma β is typically enhanced in jets. For low IMF cone angles ($< 30^\circ$), the favorability for reconnection was similar between jet and non-jet observations, both during northward and southward IMF B_Z. However, for increasing cone angles jet plasma was found to be consistently less favorable for reconnection, indicating that the most likely effect of jets is to suppress reconnection. Similar to our methodology, LaMoury (2023) looked at the extreme values in jet intervals. Half of the jets during low IMF cone angle and northward IMF were estimated to contain some plasma favorable for triggering reconnection, while 70–80 % of jets during southward IMF were estimated to contain plasma favorable for suppressing reconnection during all cone angle conditions. Overall, the results of LaMoury (2023) indicate that, while jets can contain plasma both favorable and unfavorable for reconnection, suppression is expected to be the more dominant effect due to the enhanced β.

LaMoury (2023) also presented a case study of THEMIS A, D, and E observing magnetosheath jets during an interval when numerous magnetopause crossings were recorded. During this interval, the magnetopause exhibited local indentations and oscillatory motion, most likely related to the incident magnetosheath jets. The authors inferred ongoing reconnection from signatures of reconnection exhausts and found that reconnection was intermittent throughout the interval. Comparing the state of reconnection before and after jet observations, the authors found indications of different jets triggering, suppressing, and not changing reconnection all within the same 25-minute interval.

Jets have also been observed to influence magnetopause reconnection in simulations. In hybrid 2D simulations of Karimabadi et al. (2014), a flux transfer event (FTE) was formed as a consequence of a jet impacting the magnetopause during

quasi-radial IMF. Recent 3D simulations by Ng et al. (2021) showed jet impacts causing localized bursty magnetopause reconnection during quasi-radial southward IMF. They attributed these effects mainly to the intensification of the current sheet when compressed by an impacting magnetosheath jet. The authors also noted that structures of negative B_Z, most likely related to foreshock waves and turbulence, can contribute to bursty reconnection. This has also been observed in 3D hybrid simulations of Chen et al. (2021a) for quasi-radial northward IMF.

Jets can have effects inside the magnetosphere, in the ionosphere, and even observable signatures in ground magnetometers. Hietala et al. (2012) reported observations of transient convection flow channels in the high-latitude ionosphere around the time of jet observations in the magnetosheath and suggested that jets caused enhanced precipitation into the ionosphere. A possible, but still not confirmed, connection has been inferred between magnetosheath jets and throat aurora, which occur preferentially during low IMF cone angles (Han et al., 2016, 2017, 2018). However, jets have been observed to cause brightenings of both discrete and diffuse auroral forms on the dayside auroral oval (Wang et al., 2018), indicating enhanced particle precipitation to the ionosphere. Ground magnetic disturbances associated with jets impacts have also been identified by multiple authors (Dmitriev and Suvorova, 2012; Norenius et al., 2021; Wang et al., 2022; Dmitriev and Suvorova, 2023). While strong ground magnetic disturbances may lead to space weather effects also on ground, Norenius et al. (2021) estimated that harmful effects from jets are not likely.

5 Data and Methods

In this chapter, we present the data and methodology of this thesis. We introduce the spacecraft missions and data sets along with the multiple empirical models employed in this thesis. Finally, we introduce the test-particle Monte Carlo model developed for studying electron acceleration at a jet-driven shock in the magnetosheath.

5.1 Spacecraft observations

In this thesis, we rely on in-situ spacecraft observations from the Earth's magnetosheath. We mainly use data from Time History of Events and Macroscale Interactions during Substorms (THEMIS) mission (Angelopoulos, 2008), but data from the Magnetospheric Multiscale (MMS) mission (Burch et al., 2016) is also used. For context on the solar wind conditions at any particular time, we also use data from the OMNI data set, which combines in-situ data from multiple spacecraft at Lagrange point 1 (L1) (King and Papitashvili, 2005).

5.1.1 THEMIS

THEMIS is a mission operated by the National Aeronautics and Space Administration (NASA). It was launched into a highly elliptical geocentric orbit on February 17, 2007 as a constellation of five identical satellites (see a model the spacecraft in Figure 12) named THEMIS A, B, C, D, and E. Its primary scientific goal was to determine what triggers substorms in the Earth's magnetotail and how these substorms evolve in time. In 2010, THEMIS B and C were repurposed into the Acceleration, Reconnection, Turbulence and Electrodynamics of the Moon's Interaction with the Sun (ARTEMIS) mission and inserted to lunar orbits. THEMIS near-equatorial orbits are fixed to the stars, drifting around the Earth throughout the year. For part of the year, THEMIS apogees are on the dayside, enabling research on the foreshock, bow shock, magnetosheath, and the magnetopause. One of the mission's scientific goals was to investigate dayside processes as part of solar wind–magnetosphere coupling. As THEMIS spacecraft have been gathering measurements of the subsolar magnetosheath since 2008, their observations have been an integral part of the study of magnetosheath jets. In this thesis, we utilize these large statistical THEMIS data sets.

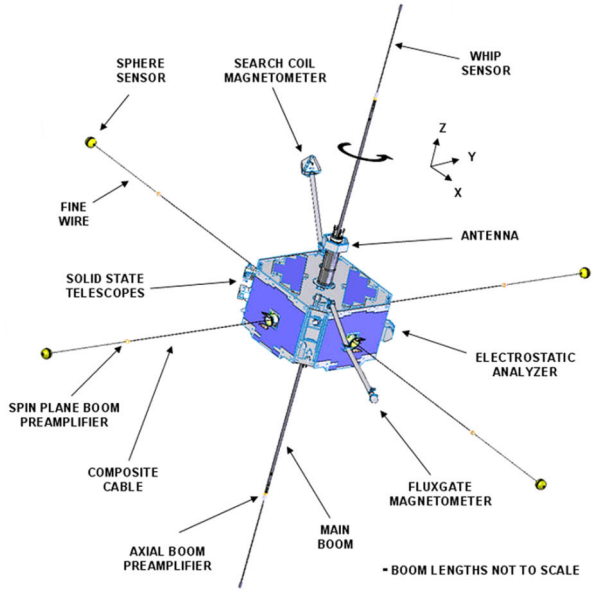

Figure 12. A model of the THEMIS satellites. Figure is adapted from Bonnell et al. (2008), reproduced with permission from SNCSC.

THEMIS probes are equipped with extensive scientific instrumentation to measure charged particles and magnetic and electric fields. We use THEMIS data in **Papers I–V**, and the studies require moments and velocity distribution functions (VDFs) of the thermal ion population, magnetic field observations, and suprathermal electron measurements. These observations are obtained from the following instruments on-board the THEMIS spacecraft, respectively: the Electrostatic Analyzer (ESA; McFadden et al., 2008), the FluxGate Magnetometer (FGM; Auster et al., 2008), and the Solid State Telescope (SST; Angelopoulos, 2008).

5.1.2 MMS

MMS mission is operated by NASA, and it has been on a highly elliptical orbit around the Earth since its launch on March 13, 2015. This mission consists of four identical satellites whose distance from each other can be as low as tens of kilometers. Together with high temporal resolution measurements, MMS allows for observations of phenomena on unprecedentedly small scales and for disambiguating spatial and temporal variations. The main scientific goal of the MMS mission is to study microphysics of magnetic reconnection, and thus, along with the magnetotail, a major region of interest is the dayside magnetopause. MMS observations have also been utilized for studying the kinetic physics of the Earth's bow shock and they have spent substantial amounts of time in the dayside magnetosheath, making MMS an

important mission for magnetosheath jet studies. We have utilized MMS observations of jets to support the analysis of **Paper II** and to analyze the event studied by Nykyri et al. (2019) in **Paper V**. We have utilized plasma moment data from the Fast Plasma Investigation instrument (FPI; Pollock et al., 2016) and magnetic field data from the FIELDS fluxgate magnetometer (Torbert et al., 2016).

5.1.3 OMNI data set

We link observations in the magnetosheath to upstream solar wind conditions by using the high-resolution (1-min cadence) OMNI data set (King and Papitashvili, 2005). OMNI data is a combination of measurements from multiple spacecraft located at L1, 1.5 million kilometers from Earth, but most importantly from the Advanced Composition Explorer (ACE; Smith et al., 1998; McComas et al., 1998) and Wind (Lepping et al., 1995; Ogilvie et al., 1995) spacecraft. At this location, we can measure the solar wind that is coming towards the Earth approximately an hour in advance. OMNI data is propagated to the nose of the Earth's bow shock to account for the estimated time lag between the L1 point and the Earth.

OMNI observations do not always accurately represent the local conditions upstream of the Earth's bow shock, and in fact fail relatively often (e.g., Walsh et al., 2014; Vokhmyanin et al., 2019). This is because the propagation inherently contains uncertainty and the solar wind may develop along the way to the Earth. Additionally, the observing spacecraft and the Earth may not be in the same flux tube and the solar wind can exhibit significant variations on scales comparable to the transverse size of the Earth's magnetosphere. When studying individual events, it is especially important to consider the possibility for large uncertainties in the solar wind conditions as estimated by the OMNI data set. In such studies, local upstream measurements from a nearby spacecraft are preferred.

The significant advantage of the OMNI data set is its almost continuous coverage, which enables statistical studies of how solar wind conditions affect phenomena at the Earth. During the years when the research of this thesis has been conducted, large statistical data sets combining magnetosheath observations with local upstream measurements have not been available, and OMNI data has been the only option available for large statistical studies. When using large data sets, random errors can be expected to average out, but any systematic errors will remain. As the list of suitable conjunctions, where there is a spacecraft observing jets in the magnetosheath and also a spacecraft present in the local upstream region, is growing, data sets utilizing local upstream conditions have started to appear at the time of writing this thesis. Statistical studies of jets should also be performed using these data, and these results should be compared to previous results obtained using OMNI data. While the uncertainty in propagation vanishes, it must be noted that magnetospheric missions are not designed for the accurate measurement of the narrow solar wind beam and

thus the quality of plasma measurements can be poor depending on the instrument modes. While many spacecraft instruments have a solar wind mode, this is often not used in the presence of the foreshock region as wide angular coverage is prioritized. This is especially true for the temperature measurement, while ion number density measurement can be often cross-checked with electron measurement and the estimate derived from the spacecraft potential.

5.1.4 Subsolar magnetosheath data set

Most of the work presented in this thesis utilizes a large statistical data set consisting of THEMIS spacecraft measurements from the subsolar magnetosheath and the jet observations adhering to the jet definition by Plaschke et al. (2013). This was first published by Plaschke et al. (2013) for the purpose of studying anti-sunward high speed jets, and this first version of the data set contained data from the years 2008–2011. Since then, it has been extended, with LaMoury et al. (2021) using observations from years 2008–2018 and Koller et al. (2022) from years 2008–2020. In **Paper I** and **Paper V**, we utilize data from 2008–2011. In **Paper II** and **Paper III**, we use the latest version consisting of measurements in 2008–2020, notably for the first time spanning over an entire solar cycle (Solar Cycle 24, Dec 2008–Dec 2019; Solar Influences Data Analysis Center, 2023). The growing size of this data set has ensured a wide coverage of different solar wind conditions and enabled increasingly detailed statistical studies of jets.

In the following, we summarize how these data sets have been assembled, as originally defined by Plaschke et al. (2013). THEMIS spacecraft were in the region of interest near the subsolar magnetosheath when they were located within a 30°-wide Sun-centered cone with its tip at Earth and within a 7–18 R_E geocentric distance. The corresponding solar wind conditions for each measurement were obtained from the OMNI data set as a running average of the preceding five minutes. To ensure that the spacecraft were not in the upstream solar wind, the density observed by THEMIS ESA instrument was required to be twice of that in the solar wind. Additionally, the energy flux of 1 keV ions was required to exceed that of 10 keV ions to exclude observations from inside the magnetosphere. Data from different instruments (here ESA and FGM) were interpolated to common timestamps with a 1-s cadence. Due to their best availability, ESA on-board moment data and FGM spin-resolution data, both with nominal cadence of 3 s, were used when assembling the data set. When taking magnetosheath intervals longer than two minutes and applying the Plaschke et al. (2013) jet criteria introduced in Section 4.1 (Equations 14–15), these criteria yielded around 2,700 (11,000) hours of subsolar magnetosheath data along with 2,859 (16,494) observed jets during years 2008–2011 (2008–2020; Koller et al., 2022).

5.2 Magnetospheric coordinate systems

Perhaps the most commonly used magnetospheric coordinate system is the *Geocentric Solar Ecliptic* (GSE) coordinate system (e.g., Russell, 1971). The X_{GSE}-axis points sunward along the Sun-Earth line and the Y_{GSE}-axis points duskward in the ecliptic plane opposite to the direction of Earth's orbital motion. The Z_{GSE}-axis completes the right-handed coordinate system, pointing towards the ecliptic north pole.

When studying dayside magnetopause reconnection, *Geocentric Solar Magnetospheric* (GSM) coordinate system (e.g., Russell, 1971) is typically used, which is defined with respect to the Earth's dipole magnetic field axis. The orientation of this axis with respect to the ecliptic plane varies due to the orbital motion of the Earth around the Sun and due to the Earth's rotation around its own orbital axis (which is tilted with respect to the magnetic dipole axis). The X_{GSM}-axis is defined identically to the X_{GSE}-axis. The Y_{GSM}-axis is defined to be perpendicular to both the X_{GSE}-axis and the Earth's magnetic dipole axis in this right-handed coordinate system. Now the X_{GSM}–Z_{GSM} plane contains the Earth's magnetic dipole axis, and the direction of Z_{GSM} is chosen such that the positive direction corresponds to the north magnetic pole. Thus, at the subsolar magnetopause, the Earth's magnetic field points northward ($B_{Z,\mathrm{GSM}} > 0$). Therefore, southward magnetic field ($B_{Z,\mathrm{GSM}} < 0$) in the solar wind and/or in the magnetosheath is of interest when studying magnetopause reconnection.

As described in Section 3.2.1, the orientation of the interplanetary magnetic field controls the location of the foreshock and the quasi-parallel and quasi-perpendicular shock regions. We use the *Geocentric InterPlanetary Medium* (GIPM) coordinate system (Bieber and Stone, 1979), which is defined by the IMF and thus allows us to compare spacecraft locations with respect to the expected foreshock location in a relatively simple manner. This coordinate system has been previously utilized in magnetosheath studies (e.g., Verigin et al., 2006; Dimmock and Nykyri, 2013). The unit vectors of the GIPM coordinate system can be determined in GSE coordinates as follows (Verigin et al., 2006):

$$\hat{\mathbf{X}}_{\mathrm{GIPM}} = \frac{(-V_X, -V_Y - 30\ \mathrm{km/s}, -V_Z)}{\sqrt{V_X^2 + (V_Y + 30\ \mathrm{km/s})^2 + V_Z^2}} \tag{16}$$

$$\hat{\mathbf{Y}}_{\mathrm{GIPM}} = \begin{cases} \dfrac{(-\mathbf{B} + (\mathbf{B}\cdot\hat{\mathbf{X}}_{\mathrm{GIPM}})\hat{\mathbf{X}}_{\mathrm{GIPM}})}{|\mathbf{B} - (\mathbf{B}\cdot\hat{\mathbf{X}}_{\mathrm{GIPM}})\hat{\mathbf{X}}_{\mathrm{GIPM}}|}, & \text{if } \mathbf{B}\cdot\hat{\mathbf{X}}_{\mathrm{GIPM}} > 0 \\ \dfrac{(\mathbf{B} - (\mathbf{B}\cdot\hat{\mathbf{X}}_{\mathrm{GIPM}})\hat{\mathbf{X}}_{\mathrm{GIPM}})}{|\mathbf{B} - (\mathbf{B}\cdot\hat{\mathbf{X}}_{\mathrm{GIPM}})\hat{\mathbf{X}}_{\mathrm{GIPM}}|}, & \text{if } \mathbf{B}\cdot\hat{\mathbf{X}}_{\mathrm{GIPM}} < 0 \end{cases} \tag{17}$$

$$\hat{\mathbf{Z}}_{\mathrm{GIPM}} = \hat{\mathbf{X}}_{\mathrm{GIPM}} \times \hat{\mathbf{Y}}_{\mathrm{GIPM}}. \tag{18}$$

Here $\mathbf{V} = (V_X, V_Y, V_Z)$ is the solar wind velocity and $\mathbf{B} = (B_X, B_Y, B_Z)$ is the

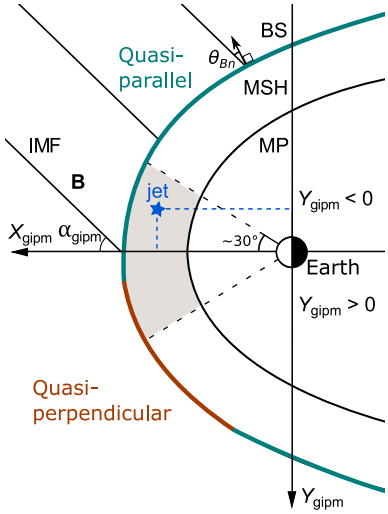

Figure 13. A cartoon of the GIPM X–Y plane, which contains the X_{GIPM}-axis (anti-parallel to the aberrated solar wind velocity) and the IMF vector. The IMF cone angle α_{GIPM} always opens towards the $-Y_{\mathrm{GIPM}}$ direction. The gray-shaded area estimates the subsolar magnetosheath region from where the spacecraft observations are taken. The figure is adapted from Vuorinen et al. (2019) and licensed under CC BY.

IMF vector, both in GSE. The X_{GIPM}-axis is anti-parallel to the solar wind velocity, but with a correction for orbital aberration. The Y_{GIPM}-axis is defined such that the IMF is in the X_{GIPM}–Y_{GIPM} plane, or in other words, X_{GIPM}–Y_{GIPM} is the plane spanned by the aberrated solar wind velocity vector and the IMF vector.

The X_{GIPM}–Y_{GIPM} plane is illustrated in Figure 13. As the IMF cone angle increases, the foreshock (and the quasi-parallel shock region) moves towards the $-Y_{\mathrm{GIPM}}$ direction. Therefore, by investigating jet occurrence as a function of Y_{GIPM} for different IMF obliquities, we can map the spatial occurrence of jets downstream of the quasi-parallel and quasi-perpendicular shock regions. Instead of defining the cone angle with respect to the Sun-Earth line, we define the GIPM IMF cone angle with respect to the X_{GIPM}-axis:

$$\alpha_{\mathrm{GIPM}} = \arccos\left(\frac{|\mathbf{B}\cdot\hat{\mathbf{X}}_{\mathrm{GIPM}}|}{B}\right) \in [0^\circ, 90^\circ]. \tag{19}$$

These angles are almost identical, because the solar wind velocity is typically closely aligned with the Sun-Earth line, and the orbital aberration effect is $\sim 5^\circ$.

5.3 Conditional probabilities

Bayes' theorem describes conditional probabilities and is written as

$$P(A|B) = \frac{P(B|A)P(A)}{P(B)}, \tag{20}$$

where $P(A)$ and $P(B)$ are probabilities of observing events A and B, respectively, and $P(A|B)$ and $P(B|A)$ are conditional probabilities of observing event A given that B is true and observing event B given that A is true, respectively. In this thesis, we study how different solar wind conditions and/or the location of the spacecraft (here we call them simply "conditions") affect the number of observed jets. As an example, the apogee of THEMIS orbits are such that there are significantly more observations close to the magnetopause than to the bow shock. This causes jets close to the magnetopause to be over-represented in our data set compared to jets close to the bow shock. We use conditional probabilities to take such biases into account. In our case Bayes' rule is written

$$P(\text{jet}|\text{conditions}) = \frac{P(\text{conditions}|\text{jet})P(\text{jet})}{P(\text{conditions})}. \tag{21}$$

The probabilities on the right-hand side can be estimated by using the numbers of observations: $P(\text{jet}) = N(\text{jet})/N$, $P(\text{conditions}) = N(\text{conditions})/N$, and $P(\text{conditions}|\text{jet}) = N(\text{conditions} \wedge \text{jet})/N(\text{jet})$. Thus, the conditional probability (or *normalized* probability as referred to in this thesis) becomes simply

$$P(\text{jet}|\text{conditions}) = \frac{N(\text{conditions} \wedge \text{jet})}{N(\text{conditions})}. \tag{22}$$

As the data cadence is 1 s in the statistical magnetosheath jet data set we use, we can convert the number of observations into observation time and write a jet occurrence (observation) rate

$$\begin{aligned} R(\text{jet}|\text{conditions}) &= \frac{N(\text{conditions} \wedge \text{jet})}{N(\text{conditions})} \frac{N(\text{conditions})}{1\,\text{s}} \\ &= \frac{N(\text{conditions} \wedge \text{jet})}{\text{s}} \\ &= 60 \times 60 \times \frac{N(\text{conditions} \wedge \text{jet})}{\text{h}}. \end{aligned}$$

5.4 Empirical models

In this thesis, we utilize multiple empirical (statistical) models, which have been built based on large numbers of spacecraft observations. We use these models to estimate where the bow shock and the magnetopause are located, how often jets hit the magnetopause, and how jet occurrence rates vary throughout the solar cycle.

5.4.1 Bow shock and magnetopause models

We apply empirical models of the bow shock and the magnetopause to estimate the relative position of the spacecraft in the magnetosheath. Inferring the relative location of the spacecraft in the magnetosheath is important for understanding different jet formation mechanisms, jet propagation, and their likelihood to impact the magnetopause. These models are needed because these boundaries are not fixed in space, but their position and form changes in response to upstream solar wind variations. Most significantly, the bow shock and the magnetopause move closer and further from the Earth in response to upstream dynamic pressure variations. The models are semi-empirical, meaning that they assume a functional form and then the fit parameters are estimated from actual measurements of spacecraft crossing the bow shock and the magnetopause. We use the bow shock model by Merka et al. (2005), which takes as input parameters the solar wind dynamic pressure and the Alfvén Mach number M_{A}. For the magnetopause, we use the model by Shue et al. (1998), which is dependent on the solar wind dynamic pressure and the IMF Z_{GSM}-component B_Z. The relative radial position F of the spacecraft between the model bow shock (at $F = 1$) and the model magnetopause (at $F = 0$) can be calculated as

$$F = \frac{r - r_{\mathrm{MP}}}{r_{\mathrm{BS}} - r_{\mathrm{MP}}}. \tag{23}$$

Here r is the geocentric distance of the spacecraft. r_{BS} and r_{MP} are the geocentric distances of the model bow shock and the model magnetopause measured along that same radial line.

Although the empirical bow shock and magnetopause models statistically represent the observations, they can be highly uncertain for individual events, as the bow shock-magnetosphere system has a finite response time to variations in the solar wind. At this moment, we do not have continuous data of the bow shock and magnetopause locations, and single spacecraft crossings, of especially the magnetopause, can be relatively far from the nominal position due to local corrugations. The first step toward improving these estimates would be to improve the quality of inputs (the estimated upstream conditions propagated from L1 measurements) to these models. However, perhaps local magnetosheath properties could also be used to infer position in the magnetosheath. Such an idea was recently pursued by Sibeck et al. (2022), who showed that it is possible to infer the locations of the boundaries from the observed velocity gradient between two spacecraft in the magnetosheath.

5.4.2 Magnetopause impact rates of jets

As discussed in Section 4.3.3, jets can cause effects inside the magnetosphere when they impact the magnetopause. Thus, the first step towards assessing their geoeffectiveness is to estimate how often jets hit the magnetopause. Plaschke et al. (2016)

developed an empirical model for this purpose using the subsolar magnetosheath data set by Plaschke et al. (2013) (see the original paper for a full description), but only considering measurements of THEMIS A, D, and E which had orbits close to the magnetopause. They used the jet observation rate Q_{obs} near the magnetopause to estimate the number of jets that will go on to hit the magnetopause per unit time. However, the jets observed by the spacecraft are only a small fraction of all jets, because spacecraft observations are limited to essentially singular points in space. Thus, an estimation of the magnetopause impact rates of jets requires a correction for the jets that were not observed. The probability to observe a jet increases for jets of larger size. Therefore, knowledge of the size distribution of jets is needed to perform this correction.

Plaschke et al. (2016) found 662 jet observations where two spacecraft were approximately in the same plane transverse to the propagation direction of the jet. Based on these events, they estimated the probability for two spacecraft at a given separation to both observe the same jet. Assuming circular cross-sections of jets, an exponential distribution $P_\perp$ of perpendicular jet diameters $D_\perp$ was found to provide a good fit with the observations:

$$P_\perp = \exp\left(-D_\perp / D_{\perp 0}\right) / D_{\perp 0}, \tag{24}$$

with $D_{\perp 0} = 1.34\,R_{\text{E}}$. The observation rate of jets larger than a given minimum size $D_{\perp\text{min}}$ could then be estimated as

$$\int_{D_{\perp\text{min}}}^{\infty} Q_{\text{obs}} P_\perp(D_\perp)\,\mathrm{d}D_\perp. \tag{25}$$

Here Q_{obs} is the number of jets observed per unit time by a single spacecraft. This parameter is a constant in the integral, as it does not depend on $D_\perp$, but its value can be varied when considering different solar wind conditions. Finally, adding a correction factor for the jets not observed, Plaschke et al. (2016) obtained the following formula for the estimated magnetopause impact rate of these jets on a reference magnetopause area A_{ref}:

$$Q_{\text{imp}} = \int_{D_{\perp\text{min}}}^{\infty} \frac{A_{\text{ref}}}{A_{\text{jet}}(D_\perp)} Q_{\text{obs}} P_\perp(D_\perp)\,\mathrm{d}D_\perp \tag{26}$$

$$= 4\,A_{\text{ref}} \cos\phi\, Q_{\text{obs}} \int_{D_{\perp\text{min}}}^{\infty} \frac{P_\perp(D_\perp)}{D_\perp^2}\,\mathrm{d}D_\perp \tag{27}$$

$$= \frac{4\,A_{\text{ref}} \cos\phi\, Q_{\text{obs}}}{\pi D_{\perp 0}} \int_{D_{\perp\text{min}}}^{\infty} e^{-D_\perp / D_{\perp 0}} \frac{\mathrm{d}D_\perp}{D_\perp^2}. \tag{28}$$

$A_{\text{jet}} = \pi(D_\perp/2)^2/\cos\phi$ is the projection of the jet's cross-sectional area onto the reference area that is on a plane perpendicular to the Sun-Earth line (see Figure 14). ϕ is the mean of the angle between the jet propagation direction and the Sun-Earth

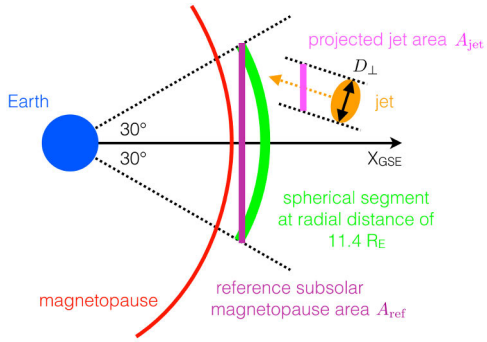

Figure 14. A cartoon illustrating the reference magnetopause area $A_{\rm ref}$ and projected jet area $A_{\rm jet}$. The figure is from Plaschke et al. (2016) and licensed under CC BY.

line. The reference area used by Plaschke et al. (2016) (and also in this thesis) was a $A_{\rm ref} = 102\,R_{\rm E}^2$ circular area defined by a 30° Earth-tipped and Sun-facing cone and the average radial distance $11.4\,R_{\rm E}$ of the observations from the center of Earth.

We note that Plaschke et al. (2020a) have since updated this model. They found that after multiplying $P_\perp$ by the correction factor $1/D_\perp^2$ (see Equation 27) it could not be normalized. According to their new results based on an updated log-normal size distribution, the previous form used by Plaschke et al. (2016) led to an overestimation of smallest-scale jets. However, the results of Plaschke et al. (2016) and the results presented in **Paper I** for large-scale (and the most likely geoeffective) jets remain largely unchanged.

5.4.3 Reconstruction of yearly jet occurrence rates over a solar cycle

In **Paper III**, we use THEMIS data over years 2008–2020 spanning across the solar cycle 24 (from December 2008 to December 2019) in concordance with the OMNI solar wind data set to study how the occurrence of jets varies across the solar cycle. As shown in the paper, a comparison of the yearly occurrence rates of jets is susceptible to biases related to variations in the apogees of THEMIS spacecraft during these years. These biases render the observed yearly jet occurrence rates non-comparable from year to year. However, this extensive data set (Koller et al., 2022) of over 16,000 jets together with the OMNI solar wind data set contains a lot of statistical information on jet occurrence rates under different solar wind conditions. We use this data to create an empirical statistical model of jet occurrence as a function of solar wind conditions and apply this model to all OMNI observations of the solar cycle 24, and also of the previous solar cycle 23.

Figure 15a shows an illustration of our model, which is essentially a “data cube” or a “look-up table”, where we divide the solar wind parameter space into bins and

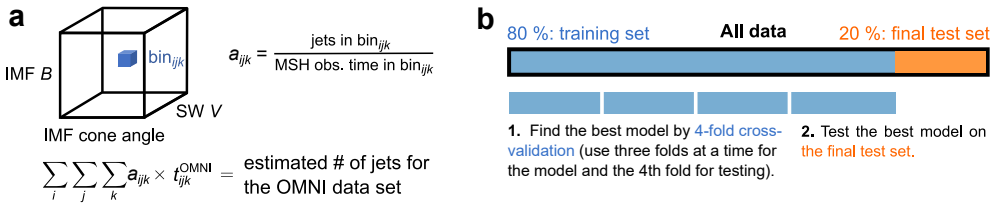

Figure 15. A cartoon describing (a) the model, in which we use THEMIS and OMNI data to estimate jet occurrence rates in the solar wind parameter space bins. New OMNI solar wind data can be then input to the model, obtaining an estimate for number of jets in the new data; (b) using K-fold cross-validation (with $K = 4$) on a training set (80 % of the data) to find the best model using, and obtaining the error estimates of the model by testing it on the final test set (20 % of the data). The figure is from Vuorinen et al. (2023b) and licensed under CC BY.

calculate the number of jets per unit time in each of the bins. When we have a new interval of solar wind data, we can then estimate/predict the number of jets for that data by first counting how much time was spent in each of the bins and then multiplying these times by the jet occurrence rates of the model, obtaining a number of jets. A model (jet occurrence rates in the solar wind parameter space) is defined by the solar wind parameters used and the number of bins in the parameter space. Figure 15b illustrates the process of developing the model with our data set: we first train the model with 80 % of the data and in the end test the model with the remaining 20 % of the data. During training, we systematically change the model (the parameters included and the numbers of bins) and use K-fold cross-validation (with $K = 4$) (Hastie et al., 2009) to determine which model performs the best. During final testing, applying the model to unseen data allows us to estimate the error of the model. The performance of the models is quantified with two error measures, one comparing the yearly jet occurrence rates to the observed rates and the other measuring the stability of the jet occurrence rates in each bin of the solar wind parameter space. After training the model and testing its performance on unseen data, we apply it to new OMNI data spanning the entire solar cycles 23 and 24 to obtain estimations of the unbiased jet occurrence rates.

5.5 Test-particle simulation model of electron shock acceleration

In **Paper IV**, we study electron acceleration at bow waves driven by supermagnetosonic jets in the magnetosheath. We model this with test-particle Monte Carlo simulations (e.g., Jones and Ellison, 1991) of electrons on a single magnetic field line with the jet-driven bow wave modelled as an MHD shock wave. A schematic of the simulation setup is shown in Figure 16, and the full description of the model can be found in the paper (Vuorinen et al., 2022). Electrons with energies 0.1 keV–1 MeV are introduced uniformly on the field line at the beginning of the simulation, follow-

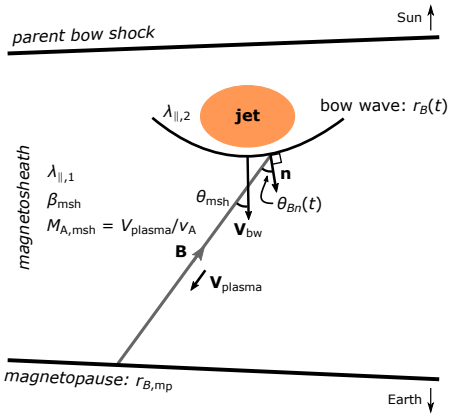

Figure 16. The simulation setup and the key parameters, shown in the frame fixed with the magnetopause. The model follows electrons on a single field line between two magnetic mirrors: a moving bow wave (MHD shock) driven by a jet and the stationary magnetopause. The model includes pitch-angle scattering upstream and downstream of the bow wave, controlled by the parallel mean free paths $\lambda_{||,1}$ and $\lambda_{||,2}$. The field line sweeps across the bow wave as the bow wave propagates and the local shock parameters change as a function of time. The figure is adapted from Vuorinen et al. (2022) and licensed under CC BY.

ing a background energy distribution motivated by magnetosheath observations of Liu et al. (2020b). We follow the electrons under the guiding center approximation and also include isotropic pitch-angle scattering of off magnetic fluctuations frozen-in into the background plasma flow. The shock acts as a moving magnetic mirror, and this interaction between the particles and the shock is treated by moving to the de Hoffmann–Teller frame (HT-frame) of the shock, where the convectional electric field vanishes (as discussed in Section 2.2.3). We apply Lorentz transformations to move between the frames of reference. In the HT-frame, the particle is simply magnetically mirrored or transmitted to downstream depending on its pitch-angle (assuming conservation of the first adiabatic invariant). We ignore the cross-shock potential in our simulation, which would only slightly decrease the probability of reflection for electrons. We also include another, standing, magnetic mirror which can be considered as the magnetopause or a strong magnetic structure in the magnetosheath. In the simulation, the electrons are accelerated at the shock by the convective electric field in line with the shock drift acceleration process. The two mirrors form a collapsing trap, which substantially amplifies the acceleration by allowing electrons to interact with the shock numerous times.

This simplified setup is a natural first step for probing the acceleration of electrons at jet-driven bow waves. In the future, more sophisticated simulations are needed to study this process in more detail. For example, hybrid-PIC simulations with suprathermal test-particles would offer a more realistic setup and shock structure.

6 Summary of the Results

In this chapter, we summarize the results of this thesis published in **Papers I–V**.

6.1 Solar wind and IMF control of jet occurrence

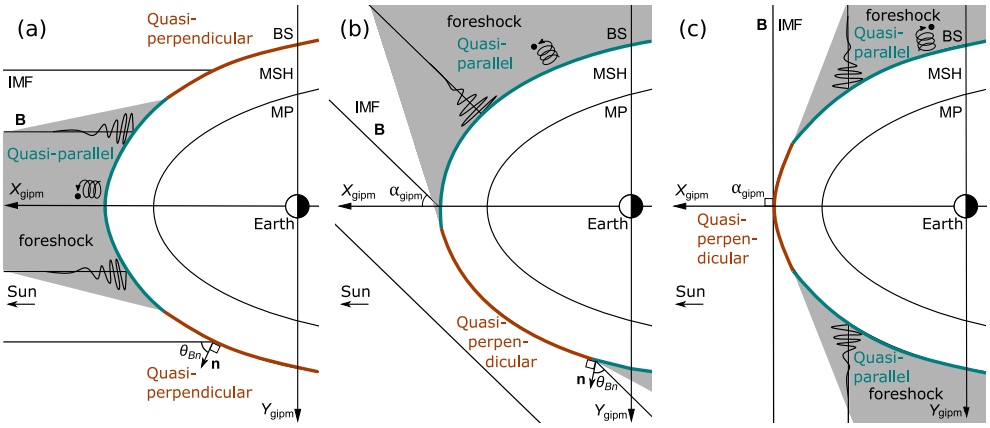

Figure 17. A cartoon showing the approximate locations of the foreshock region (gray area) and the quasi-parallel (turquoise) and the quasi-perpendicular (brown) shock regions in the X–Y GIPM plane for varying IMF cone angles: (a) $\alpha_{\mathrm{GIPM}} = 0°$, (b) $\alpha_{\mathrm{GIPM}} = 45°$, and (c) $\alpha_{\mathrm{GIPM}} = 90°$. The figure is adapted from Vuorinen et al. (2019) and licensed under CC BY.

In **Paper I**, we performed a statistical study on how the IMF orientation affects where and how often magnetosheath jets are observed. We utilized THEMIS observations from the subsolar magnetosheath from years 2008–2011 (the data set used by Plaschke et al., 2013). The corresponding solar wind conditions were obtained from the OMNI data set as running averages of the preceding five minutes. We moved to the GIPM coordinate system (see Section 5.2) where the X-axis is anti-parallel to the (aberrated) solar wind velocity vector and the IMF vector lies in the X–Y plane. In this coordinate system, the quasi-parallel region moves towards the $-Y$ side as the IMF obliquity increases (see Figure 17). We divided the data into three subsets based on IMF cone angles: quasi-radial IMF ($[0°, 30°)$), oblique IMF ($[30°, 60°)$), and high cone angle IMF ($[60°, 90°]$). We presented the spatial distribution of jet occurrence in this X–Y plane and found, similar to previous studies, that jets are more frequent near the bow shock and their occurrence is the highest downstream of

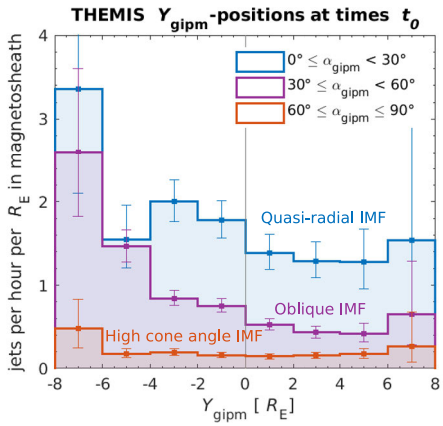

Figure 18. The jet observation rates as a function of Y_{GIPM} shown separately for the three IMF cone angle ranges. The spacecraft positions have been scaled to the mean solar wind $P_{\mathrm{dyn}} = 1.76$ nPa. The figure is adapted from Vuorinen et al. (2019) and licensed under CC BY.

the quasi-parallel shock. Figure 18 shows the jet observation rate as a function of Y for these three subsets. According to our results, jets occur 9 times more frequently during quasi-radial IMF (downstream of the quasi-parallel shock) than during high cone angle IMF (downstream of the quasi-perpendicular shock). For oblique IMF, the occurrence rates monotonically increase towards the quasi-parallel side. These results explicitly showed for the first time that the spatial occurrence of jets follows the location of the quasi-parallel shock, gradually decreasing toward the quasi-perpendicular shock. We also used the statistical model of jet magnetopause impact rates by Plaschke et al. (2016) and found that jets of diameters $> 1\ R_{\mathrm{E}}$ perpendicular to the propagation direction are estimated to hit the subsolar magnetopause defined by a 30° solar zenith angle approximately once per minute during quasi-radial IMF and five times per hour during high cone angle IMF.

In **Paper II**, we continued to investigate the solar wind control of jet occurrence. While the IMF cone angle has been considered the only important parameter affecting jet occurrence, a recent study by LaMoury et al. (2021) on an extended THEMIS data set from 2008–2018 indicated that other solar wind parameters influence it too. We further investigated their influence by studying THEMIS measurements from the years 2008–2020, again taking the corresponding solar wind conditions from the OMNI data set. We divided the observations into two categories by the IMF cone angle conditions: low ($[0^{\circ}, 30^{\circ}]$) and high ($[60^{\circ}, 90^{\circ}]$) IMF cone angles, corresponding to the two shock regimes, quasi-parallel and quasi-perpendicular, respectively. This was motivated both from a physical and a statistical perspective. First, the structure and dynamics of quasi-parallel and quasi-perpendicular shock regimes are different (see Sections 2.2.2 and 3.2.1). Consequently, the suggested jet formation mechanisms also differ for these two regimes (see Section 4.3.1). Second, because the IMF

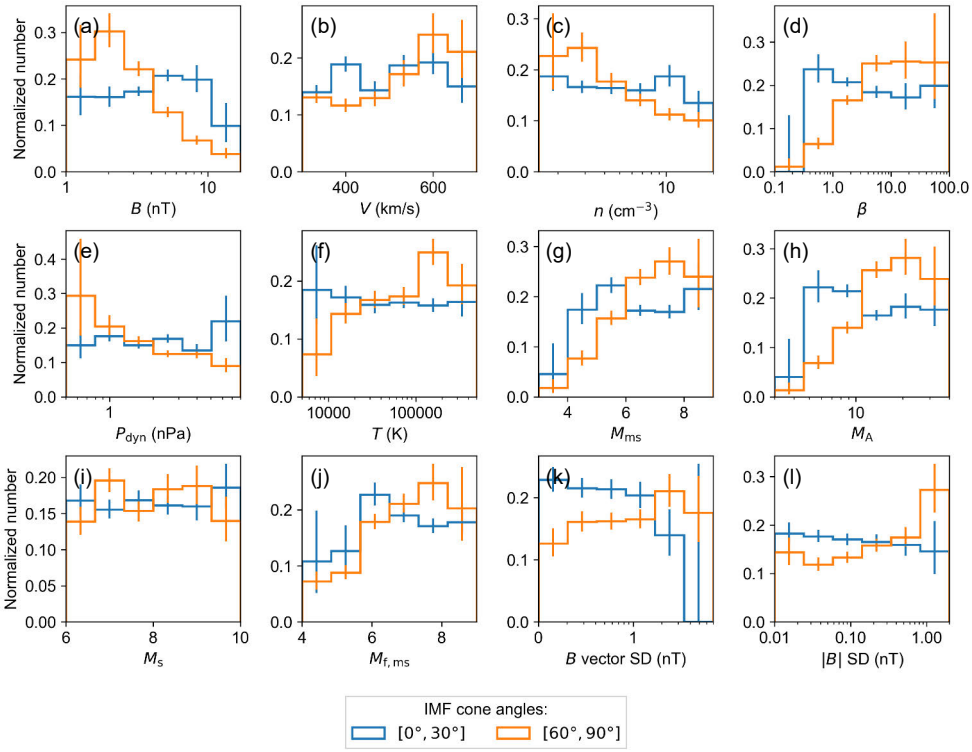

Figure 19. Distributions of the normalized occurrence rates of jets during low ($[0°, 30°]$; blue) and high IMF cone angles ($[60°, 90°]$; orange) as functions of other solar wind parameters: (a) IMF magnitude, (b) speed, (c) density, (d) β, (e) dynamic pressure, (f) ion temperature, (g) magnetosonic Mach number, (h) Alfvénic Mach number, (i) sonic Mach number, (j) fast magnetosonic Mach number, (k) IMF vector standard deviation, and (l) IMF magnitude standard deviation. The error bars denote 95 % proportional confidence intervals. The figure is from Vuorinen et al. (2023a) and licensed under CC BY.

cone angle is such an important parameter controlling jet occurrence, there is a large difference in the IMF cone angle distributions between the jet and all magnetosheath data. Therefore, taking IMF cone angle conditions into account is important when calculating the normalized jet occurrence rates (conditional probabilities; see Section 5.3) to avoid interdependecies between the IMF cone angle and other solar wind parameters to bias the results. Following the conclusions of LaMoury et al. (2021), we only considered the observations close to the bow shock ($0.5 \leq F \leq 1.1$; see Section 5.4.1) with the aim of focusing on solar wind control on jet formation and excluding propagation effects.

Our statistical results are shown in Figure 19, where we present normalized jet occurrence rates as a function of solar wind parameters separately for the low (blue) and high (orange) IMF cone angle subsets. The results indicate that when the IMF cone angle is low, i.e., the subsolar magnetosheath is downstream of a quasi-parallel

shock, other solar wind parameters do not significantly influence jet occurrence. In this data set, jet occurrence commences when the solar wind Alfvénic Mach number $M_{\mathrm{A}} \gtrsim 5$, which could be related to the condition of supercriticality for the Earth's bow shock. However, this condition is rarely not satisfied at 1 AU and the statistics are low. Similarly, high variability in the IMF direction (panel k) seems to be unfavorable for jet generation, but the statistics are of low confidence. All in all, these results indicate that simply the steady presence of a foreshock region is enough for jet generation, again simplifying our picture of jet occurrence at the quasi-parallel shock. In contrast, when the IMF cone angle is high and the subsolar shock region is quasi-perpendicular, we find that other upstream parameters do have an effect on the observed jet occurrence rates. More favorable conditions for jet formation are in particular high M_{A}, high β, low magnetic field magnitude B, and low density n. A correlation analysis suggests that IMF magnitude is most often responsible for variations in M_{A} and β and can therefore be considered as the most important parameter. In accordance with previous studies (Goncharov et al., 2020; Raptis et al., 2020), we found that the quasi-perpendicular jets tend to be small. While jets of all sizes are more prevalent during M_{A} and β, jets associated with these conditions are smaller on average.

As the statistical results imply that solar wind M_{A} and β control jet occurrence downstream of a quasi-perpendicular shock, we investigated quasi-perpendicular bow shock crossings at different M_{A} and β conditions to understand how the shock transition changes. Jet occurrence in this regime had not been studied before, and our understanding of the ability of quasi-perpendicular shocks to generate jets had been generally poor. The high M_{A} and β observations show, similarly to previous studies (Sulaiman et al., 2015; Sundberg et al., 2017; Madanian et al., 2021; Petrukovich and Chugunova, 2021), that with increasing M_{A} (and β, as these two parameters are highly correlated at 1 AU) the shock crossing exhibits a more extended transition from the upstream state to the downstream state. This is related to the increased gyroscales in low $|B|$ conditions. In our example events, spacecraft near the shock observed jets in the highly structured transition region, but spacecraft deeper in the magnetosheath did not observe jets, indicating that these jets do not propagate far and are not expected to be geoeffective. In Figure 20 we show one of the example events, where THEMIS A in the upstream confirms highly perpendicular magnetic field geometry ($B_{Z,\mathrm{GSE}}$ dominates), THEMIS E crosses the shock from the magnetosheath to the solar wind observing dynamic pressure enhancements in the transition region of the shock, and THEMIS D deeper in the magnetosheath does not observe jets, indicating that the structures have already dissipated or that they were simply temporal variations instead of propagating structures. For our other example event (not shown here, see the original paper Vuorinen et al., 2023a), burst-level data allowed for a more detailed look into the velocity distribution functions (VDFs) of one of these jets. They revealed the presence of a non-gyrotropic gyrating ion popula-

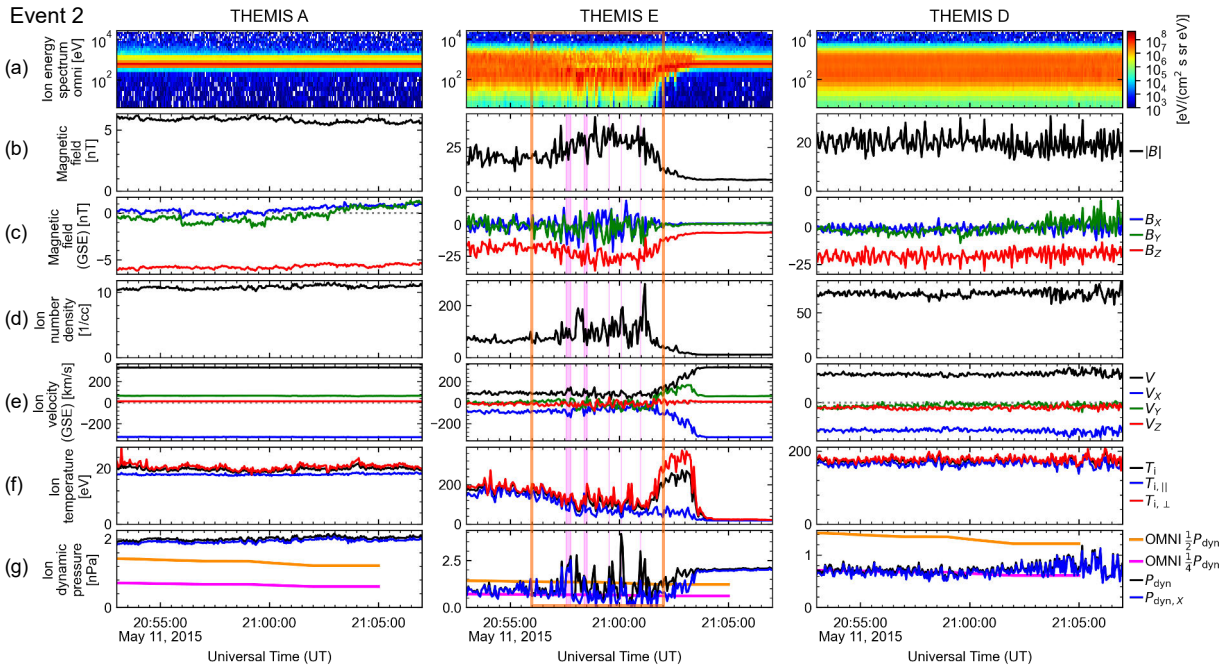

Figure 20. Observations by THEMIS A (in the solar wind), E (crossing from magnetosheath to the solar wind), and D (in the magnetosheath) on May 11, 2015. (a) ion omni-directional energy spectrogram, (b) magnetic field magnitude, (c) magnetic field GSE components, (d) ion number density, (e) ion velocity magnitude and GSE components, (f) ion total, parallel, and perpendicular temperatures, and (g) total and GSE $-X$ aligned dynamic pressures with $1/2$ (orange) and $1/4$ (magenta) of OMNI solar wind dynamic pressure. We have highlighted jets that fulfill the Plaschke et al. (2013) criteria by a magenta shading. The figure is from Vuorinen et al. (2023a) and licensed under CC BY.

tion, which can periodically increase the earthward dynamic pressure causing jet-like enhancements. This is most likely related to ion motion near the shock, but with extended spatial scales due to the low IMF magnitude. While these structures fulfill the jet criteria, they likely do not fit our typical picture of jets as coherent propagating structures.

The characteristics of the solar wind change during the solar cycle, as the structure of the Sun's magnetic field becomes more complicated and the Sun more active near the solar maximum. The size of large-scale solar wind structures is much larger than the Earth's dayside magnetosphere, and they manifest as variations in the solar wind conditions observed at the Earth. Koller et al. (2022) studied magnetosheath jets in relation to large-scale solar wind structures, SIRs and CMEs. Motivated both by previous studies of solar wind control of jet occurrence and the results of Koller et al. (2022), in **Paper III**, we investigated how jet occurrence varies during the solar cycle. We again utilized the extensive THEMIS data set from 2008-2020 (Koller

et al., 2021), which spans over the solar cycle 24 (December 2008 to December 2019).

While comparing the yearly average jet occurrence rates (jets per observation time), we found that the observations were biased due to orbital variations throughout the years. Previous studies (and this data set) show that jets are much more common close to the bow shock than close to the magnetopause. Therefore, fewer jets were observed during the years when the apogees of spacecraft orbits were lower. We controlled for this bias by only considering jets close to the model the bow shock. However, this selection introduced another bias: during the years when the apogees were low, the spacecraft were close to the model bow shock during solar wind conditions when the magnetosphere was compressed and the bow shock was closer to the Earth. This happens during high solar wind dynamic pressure conditions. Consequently, the resulting distributions of OMNI solar wind conditions during THEMIS observation times were different from the distribution of all OMNI measurements in those years. Curiously, this bias also led to high IMF cone angle conditions being over-represented in some of the years, by an interrelation of high solar wind dynamic pressure and high IMF cone angle. Overall, the changes in orbital apogees of THEMIS spacecraft yielded non-comparable the jet occurrence rates between the solar maximum and the solar minimum.

As a direct comparison of the jet occurrence rates during different years is not possible, we instead created a statistical model utilizing the vast amount of THEMIS and OMNI data which contain information on how jet occurrence depends on the solar wind conditions. Using geocentric coordinate systems (see Section 5.2), the calendar year of the observations is not important, so with a model of how jet occurrence varies as a function of solar wind conditions we can estimate the unbiased yearly jet occurrence rates by giving all the yearly OMNI observations as an input. This statistical model is introduced in Section 5.4.3 and thoroughly described in the paper. After building and testing the model, we found that the best model uses IMF cone angle and IMF magnitude (in line with the results of **Paper II**). Notably, IMF cone angle alone was enough to recreate the significant variations.

We applied the models to OMNI data from the solar cycles 23 and 24 to get the first-ever estimations of how jet occurrence varies throughout the solar cycle. The obtained results for the models using only IMF cone angle and the best model using IMF cone angle and IMF magnitude are shown in Figure 21. Our reconstructions indicated that the jet occurrence does not vary strongly across a solar cycle, but there may be a 10–20 % decrease during solar maxima, which was within the uncertainties of the model. Jets can thus be expected to be a relatively constant phenomenon present throughout the solar cycle. These yearly averages of the number of observed jets per hour ($\sim$ 3–4 jets/h) would correspond to 26,000–35,000 observable jets/year. These numbers are based on the numbers of jets observed by a single THEMIS spacecraft, but since a spacecraft cannot observe every jet, the true number

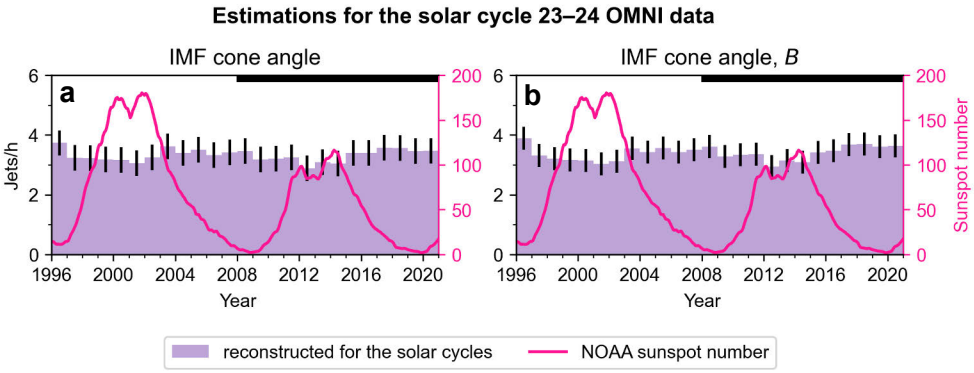

Figure 21. Estimations of the yearly jet occurrence rates obtained by applying the statistical models using (a) IMF cone angle and (b) IMF cone angle and IMF magnitude on all OMNI data from years 1996–2020 (solar cycles 23 & 24). The error bars show the estimated uncertainties of the models. The pink line shows the smoothed sunspot number from NOAA. The figure is adapted from Vuorinen et al. (2023b) and licensed under CC BY.

of jets forming is higher. Magnetosheath jets are evidently very frequently formed at the Earth's bow shock, and their role in the solar wind–magnetosphere interaction needs to be determined.

6.2 Electron acceleration at jet-driven bow waves

In **Paper IV**, we presented the first modelling results of electron acceleration at bow waves that can form ahead of supermagnetosonic jets propagating in the magnetosheath. This simple 1D test-particle model (introduced in Section 5.5 and described in detail in the paper) follows electrons on a single field line between the jet-driven bow wave (which is modelled as a curved MHD shock) and a standing mirror (e.g., the magnetopause or another standing mirror in the magnetosheath). These two mirrors form a collapsing magnetic trap. We performed a parameter study in which we studied the relative significance of the magnetic trap and pitch-angle scattering and compared the electron spectra to those observed by Liu et al. (2020b).

To obtain results that are similar to observations, we found that the magnetic trap has to keep particles trapped for a long enough time to allow the electrons interact with the shock many times. The role of scattering was found to be unimportant in comparison to the collapsing trap. In the simulations, particles were accelerated due to the collapsing trap between the bow wave and the magnetopause with shock drift acceleration at the moving bow wave. The free energy comes from the relative motion between the fast jet and the surrounding magnetosheath plasma. We ran simulations with two different background plasma conditions corresponding to representative conditions in the Earth's magnetosheath (as determined from the THEMIS

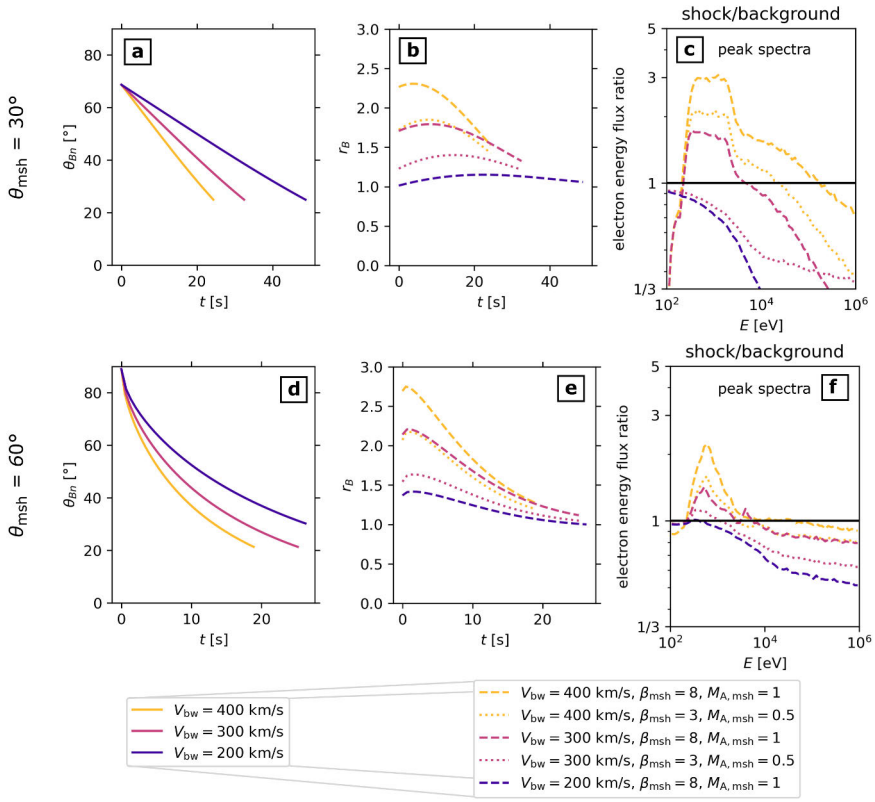

Figure 22. Simulations with magnetosheath field obliquity (a–c) $\theta_{\mathrm{msh}} = 30°$ and (d–f) $60°$. (a,d) The time variation of θ_{Bn} at the shock for the three different bow wave speeds. (b,e) The time variation of the magnetic compression ratio of the bow wave for bow waves of different speeds with magnetosheath conditions ($\beta_{\mathrm{msh}} = 8$, $M_{\mathrm{A,msh}} = 1$; dashed line) and ($\beta_{\mathrm{msh}} = 3$, $M_{\mathrm{A,msh}} = 0.5$; dotted line). (c,f) The ratios of peak energy flux spectra to the initial spectrum. The figure is from Vuorinen et al. (2022) and licensed under CC BY.

subsolar magnetosheath data set). We also presented results for two different background magnetic field obliquities and varied the speed of the jet-driven bow wave. All the varied parameters were found to be important for the efficiency of acceleration in our simulations, but we note that the bow wave speed especially has to be high (300–400 km/s) for acceleration to occur. According to our results shown in Figure 22, these bow waves are able to accelerate electrons with energies ~ 100 eV to ~ 10 keV, even up to a few hundred keV (see Figure 22c&f). The final energy fluxes at these energies were 1–3 times the initial values, which were similar to the energy flux increases observed by Liu et al. (2020b). Our simulation results suggest that in the spatial and temporal scales corresponding to the jets in the Earth's magnetosheath, a collapsing trap with shock drift acceleration at the jet-driven bow wave could explain the observed energization of electrons.

6.3 B_Z in magnetosheath jets

In **Paper V**, we presented the first statistical study with the aim to understand how magnetosheath jets could influence magnetopause reconnection. Observations reported by Hietala et al. (2018) and Nykyri et al. (2019), and later in the PhD thesis of LaMoury (2023), suggest that jets can trigger reconnection as they impact the magnetopause. This paper focused on studying the B_Z (GSM) magnetic field component in jets, to determine whether jets alter the magnetic shear at the magnetopause in a statistical sense. We used data from the THEMIS spacecraft from years 2008–2011 (the data set used by Plaschke et al., 2013) and complemented these observations with OMNI solar wind observations. We divided the data to northward ($B_Z^{\mathrm{IMF}} > 0$) and southward IMF ($B_Z^{\mathrm{IMF}} < 0$) subsets. We considered THEMIS observations close to the model magnetopause ($-0.1 \leq F \leq 0.3$; see Section 5.4.1) and compared the B_Z measurements during jet intervals to those during similar-duration non-jet intervals sampled from the magnetosheath data set. We performed the sampling of non-jet intervals such that their IMF cone angle distribution matched that of jet intervals to remove bias related to the IMF cone angle. Using bootstrap sampling (Efron and Tibshirani, 1993), we were also able to estimate the uncertainty in the results.

According to our results, both jet and non-jet magnetosheath B_Z observations are roughly as likely ($\sim$ 20–30 %) to be of the opposite polarity to the IMF B_Z. However, there is a clear difference how these observations are distributed between individual intervals. When we investigate how the magnetic field varies within individual intervals, we find that most jets (60–70 %) contain at least some B_Z opposite to the IMF B_Z in comparison to $\sim$ 40 % of non-jet intervals. This suggests that the magnetic field within jets is more variable. In fact, opposite B_Z pulses of up to $\sim$ 10 s are more frequent in jet intervals than in non-jet intervals. Therefore, as jets approach the magnetopause, they statistically introduce variations to the magnetic field conditions, which may be favorable for locally triggering magnetopause reconnection during northward IMF and suppressing it during southward IMF.

It is not clear what type of variations in the magnetic shear angle are enough to have an effect on magnetopause reconnection. However, we used the observations reported by Nykyri et al. (2019) as a benchmark. They observed strong southward pulses within jets, of which one was 4 s in duration and had $B_Z = -24$ nT. Such pulses are observed in around 12 % of jets during northward IMF, being two times more common than in the non-jet magnetosheath intervals.

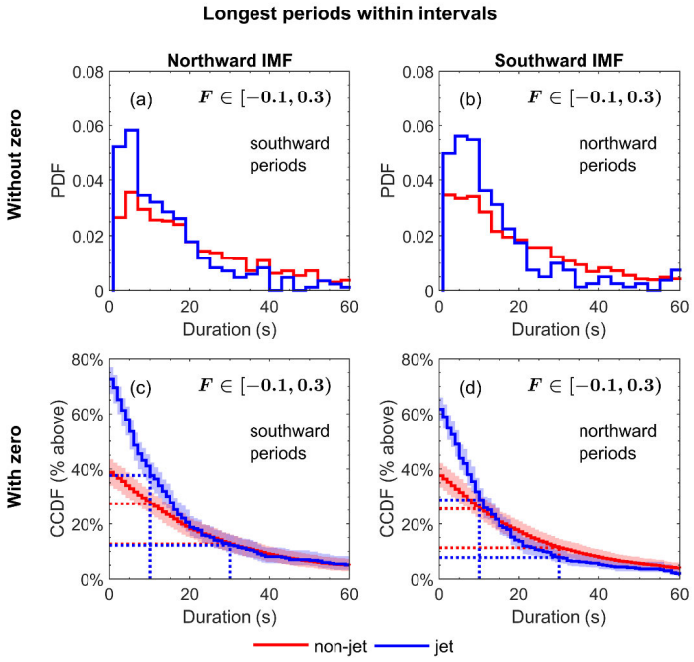

Figure 23. The durations of the longest (a,c) southward B_Z periods during northward IMF and (b,d) northward B_Z periods during southward IMF within jet (blue) and non-jet (red) intervals. Panels (a,b) show the probability density functions (PDFs) without 0-s-duration intervals and panels (c,d) show complementary cumulative distribution functions (CCDFs, i.e., the proportions of intervals longer than a certain duration) containing 0-s durations. 10 s and 30 s are marked with dashed lines. The figure is from Vuorinen et al. (2021) and licensed under CC BY.

7 Conclusions and Outlook

In this thesis, we have focused on dynamic pressure enhancements downstream of the Earth's bow shock for which the research community has presently widely adopted the term "magnetosheath jets". This research topic has gained interest and popularity in recent years, and our understanding of their occurrence, formation, properties, and effects has grown substantially. This progress has been largely driven by new observations, in particular from THEMIS and MMS missions, that have enabled both larger statistical studies and fortuitous observations of individual events. With growing maturity of the field, our picture of jets is becoming more intricate and newly-found complexities also arise.

Following the life of a jet, here we have gradually moved from the bow shock towards the magnetopause. Magnetosheath jets form sporadically due to the dynamics of the Earth's bow shock both in the presence and, importantly, in the absence of localized solar wind variations. Their formation is believed to be inherently related to the kinetic processes at the shock, namely ion reflection and the foreshock region upstream of the shock, which influence the corrugated and non-stationary quasi-parallel shock. Jets represent a way of transporting solar wind energy and momentum into the magnetosphere as jets of high dynamic pressure can deform the magnetopause and launch effects into the magnetosphere and the ionosphere. During their propagation through the magnetosheath, they also perturb the surrounding plasma and can even accelerate particles due to the bow waves that they drive ahead of them.

We have used THEMIS spacecraft observations to perform several statistical studies to understand the connection between upstream solar wind conditions and jet occurrence. Investigating how often, where, and under which conditions jets occur helps us understand how they may form, how prevalent their effects are expected to be, and make predictions of their existence in other shock environments. In **Paper I**, we studied how the IMF orientation controls where and how often magnetosheath jets occur. Due to combined effect of the varying IMF orientation and the curvature of the Earth's bow shock, the quasi-parallel and quasi-perpendicular shock regions are not fixed in place, but they change location. We find that jet occurrence indeed responds to these changes: jet occurrence is the highest downstream of the quasi-parallel shock region and monotonically decreases towards the quasi-perpendicular region. Unfortunately, the statistical data set used at the time did not allow for a more detailed probing of the spatial occurrence of jets near the foreshock boundary,

where the ion foreshock and the ULF foreshock diverge. This could be investigated in future simulation studies.

The view of the IMF cone angle being the only parameter controlling jet occurrence has been challenged by new statistical studies employing more extensive data sets (Goncharov et al., 2020; LaMoury et al., 2021; Koller et al., 2022, 2023). In **Paper II**, we statistically study how solar wind conditions influence jet occurrence by looking separately at the two distinct shock regimes: the quasi-parallel and quasi-perpendicular shock. The subsets of data from the quasi-parallel and quasi-perpendicular regimes near the subsolar region were obtained by taking observations during low IMF cone angles ($< 30°$; quasi-radial IMF) and high IMF cone angles ($\geq 60°$), respectively. Our results indicate that when the subsolar bow shock region is quasi-parallel, other solar wind parameters are not important for jet occurrence, albeit the occurrence seemed to drop for very low M_{A}. This indicates that simply the presence of the foreshock region and the quasi-parallel shock are enough for jet generation. We note that, while quasi-radial IMF is the most favorable condition for observing jets in the subsolar magnetosheath, such conditions constitute only 10 % of IMF conditions in our extensive data set (by Koller et al., 2021, 2022), which includes almost 11,000 hours of data from the subsolar magnetosheath (and of which 3,400 hours is estimated to be from the region near the bow shock) from 2008–2020, spanning over a solar cycle. 30 % of all jets are observed during quasi-radial IMF conditions, while 50 % of all jets are observed during oblique IMF with cone angles $\alpha \in [30°, 60°)$. Due to the nominal Parker spiral configuration of the IMF, the quasi-parallel area of the Earth's bow shock is typically located on the dawnside. Therefore, the effects of magnetosheath jets can be expected to be most influential on the dawnside magnetosphere, and this oblique regime should be a subject of further study.

It has thus far been unclear whether jets in the quasi-perpendicular magnetosheath can form at the shock or whether they are only due to local magnetosheath processes (e.g., mirror-mode waves) or jets formed at the quasi-parallel shock and travelled to the quasi-perpendicular magnetosheath (Raptis et al., 2020). According to our results, low IMF magnitude, high M_{A}, and high β favor jet formation in the quasi-perpendicular regime. We study two bow shock crossings, where jets are observed in the transition region of the shock, but not deeper in the magnetosheath. One of these jets reveals a non-gyrotropic gyrating ion population, which can periodically increase the earthward dynamic pressure. These observations suggest that these jets are most likely not propagating structures but rather temporal variations. This leads us to call them jet-like structures, albeit the definition of jets only based on a dynamic pressure threshold in itself is not exclusionary.

This question of what is a jet has become increasingly more relevant the more we study them. The simple definition based on a dynamic pressure threshold can be viewed as arbitrary as many different transients can fulfill the criteria. An appropriate

sub-categorization of different types of structures that are identified as jets would be beneficial, and as a long-term goal, it would be important to assess the relative prevalence of jets formed by different mechanisms and correspondingly assess their contribution to the solar wind–magnetosphere interaction.

Ever since jets were first studied, their relevance for the Sun-Earth interaction and their solar cycle dependence have been important open questions. As the solar wind conditions vary across the solar cycle, the occurrence of jets is expected to vary, as well. Koller et al. (2022) have also shown that jet occurrence changes during large-scale solar wind structures. However, the results of **Paper III** indicate that jet occurrence does not have a strong solar cycle dependence on a yearly level. Temporal variations in jet occurrence effectively even out when averaging over a year. This is because there is no strong long-term variability in the most important parameter controlling jet occurrence — the IMF cone angle. However, there may be a 10–20 % decrease in jet occurrence rates during the solar maximum. This could be attributed to the high IMF cone angle, low-M_{A} conditions present in coronal mass ejections (Koller et al., 2023). We also see indications of the jet occurrence rate quickly recovering during the declining phase of the solar cycle, which we attribute to the increased occurrence of SIRs. We know that during solar maximum, the solar wind–magnetosphere coupling is clearly dominated by solar wind structures. Therefore, the relative importance of magnetosheath jets and other dayside transient phenomena is most likely higher during quiet activity times.

As jets propagate in the magnetosheath, they influence the surrounding magnetosheath plasma. In particular, the fastest jets can be supermagnetosonic with respect to their surroundings and consequently drive bow shocks in front of them. Motivated by previous observations of both ion and electron energization, in **Paper IV** we studied electron acceleration by these bow waves. We applied a simple test-particle Monte Carlo model, where the bow wave was modelled as an MHD shock. In our simulations, the particles were accelerated due to a combined effect of shock drift acceleration and a collapsing trap forming between the bow wave and a second, standing, magnetic mirror, e.g., the magnetopause. Perhaps SLAMSs and other types of transient structures in the magnetosheath with substantial magnetic field enhancements could also act as the secondary mirror and form such a collapsing trap downstream of the quasi-parallel shock. We found a relatively good match with observations, which indicates that in the temporal and spatial scales relevant for jets in the Earth's magnetosheath such a mechanism could qualitatively explain the observed increases in electron energy fluxes. In the future, this phenomenon should be further studied in simulations, where the bow wave structure is more realistic, e.g., following test-particles in a hybrid-PIC plasma simulation. Although the energization is modest, jets provide additional acceleration of particles in the Earth's bow shock environment. As with other jet-related effects on the bow shock–magnetosphere system, the total contribution of jets is ultimately a sum of many jets. Previous studies

(e.g., Liu et al., 2017) have shown that upstream foreshock transients can also accelerate particles, and thus additional acceleration happens at transient structures both upstream and downstream of the Earth's bow shock.

Eventually, most jets dissipate during their propagation towards the Earth, but some of them survive all the way and collide into the boundary of the magnetosphere. With their high dynamic pressure, they can indent the magnetopause — individual jets simultaneously at multiple points at the magnetopause. These perturbations can be transmitted into the magnetosphere in multiple different ways, e.g., by launching waves, by exciting field-aligned currents, or by triggering reconnection. Direct evidence of a jet influencing magnetosheath reconnection was reported by Hietala et al. (2018). In this event, the plasma and magnetic field conditions were favorable for a reconnection onset, but the current sheet was unusually thick. The high dynamic pressure of a jet allowed for compression of the current sheet, which was then observed reconnecting. Additionally, Nykyri et al. (2019) related strong southward B_Z (in GSM coordinates, see Section 5.2) pulses within magnetosheath jets during positive IMF B_Z conditions to a later observed substorm onset via a timing analysis. They proposed that these jets triggered magnetopause reconnection and acted as the final trigger for the substorm onset.

It is reasonable to believe that jets may locally modulate magnetopause reconnection both via the inherent ability to compress the magnetopause and by changing the local plasma and magnetic field conditions. In **Paper V**, we studied B_Z within magnetosheath jets close to the magnetopause and found that the magnetic field within jets is more variable than typically in the magnetosheath. Thus jets can introduce B_Z variations of opposite polarity to the prevailing IMF at the magnetopause. An important take-away from this paper is that the non-jet magnetosheath itself also exhibits more fluctuations whenever downstream of the quasi-parallel shock. Therefore, the effects of foreshock-related fluctuations and transient structures, more generally, on magnetopause reconnection should be investigated. Jets are one manifestation of this variability with the definitional property of enhanced dynamic pressure.

Recently, LaMoury (2023) have built upon our results by studying the additional effect of the plasma β in the $\Delta\beta$-shear condition for diamagnetic suppression of reconnection. They found that the high β observed in jets makes jets more likely to suppress reconnection. Therefore, based on these statistical results, the most substantial effect would be expected to be local suppression of magnetopause reconnection during southward IMF. Interestingly, they also presented a case study where they found evidence of jets both suppressing and triggering reconnection, and also not changing its state. Notably, the $\Delta\beta$-shear condition was found to be unreliable for predicting the state of reconnection in this complex interval containing multiple jets.

It is not clear what type of variations are able to locally alter the state of reconnection at the magnetopause, i.e., how strong and long-lasting the variations should be. While more direct observations of jets influencing reconnection are needed, it is

difficult to disentangle the relative importance of different parameters and physical effects at play from the inherently limited spacecraft observations. Therefore, jets influencing reconnection should also be investigated in simulation studies. On the other hand, statistical studies relating jet observations and possible indirect/remote signatures of magnetopause reconnection will help us understand whether jets do in fact statistically influence reconnection, and how, and whether this affects the global reconnection rate. Remote observations of interest could include FTEs, auroral imaging, and the polar cap potential measurements. Kullen et al. (2019) reported that the occurrence rate of isolated FTEs is enhanced under low IMF cone angle conditions and proposed that their generation could be linked to jet-related reconnection events. Similarly, the possible connection between throat aurora signatures (e.g., Han et al., 2016, 2017, 2018) and jet-related reconnection should be investigated.

Statistically speaking, reconnection at the duskward (quasi-perpendicular) sector of the dayside magnetopause is modulated by magnetosheath mirror-mode waves (Laitinen et al., 2010; Hoilijoki et al., 2017) and the presence of the plasmaspheric plume (a cold dense plasma population) on the magnetospheric side (Walsh et al., 2013, 2014), while on the dawnward (quasi-parallel) side it is modulated by foreshock-related effects, including magnetosheath jets. These effects may result in global-scale differences in the nature of magnetopause reconnection.

In the statistical studies of this thesis, we have employed OMNI solar wind data to infer conditions upstream solar wind conditions at the Earth. Due to its almost continuous coverage, OMNI data enables large statistical studies. However, the propagation of OMNI data from L1 to the Earth contains uncertainty and the inferred conditions may sometimes largely deviate from the true conditions at the Earth's bow shock. This is especially important to consider when studying individual events. However, as the number of suitable observations with a local upstream monitor grow, statistical studies of jets should also be conducted using that data in order to rule out any systematic errors in OMNI data. Reliable solar wind measurements ahead of Earth are crucial not only for the study of magnetosheath jets and magnetospheric research in general, but they are of utmost importance also for space weather monitoring and forecasting. Novel methods to improve the propagation of the solar wind from the L1 to the Earth are being developed (Burkholder et al., 2020; O'Brien et al., 2023). New L1 spacecraft missions, such as the Interstellar Mapping and Acceleration Probe (IMAP; McComas et al., 2018), will be important additions to the aging set of L1 monitors and improve the estimations by providing additional points of measurements.

In this thesis, we have studied multiple features of magnetosheath jets from their occurrence in relation to the upstream solar wind conditions to their potential effects both during their propagation in the magnetosheath and upon impacting the magnetopause. As part of the work of the growing research community investigating this topic, our results help establish jets as an inherent part of solar wind–magnetosphere

interaction, which perturb the surrounding magnetosheath and the magnetosphere in various ways. Jets of different sizes are expected to continuously impact the Earth's magnetopause downstream of the quasi-parallel shock, and ultimately their total contribution is related to their prevalence. Understanding the importance of different jet formation mechanisms, quantifying the effects and significance of jets, and determining jets as a possibly inherent property of other collisionless shock environments remain subjects of many future studies.

List of References

Amata, E., Savin, S., Ambrosino, D., Bogdanova, Y., Marcucci, M., Romanov, S., and Skalsky, A.: High kinetic energy density jets in the Earth's magnetosheath: A case study, Planetary and Space Science, 59, 482–494, https://doi.org/10.1016/j.pss.2010.07.021, Cross-Scale Coupling in Plasmas, 2011.

Angelopoulos, V.: The THEMIS Mission, Space Science Reviews, 141, 5, https://doi.org/10.1007/s11214-008-9336-1, 2008.

Archer, M. O. and Horbury, T. S.: Magnetosheath dynamic pressure enhancements: occurrence and typical properties, Annales Geophysicae, 31, 319–331, https://doi.org/10.5194/angeo-31-319-2013, 2013.

Archer, M. O., Horbury, T. S., and Eastwood, J. P.: Magnetosheath pressure pulses: Generation downstream of the bow shock from solar wind discontinuities, Journal of Geophysical Research, 117, 1–13, https://doi.org/10.1029/2011JA017468, 2012.

Archer, M. O., Hartinger, M. D., and Horbury, T. S.: Magnetospheric "magic" frequencies as magnetopause surface eigenmodes, Geophysical Research Letters, 40, 5003–5008, https://doi.org/10.1002/grl.50979, 2013.

Archer, M. O., Hietala, H., Hartinger, M. D., Plaschke, F., and Angelopoulos, V.: Direct observations of a surface eigenmode of the dayside magnetopause, Nature Communications, 10, 615, https://doi.org/10.1038/s41467-018-08134-5, 2019.

Auster, H. U., Glassmeier, K. H., Magnes, W., Aydogar, O., Baumjohann, W., Constantinescu, D., Fischer, D., Fornacon, K. H., Georgescu, E., Harvey, P., Hillenmaier, O., Kroth, R., Ludlam, M., Narita, Y., Nakamura, R., Okrafka, K., Plaschke, F., Richter, I., Schwarzl, H., Stoll, B., Valavanoglou, A., and Wiedemann, M.: The THEMIS Fluxgate Magnetometer, Space Science Reviews, 141, 235–264, https://doi.org/10.1007/s11214-008-9365-9, 2008.

Bale, S. D., Balikhin, M. A., Horbury, T. S., Krasnoselskikh, V. V., Kucharek, H., Möbius, E., Walker, S. N., Balogh, A., Burgess, D., Lembège, B., Lucek, E. A., Scholer, M., Schwartz7 10, S. J., and Thomsen, M. F.: Quasi-perpendicular Shock Structure and Processes, Space Science Reviews, 118, 161–203, https://doi.org/10.1007/s11214-005-3827-0, 2005.

Bieber, J. W. and Stone, S. C.: Energetic electron bursts in the magnetopause electron layer and in interplanetary space, in: Magnetospheric Boundary Layers, edited by Battrick, B., Mort, J., Haerendel, G., and Ortner, J., vol. 148 of *ESA Special Publication*, pp. 131–135, European Space Agency, Paris, France, 1979.

Biskamp, D.: Magnetic Reconnection in Plasmas, Cambridge Monographs on Plasma Physics, Cambridge University Press, 2000.

Bonnell, J. W., Mozer, F. S., Delory, G. T., Hull, A. J., Ergun, R. E., Cully, C. M., Angelopoulos, V., and Harvey, P. R.: The Electric Field Instrument (EFI) for THEMIS, Space Science Reviews, 141, 303–341, https://doi.org/10.1007/s11214-008-9469-2, 2008.

Bothmer, V. and Daglis, I. A.: Introduction, in: Space Weather: Physics and Effects, edited by Bothmer, V. and Daglis, I. A., Springer-Verlag Berlin Heidelberg and Praxis Publishing, Berlin, Germany and Chichester, United Kingdom, 1st edition, 2007.

Bothmer, V. and Zhukov, A.: The Sun as the prime source of space weather, in: Space Weather: Physics and Effects, edited by Bothmer, V. and Daglis, I. A., Springer-Verlag Berlin Heidelberg and Praxis Publishing, Berlin, Germany and Chichester, United Kingdom, 1st edition, 2007.

Burch, J. L., Moore, T. E., Torbert, R. B., and Giles, B. L.: Magnetospheric Multiscale Overview and Science Objectives, Space Science Reviews, 199, 5–21, https://doi.org/10.1007/s11214-015-0164-9, 2016.

Burgess, D. and Scholer, M.: Collisionless Shocks in Space Plasmas, Cambridge University Press, Cambridge, United Kingdom, 2015.

Burgess, D., Lucek, E. A., Scholer, M., Bale, S. D., Balikhin, M. A., Balogh, A., Horbury, T. S., Krasnoselskikh, V. V., Kucharek, H., Lembège, B., Möbius, E., Schwartz, S. J., Thomsen, M. F., and Walker, S. N.: Quasi-parallel Shock Structure and Processes, Space Science Reviews, 118, 205–222, https://doi.org/10.1007/s11214-005-3832-3, 2005.

Burgess, D., Möbius, E., and Scholer, M.: Ion Acceleration at the Earth's Bow Shock, Space Science Reviews, 173, 5–47, 2012.

Burkholder, B. L., Nykyri, K., and Ma, X.: Use of the L1 Constellation as a Multispacecraft Solar Wind Monitor, Journal of Geophysical Research: Space Physics, 125, e2020JA027 978, https://doi.org/10.1029/2020JA027978, 2020.

Cassak, P. A. and Fuselier, S. A.: Reconnection at Earth's Dayside Magnetopause, in: Magnetic Reconnection, edited by Gonzalez, W. and Parker, E., pp. 213–276, Springer International Publishing, Cham, Switzerland, 1st edition, https://doi.org/10.1007/978-3-319-26432-5, 2016.

Chen, L.-J., Ng, J., Omelchenko, Y., and Wang, S.: Magnetopause Reconnection and Indents Induced by Foreshock Turbulence, Geophysical Research Letters, 48, e2021GL093 029, https://doi.org/10.1029/2021GL093029, 2021a.

Chen, L.-J., Wang, S., Ng, J., Bessho, N., Tang, J.-M., Fung, S. F., Le, G., Gershman, D., Giles, B., Russell, C. T., Torbert, R., and Burch, J.: Solitary Magnetic Structures at Quasi-Parallel Collisionless Shocks: Formation, Geophysical Research Letters, 48, e2020GL090 800, https://doi.org/doi.org/10.1029/2020GL090800, 2021b.

Desai, M. and Giacalone, J.: Large gradual solar energetic particle events, Living Reviews in Solar Physics, 13, 3, https://doi.org/10.1007/s41116-016-0002-5, 2016.

Dimmock, A. P. and Nykyri, K.: The statistical mapping of magnetosheath plasma properties based on THEMIS measurements in the magnetosheath interplanetary medium reference frame, Journal of Geophysical Research: Space Physics, 118, 4963–4976, https://doi.org/10.1002/jgra.50465, 2013.

Dmitriev, A. V. and Suvorova, A. V.: Traveling magnetopause distortion related to a large-scale magnetosheath plasma jet: THEMIS and ground-based observations, Journal of Geophysical Research: Space Physics, 117, https://doi.org/10.1029/2011JA016861, 2012.

Dmitriev, A. V. and Suvorova, A. V.: Large-scale jets in the magnetosheath and plasma penetration across the magnetopause: THEMIS observations, Journal of Geophysical Research: Space Physics, 120, 4423–4437, https://doi.org/10.1002/2014JA020953, 2015.

Dmitriev, A. V. and Suvorova, A. V.: Atmospheric Effects of Magnetosheath Jets, Atmosphere, 14, 45, https://doi.org/10.3390/atmos14010045, 2023.

Drury, L. O.: An introduction to the theory of diffusive shock acceleration of energetic particles in tenuous plasmas, Reports on Progress in Physics, 46, 973–1027, https://doi.org/10.1088/0034-4885/46/8/002, 1983.

Eastwood, J. P., Lucek, E. A., Mazelle, C., Meziane, K., Narita, Y., Pickett, J., and Treumann, R. A.: The foreshock, Space Science Reviews, 118, 41–94, https://doi.org/10.1007/s11214-005-3824-3, 2005.

Eastwood, J. P., Hietala, H., Toth, G., Phan, T. D., and Fujimoto, M.: What Controls the Structure and Dynamics of Earth's Magnetosphere?, Space Science Reviews, 188, 251–286, https://doi.org/10.1007/s11214-014-0050-x, 2015.

Efron, B. and Tibshirani, R. J.: An Introduction to the Bootstrap, Chapman & Hall, New York, NY, The United States, 1993.

Escoubet, C. P., Hwang, K.-J., Toledo-Redondo, S., Turc, L., Haaland, S. E., Aunai, N., Dargent, J., Eastwood, J. P., Fear, R. C., Fu, H., Genestreti, K. J., Graham, D. B., Khotyaintsev, Y. V., Lapenta, G., Lavraud, B., Norgren, C., Sibeck, D. G., Varsani, A., Berchem, J., Dimmock, A. P.,

Paschmann, G., Dunlop, M., Bogdanova, Y. V., Roberts, O., Laakso, H., Masson, A., Taylor, M. G. G. T., Kajdič, P., Carr, C., Dandouras, I., Fazakerley, A., Nakamura, R., Burch, J. L., Giles, B. L., Pollock, C., Russell, C. T., and Torbert, R. B.: Cluster and MMS Simultaneous Observations of Magnetosheath High Speed Jets and Their Impact on the Magnetopause, Frontiers in Astronomy and Space Sciences, 6, 78, https://doi.org/10.3389/fspas.2019.00078, 2020.

Fairfield, D. H.: The ordered magnetic field of the magnetosheath, Journal of Geophysical Research (1896-1977), 72, 5865–5877, https://doi.org/10.1029/JZ072i023p05865, 1967.

Farris, M. H., Petrinec, S. M., and Russell, C. T.: The thickness of the magnetosheath: Constraints on the polytropic index, Geophysical Research Letters, 18, 1821–1824, https://doi.org/10.1029/91GL02090, 1991.

Giacalone, J., Schwartz, S. J., and Burgess, D.: Observations of suprathermal ions in association with SLAMS, Geophysical Research Letters, 20, 149–152, https://doi.org/10.1029/93GL00067, 1993.

Goncharov, O., Gunell, H., Hamrin, M., and Chong, S.: Evolution of High-Speed Jets and Plasmoids Downstream of the Quasi-Perpendicular Bow Shock, Journal of Geophysical Research: Space Physics, 125, e2019JA027 667, https://doi.org/10.1029/2019JA027667, 2020.

Gunell, H., Stenberg Wieser, G., Mella, M., Maggiolo, R., Nilsson, H., Darrouzet, F., Hamrin, M., Karlsson, T., Brenning, N., De Keyser, J., André, M., and Dandouras, I.: Waves in high-speed plasmoids in the magnetosheath and at the magnetopause, Annales Geophysicae, 32, 991–1009, https://doi.org/10.5194/angeo-32-991-2014, 2014.

Gutynska, O., Sibeck, D. G., and Omidi, N.: Magnetosheath plasma structures and their relation to foreshock processes, Journal of Geophysical Research: Space Physics, 120, 7687–7697, https://doi.org/10.1002/2014JA020880, 2015.

Han, D.-S., Nishimura, Y., Lyons, L. R., Hu, H.-Q., and Yang, H.-G.: Throat aurora: The ionospheric signature of magnetosheath particles penetrating into the magnetosphere, Geophysical Research Letters, 43, 1819–1827, https://doi.org/10.1002/2016GL068181, 2016.

Han, D. S., Hietala, H., Chen, X. C., Nishimura, Y., Lyons, L. R., Liu, J. J., Hu, H. Q., and Yang, H. G.: Observational properties of dayside throat aurora and implications on the possible generation mechanisms, Journal of Geophysical Research: Space Physics, 122, 1853–1870, https://doi.org/10.1002/2016JA023394, 2017.

Han, D. S., Liu, J. J., Chen, X. C., Xu, T., Li, B., Hu, Z. J., Hu, H. Q., Yang, H. G., Fuselier, S. A., and Pollock, C. J.: Direct Evidence for Throat Aurora Being the Ionospheric Signature of Magnetopause Transient and Reflecting Localized Magnetopause Indentations, Journal of Geophysical Research: Space Physics, 123, 2658–2667, https://doi.org/10.1002/2017JA024945, 2018.

Hansteen, V. H.: Stellar winds and magnetic fields, in: Heliophysics: Plasma Physics of the Local Cosmos, edited by Schrijver, C. J. and Siscoe, G. L., pp. 225–255, Cambridge University Press, New York, United States, https://doi.org/10.1017/CBO9781107340657.010, 2009.

Hao, Y., Lembege, B., Lu, Q., and Guo, F.: Formation of downstream high-speed jets by a rippled nonstationary quasi-parallel shock: 2-D hybrid simulations, Journal of Geophysical Research: Space Physics, 121, 2080–2094, https://doi.org/10.1002/2015JA021419, 2016a.

Hao, Y., Lu, Q., Gao, X., and Wang, S.: Ion dynamics at a rippled quasi-parallel shock: 2D hybrid simulations, The Astrophysical Journal, 823, 7, https://doi.org/10.3847/0004-637X/823/1/7, 2016b.

Hasegawa, H., Fujimoto, M., Phan, T.-D., Rème, H., Balogh, A., Dunlop, M. W., Hashimoto, C., and TanDokoro, R.: Transport of solar wind into Earth's magnetosphere through rolled-up Kelvin–Helmholtz vortices, Nature, 430, 755–758, https://doi.org/10.1038/nature02799, 2004.

Hastie, T., Tibshirani, R., and Friedman, J.: The Elements of Statistical Learning, Springer, 2 edition, 2009.

Hietala, H. and Plaschke, F.: On the generation of magnetosheath high-speed jets by bow shock ripples, Journal of Geophysical Research: Space Physics, 118, 7237–7245, https://doi.org/10.1002/2013JA019172, 2013.

Hietala, H., Laitinen, T. V., Andréeová, K., Vainio, R., Vaivads, A., Palmroth, M., Pulkkinen, T. I., Koskinen, H. E. J., Lucek, E. A., and Rème, H.: Supermagnetosonic Jets behind a Colli-

sionless Quasiparallel Shock, Physical Review Letters, 103, 245 001, https://doi.org/10.1103/PhysRevLett.103.245001, 2009.

Hietala, H., Partamies, N., Laitinen, T. V., Clausen, L. B. N., Facskó, G., Vaivads, A., Koskinen, H. E. J., Dandouras, I., Rème, H., and Lucek, E. A.: Supermagnetosonic subsolar magnetosheath jets and their effects: from the solar wind to the ionospheric convection, Annales Geophysicae, 30, 33–48, https://doi.org/10.5194/angeo-30-33-2012, 2012.

Hietala, H., Phan, T. D., Angelopoulos, V., Oieroset, M., Archer, M. O., Karlsson, T., and Plaschke, F.: In Situ Observations of a Magnetosheath High-Speed Jet Triggering Magnetopause Reconnection, Geophysical Research Letters, 45, 1732–1740, https://doi.org/10.1002/2017GL076525, 2018.

Hoilijoki, S., Ganse, U., Pfau-Kempf, Y., Cassak, P. A., Walsh, B. M., Hietala, H., von Alfthan, S., and Palmroth, M.: Reconnection rates and X line motion at the magnetopause: Global 2D-3V hybrid-Vlasov simulation results, Journal of Geophysical Research: Space Physics, 122, 2877–2888, https://doi.org/10.1002/2016JA023709, 2017.

Johlander, A., Battarbee, M., Vaivads, A., Turc, L., Pfau-Kempf, Y., Ganse, U., Grandin, M., Dubart, M., Khotyaintsev, Y. V., Caprioli, D., Haggerty, C., Schwartz, S. J., Giles, B. L., and Palmroth, M.: Ion Acceleration Efficiency at the Earth's Bow Shock: Observations and Simulation Results, The Astrophysical Journal, 914, 82, https://doi.org/10.3847/1538-4357/abfafc, 2021.

Johnson, J. R. and Cheng, C. Z.: Kinetic Alfvén waves and plasma transport at the magnetopause, Geophysical Research Letters, 24, 1423–1426, https://doi.org/10.1029/97GL01333, 1997.

Jones, F. C. and Ellison, D. C.: The plasma physics of shock acceleration, Space Science Reviews, 58, 259–346, https://doi.org/10.1007/BF01206003, 1991.

Kajdič, P., Raptis, S., Blanco-Cano, X., and Karlsson, T.: Causes of Jets in the Quasi-Perpendicular Magnetosheath, Geophysical Research Letters, 48, e2021GL093 173, https://doi.org/10.1029/2021GL093173, 2021.

Kallenrode, M.-B.: Space Physics, Springer-Verlag Berlin Heidelberg, Germany, 1998.

Karimabadi, H., Roytershteyn, V., Vu, H. X., Omelchenko, Y. A., Scudder, J., Daughton, W., Dimmock, A., Nykyri, K., Wan, M., Sibeck, D., Tatineni, M., Majumdar, A., Loring, B., and Geveci, B.: The link between shocks, turbulence, and magnetic reconnection in collisionless plasmas, Physics of Plasmas, 21, 062 308, https://doi.org/10.1063/1.4882875, 2014.

Karlsson, T., Brenning, N., Nilsson, H., Trotignon, J.-G., Vallières, X., and Facsko, G.: Localized density enhancements in the magnetosheath: Three-dimensional morphology and possible importance for impulsive penetration, Journal of Geophysical Research: Space Physics, 117, https://doi.org/10.1029/2011JA017059, 2012.

Karlsson, T., Kullen, A., Liljeblad, E., Brenning, N., Nilsson, H., Gunell, H., and Hamrin, M.: On the origin of magnetosheath plasmoids and their relation to magnetosheath jets, Journal of Geophysical Research: Space Physics, 120, 7390–7403, https://doi.org/10.1002/2015JA021487, 2015.

Kilpua, E., Koskinen, H. E. J., and Pulkkinen, T. I.: Coronal mass ejections and their sheath regions in interplanetary space, Living Reviews in Solar Physics, 14, 5, https://doi.org/10.1007/s41116-017-0009-6, 2017.

King, J. H. and Papitashvili, N. E.: Solar wind spatial scales in and comparisons of hourly Wind and ACE plasma and magnetic field data, Journal of Geophysical Research: Space Physics (1978–2012), 110, https://doi.org/10.1029/2004JA010649, 2005.

Koller, F., Plaschke, F., Temmer, M., and Preisser, L.: THEMIS local and upstream magnetosheath jet data 2008-2020., `https://osf.io/6ywjz`, 2021.

Koller, F., Temmer, M., Preisser, L., Plaschke, F., Geyer, P., Jian, L. K., Roberts, O. W., Hietala, H., and LaMoury, A. T.: Magnetosheath Jet Occurrence Rate in Relation to CMEs and SIRs, Journal of Geophysical Research: Space Physics, 127, e2021JA030 124, https://doi.org/10.1029/2021JA030124, 2022.

Koller, F., Plaschke, F., Temmer, M., Preisser, L., Roberts, O. W., and Vörös, Z.: Magnetosheath Jet Formation Influenced by Parameters in Solar Wind Structures, Journal of Geophysical Research: Space Physics, 128, e2023JA031 339, https://doi.org/10.1029/2023JA031339, 2023.

Koskinen, H. E. J.: Magnetohydrodynamics, pp. 163–190, Springer Berlin Heidelberg, Berlin, Heidelberg, https://doi.org/10.1007/978-3-642-00319-6_6, 2011a.

Koskinen, H. E. J.: Magnetic Reconnection, pp. 219–243, Springer Berlin Heidelberg, Berlin, Heidelberg, https://doi.org/10.1007/978-3-642-00319-6_8, 2011b.

Koskinen, H. E. J.: Shocks and Shock Acceleration, pp. 279–298, Springer Berlin Heidelberg, Berlin, Heidelberg, https://doi.org/10.1007/978-3-642-00319-6_11, 2011c.

Kullen, A., Thor, S., and Karlsson, T.: The Difference Between Isolated Flux Transfer Events and Flux Transfer Event Cascades, Journal of Geophysical Research: Space Physics, 124, 7850–7871, https://doi.org/10.1029/2019JA026629, 2019.

Laitinen, T. V., Khotyaintsev, Y. V., André, M., Vaivads, A., and Rème, H.: Local influence of magnetosheath plasma beta fluctuations on magnetopause reconnection, Annales Geophysicae, 28, 1053–1063, https://doi.org/10.5194/angeo-28-1053-2010, 2010.

LaMoury, A. T.: Magnetosheath jets: from the bow shock to the magnetopause, PhD thesis, Imperial College London, London, United Kingdom, https://doi.org/10.25560/108106, 2023.

LaMoury, A. T., Hietala, H., Plaschke, F., Vuorinen, L., and Eastwood, J. P.: Solar Wind Control of Magnetosheath Jet Formation and Propagation to the Magnetopause, Journal of Geophysical Research: Space Physics, 126, e2021JA029 592, https://doi.org/10.1029/2021JA029592, 2021.

Lepping, R. P., Acũna, M. H., Burlaga, L. F., Farrell, W. M., Slavin, J. A., Schatten, K. H., Mariani, F., Ness, N. F., Neubauer, F. M., Whang, Y. C., Byrnes, J. B., Kennon, R. S., Panetta, P. V., Scheifele, J., and Worley, E. M.: The WIND magnetic field investigation, Space Science Reviews, 71, 207–229, https://doi.org/10.1007/BF00751330, 1995.

Liu, T. Z., Angelopoulos, V., Hietala, H., and Wilson III, L. B.: Statistical study of particle acceleration in the core of foreshock transients, Journal of Geophysical Research: Space Physics, 122, 7197–7208, https://doi.org/10.1002/2017JA024043, 2017.

Liu, T. Z., Hietala, H., Angelopoulos, V., Omelchenko, Y., Roytershteyn, V., and Vainio, R.: THEMIS Observations of Particle Acceleration by a Magnetosheath Jet-Driven Bow Wave, Geophysical Research Letters, 46, 7929–7936, https://doi.org/10.1029/2019GL082614, 2019.

Liu, T. Z., Hietala, H., Angelopoulos, V., Omelchenko, Y., Vainio, R., and Plaschke, F.: Statistical Study of Magnetosheath Jet-Driven Bow Waves, Journal of Geophysical Research: Space Physics, 125, e2019JA027 710, https://doi.org/10.1029/2019JA027710, 2020a.

Liu, T. Z., Hietala, H., Angelopoulos, V., Vainio, R., and Omelchenko, Y.: Electron Acceleration by Magnetosheath Jet-Driven Bow Waves, Journal of Geophysical Research: Space Physics, 125, e2019JA027 709, https://doi.org/10.1029/2019JA027709, 2020b.

Lucek, E. A., Constantinescu, D., Goldstein, M. L., Pickett, J., Pinçon, J. L., Sahraoui, F., Treumann, R. A., and Walker, S. N.: The Magnetosheath, Space Science Reviews, 118, 95–152, https://doi.org/10.1007/s11214-005-3825-2, 2005.

Lucek, E. A., Horbury, T. S., Dandouras, I., and Re, H.: Cluster observations of the Earth's quasi-parallel bow shock, Journal of Geophysical Research, 113, 1–11, https://doi.org/10.1029/2007JA012756, 2008.

Madanian, H., Desai, M. I., Schwartz, S. J., Wilson, L. B., Fuselier, S. A., Burch, J. L., Contel, O. L., Turner, D. L., Ogasawara, K., Brosius, A. L., Russell, C. T., Ergun, R. E., Ahmadi, N., Gershman, D. J., and Lindqvist, P.-A.: The Dynamics of a High Mach Number Quasi-perpendicular Shock: MMS Observations, The Astrophysical Journal, 908, 40, https://doi.org/10.3847/1538-4357/abcb88, 2021.

McComas, D. J., Bame, S. J., Barker, P., Feldman, W. C., Phillips, J. L., Riley, P., and Griffee, J. W.: Solar Wind Electron Proton Alpha Monitor (SWEPAM) for the Advanced Composition Explorer, Space Science Reviews, 86, 563–612, https://doi.org/10.1023/A:1005040232597, 1998.

McComas, D. J., Christian, E. R., Schwadron, N. A., Fox, N., Westlake, J., Allegrini, F., Baker, D. N., Biesecker, D., Bzowski, M., Clark, G., Cohen, C. M. S., Cohen, I., Dayeh, M. A., Decker, R., de Nolfo, G. A., Desai, M. I., Ebert, R. W., Elliott, H. A., Fahr, H., Frisch, P. C., Funsten, H. O., Fuselier, S. A., Galli, A., Galvin, A. B., Giacalone, J., Gkioulidou, M., Guo, F., Horanyi, M., Isenberg, P., Janzen, P., Kistler, L. M., Korreck, K., Kubiak, M. A., Kucharek, H., Larsen, B. A.,

Leske, R. A., Lugaz, N., Luhmann, J., Matthaeus, W., Mitchell, D., Moebius, E., Ogasawara, K., Reisenfeld, D. B., Richardson, J. D., Russell, C. T., Sokół, J. M., Spence, H. E., Skoug, R., Sternovsky, Z., Swaczyna, P., Szalay, J. R., Tokumaru, M., Wiedenbeck, M. E., Wurz, P., Zank, G. P., and Zirnstein, E. J.: Interstellar Mapping and Acceleration Probe (IMAP): A New NASA Mission, Space Science Reviews, 214, 116, https://doi.org/10.1007/s11214-018-0550-1, 2018.

McFadden, J. P., Carlson, C. W., Larson, D., Ludlam, M., Abiad, R., Elliott, B., Turin, P., Marckwordt, M., and Angelopoulos, V.: The THEMIS ESA Plasma Instrument and In-flight Calibration, Space Science Reviews, 141, 277–302, https://doi.org/10.1007/s11214-008-9440-2, 2008.

Merka, J., Szabo, A., Slavin, J. A., and Peredo, M.: Three-dimensional position and shape of the bow shock and their variation with upstream Mach numbers and interplanetary magnetic field orientation, Journal of Geophysical Research: Space Physics, 110, 1–13, https://doi.org/10.1029/2004JA010944, 2005.

Ng, J., Chen, L.-J., and Omelchenko, Y. A.: Bursty magnetic reconnection at the Earth's magnetopause triggered by high-speed jets, Physics of Plasmas, 28, 092 902, https://doi.org/10.1063/5.0054394, 2021.

Norenius, L., Hamrin, M., Goncharov, O., Gunell, H., Opgenoorth, H., Pitkänen, T., Chong, S., Partamies, N., and Baddeley, L.: Ground-Based Magnetometer Response to Impacting Magnetosheath Jets, Journal of Geophysical Research: Space Physics, 126, https://doi.org/10.1029/2021JA029115, 2021.

Nykyri, K. and Otto, A.: Plasma transport at the magnetospheric boundary due to reconnection in Kelvin-Helmholtz vortices, Geophysical Research Letters, 28, 3565–3568, https://doi.org/10.1029/2001GL013239, 2001.

Nykyri, K., Bengtson, M., Angelopoulos, V., Nishimura, Y., and Wing, S.: Can Enhanced Flux Loading by High-Speed Jets Lead to a Substorm? Multipoint Detection of the Christmas Day Substorm Onset at 08:17 UT, 2015, Journal of Geophysical Research: Space Physics, 124, 4314–4340, https://doi.org/10.1029/2018JA026357, 2019.

Němeček, Z., Šafránková, J., Přech, L., Sibeck, D. G., Kokubun, S., and Mukai, T.: Transient flux enhancements in the magnetosheath, Geophysical Research Letters, 25, 1273–1276, https://doi.org/10.1029/98GL50873, 1998.

Ogilvie, K. W., Chornay, D. J., Fritzenreiter, R. J., Hunsaker, F., Keller, J., Lobell, J., Miller, G., Scudder, J. D., Sittler, E. C., Torbert, R. B., Bodet, D., Needell, G., Lazarus, A. J., Steinberg, J. T., Tappan, J. H., Mavretic, A., and Gergin, E.: SWE, a comprehensive plasma instrument for the WIND spacecraft, Space Science Reviews, 71, 55–77, https://doi.org/10.1007/BF00751326, 1995.

Oka, M., Terasawa, T., Saito, Y., and Mukai, T.: Field-aligned beam observations at the quasi-perpendicular bow shock: Generation and shock angle dependence, Journal of Geophysical Research: Space Physics, 110, https://doi.org/10.1029/2004JA010688, 2005.

Orlove, S. T., Smith, C. W., Vasquez, B. J., Schwadron, N. A., Skoug, R. M., Zurbuchen, T. H., and Zhao, L.: Intervals of radial interplanetary magnetic fields at 1 AU, their association with rarefaction regions, and their apparent magnetic foot points at the Sun, The Astrophysical Journal, 774, 15, https://doi.org/10.1088/0004-637X/774/1/15, 2013.

O'Brien, C., Walsh, B. M., Zou, Y., Tasnim, S., Zhang, H., and Sibeck, D. G.: PRIME: a probabilistic neural network approach to solar wind propagation from L1, Frontiers in Astronomy and Space Sciences, 10, https://doi.org/10.3389/fspas.2023.1250779, 2023.

Palmroth, M., Laitinen, T. V., and Pulkkinen, T. I.: Magnetopause energy and mass transfer: results from a global MHD simulation, Annales Geophysicae, 24, 3467–3480, https://doi.org/10.5194/angeo-24-3467-2006, 2006.

Palmroth, M., Hietala, H., Plaschke, F., Archer, M., Karlsson, T., Blanco-Cano, X., Sibeck, D., Kajdič, P., Ganse, U., Pfau-Kempf, Y., Battarbee, M., and Turc, L.: Magnetosheath jet properties and evolution as determined by a global hybrid-Vlasov simulation, Annales Geophysicae, 36, 1171–1182, https://doi.org/10.5194/angeo-36-1171-2018, 2018.

Papitashvili, N. E. and King, J. H.: OMNI 1-min Data Set [Data set]., NASA Space Physics Data Facility, https://doi.org/10.48322/45bb-8792, 2020.

Parker, E. N.: Dynamics of the Interplanetary Gas and Magnetic Fields., Astrophysical Journal, 128, 664, https://doi.org/10.1086/146579, 1958.

Parks, G.: Magnetosphere, in: Encyclopedia of Atmospheric Sciences (Second Edition), edited by North, G. R., Pyle, J., and Zhang, F., pp. 309–315, Academic Press, Oxford, second edition edition, https://doi.org/10.1016/B978-0-12-382225-3.00211-5, 2015.

Petrukovich, A. A. and Chugunova, O. M.: Detailed Structure of Very High-β Earth Bow Shock, Journal of Geophysical Research: Space Physics, 126, e2020JA029 004, https://doi.org/10.1029/2020JA029004, 2021.

Phan, T. D., Paschmann, G., Gosling, J. T., Oieroset, M., Fujimoto, M., Drake, J. F., and Angelopoulos, V.: The dependence of magnetic reconnection on plasma β and magnetic shear: Evidence from magnetopause observations, Geophysical Research Letters, 40, 11–16, https://doi.org/10.1029/2012GL054528, 2013.

Plaschke, F. and Hietala, H.: Plasma flow patterns in and around magnetosheath jets, Annales Geophysicae, 36, 695–703, https://doi.org/10.5194/angeo-36-695-2018, 2018.

Plaschke, F., Hietala, H., and Angelopoulos, V.: Anti-sunward high-speed jets in the subsolar magnetosheath, Annales Geophysicae, 31, 1877–1889, https://doi.org/10.5194/angeo-31-1877-2013, 2013.

Plaschke, F., Hietala, H., Angelopoulos, V., and Nakamura, R.: Geoeffective jets impacting the magnetopause are very common, Journal of Geophysical Research A: Space Physics, 121, 3240–3253, https://doi.org/10.1002/2016JA022534, 2016.

Plaschke, F., Karlsson, T., Hietala, H., Archer, M., Vörös, Z., Nakamura, R., Magnes, W., Baumjohann, W., Torbert, R. B., Russell, C. T., and Giles, B. L.: Magnetosheath High-Speed Jets: Internal Structure and Interaction With Ambient Plasma, Journal of Geophysical Research: Space Physics, 122, 10,157–10,175, https://doi.org/10.1002/2017JA024471, 2017.

Plaschke, F., Hietala, H., Archer, M., Blanco-Cano, X., Kajdič, P., Karlsson, T., Lee, S. H., Omidi, N., Palmroth, M., Roytershteyn, V., Schmid, D., Sergeev, V., and Sibeck, D.: Jets Downstream of Collisionless Shocks, Space Science Reviews, 214, 81, https://doi.org/10.1007/s11214-018-0516-3, 2018.

Plaschke, F., Hietala, H., and Vörös, Z.: Scale Sizes of Magnetosheath Jets, Journal of Geophysical Research: Space Physics, 125, e2020JA027 962, https://doi.org/10.1029/2020JA027962, 2020a.

Plaschke, F., Jernej, M., Hietala, H., and Vuorinen, L.: On the alignment of velocity and magnetic fields within magnetosheath jets, Annales Geophysicae, 38, 287–296, https://doi.org/10.5194/angeo-38-287-2020, 2020b.

Pollock, C., Moore, T., Jacques, A., Burch, J., Gliese, U., Saito, Y., Omoto, T., Avanov, L., Barrie, A., Coffey, V., Dorelli, J., Gershman, D., Giles, B., Rosnack, T., Salo, C., Yokota, S., Adrian, M., Aoustin, C., Auletti, C., Aung, S., Bigio, V., Cao, N., Chandler, M., Chornay, D., Christian, K., Clark, G., Collinson, G., Corris, T., De Los Santos, A., Devlin, R., Diaz, T., Dickerson, T., Dickson, C., Diekmann, A., Diggs, F., Duncan, C., Figueroa-Vinas, A., Firman, C., Freeman, M., Galassi, N., Garcia, K., Goodhart, G., Guererro, D., Hageman, J., Hanley, J., Hemminger, E., Holland, M., Hutchins, M., James, T., Jones, W., Kreisler, S., Kujawski, J., Lavu, V., Lobell, J., LeCompte, E., Lukemire, A., MacDonald, E., Mariano, A., Mukai, T., Narayanan, K., Nguyan, Q., Onizuka, M., Paterson, W., Persyn, S., Piepgrass, B., Cheney, F., Rager, A., Raghuram, T., Ramil, A., Reichenthal, L., Rodriguez, H., Rouzaud, J., Rucker, A., Samara, M., Sauvaud, J.-A., Schuster, D., Shappirio, M., Shelton, K., Sher, D., Smith, D., Smith, K., Smith, S., Steinfeld, D., Szymkiewicz, R., Tanimoto, K., Taylor, J., Tucker, C., Tull, K., Uhl, A., Vloet, J., Walpole, P., Weidner, S., White, D., Winkert, G., Yeh, P.-S., and Zeuch, M.: Fast Plasma Investigation for Magnetospheric Multiscale, Space Science Reviews, 199, 331–406, https://doi.org/10.1007/s11214-016-0245-4, 2016.

Raptis, S., Karlsson, T., Plaschke, F., Kullen, A., and Lindqvist, P.-A.: Classifying Magnetosheath

Jets Using MMS: Statistical Properties, Journal of Geophysical Research: Space Physics, 125, e2019JA027 754, https://doi.org/10.1029/2019JA027754, 2020.

Raptis, S., Karlsson, T., Vaivads, A., Lindberg, M., Johlander, A., and Trollvik, H.: On Magnetosheath Jet Kinetic Structure and Plasma Properties, Geophysical Research Letters, 49, e2022GL100 678, https://doi.org/10.1029/2022GL100678, 2022a.

Raptis, S., Karlsson, T., Vaivads, A., Pollock, C., Plaschke, F., Johlander, A., Trollvik, H., and Lindqvist, P.-A.: Downstream high-speed plasma jet generation as a direct consequence of shock reformation, Nature Communications, 13, 598, https://doi.org/10.1038/s41467-022-28110-4, 2022b.

Reynolds, S. P.: Particle acceleration in supernova-remnant shocks, Astrophysics and Space Science, 336, 257–262, https://doi.org/10.1007/s10509-010-0559-8, 2011.

Richardson, I. G.: Solar wind stream interaction regions throughout the heliosphere, Living Reviews in Solar Physics, 15, 1, https://doi.org/10.1007/s41116-017-0011-z, 2018.

Richardson, I. G. and Cane, H. V.: Near-earth solar wind flows and related geomagnetic activity during more than four solar cycles (1963-2011), J. Space Weather Space Clim., 2, A02, https://doi.org/10.1051/swsc/2012003, 2012.

Russell, C. T.: Geophysical Coordinate Transformations, Cosmic Electrodynamics, 2, 184–196, 1971.

Savin, S., Amata, E., Zelenyi, L., Budaev, V., Consolini, G., Treumann, R., Lucek, E., Safrankova, J., Nemecek, Z., Khotyaintsev, Y., Andre, M., Buechner, J., Alleyne, H., Song, P., Blecki, J., Rauch, J. L., Romanov, S., Klimov, S., and Skalsky, A.: High energy jets in the Earth's magnetosheath: Implications for plasma dynamics and anomalous transport, JETP Letters, 87, 593–599, https://doi.org/10.1134/S0021364008110015, 2008.

Schwartz, S. J.: Magnetic field structures and related phenomena at quasi-parallel shocks, Advances in Space Research, 11, 231–240, https://doi.org/10.1016/0273-1177(91)90039-M, 1991.

Schwartz, S. J., Burgess, D., Wilkinson, W. P., Kessel, R. L., Dunlop, M., and Lühr, H.: Observations of short large-amplitude magnetic structures at a quasi-parallel shock, Journal of Geophysical Research: Space Physics, 97, 4209–4227, https://doi.org/10.1029/91JA02581, 1992.

Shapiro, V. D. and Üçer, D.: Shock surfing acceleration, Planetary and Space Science, 51, 665–680, https://doi.org/10.1016/S0032-0633(03)00102-8, collisionless Shocks, 2003.

Shue, J.-H., Song, P., Russell, C. T., Steinberg, J. T., Chao, J. K., Zastenker, G., Vaisberg, O. L., Kokubun, S., Singer, H. J., Detman, T. R., and Kawano, H.: Magnetopause location under extreme solar wind conditions, Journal of Geophysical Research: Space Physics, 103, 17 691–17 700, https://doi.org/10.1029/98JA01103, 1998.

Shue, J.-H., Song, P., Russell, C. T., Thomsen, M. F., and Petrinec, S. M.: Dependence of magnetopause erosion on southward interplanetary magnetic field, Journal of Geophysical Research: Space Physics, 106, 18 777–18 788, https://doi.org/10.1029/2001JA900039, 2001.

Shue, J.-H., Chao, J.-K., Song, P., McFadden, J. P., Suvorova, A., Angelopoulos, V., Glassmeier, K. H., and Plaschke, F.: Anomalous magnetosheath flows and distorted subsolar magnetopause for radial interplanetary magnetic fields, Geophysical Research Letters, 36, https://doi.org/10.1029/2009GL039842, 2009.

Sibeck, D. G., Silveira, M. V. D., and Collier, M. R.: Tracking the Subsolar Bow Shock and Magnetopause, Journal of Geophysical Research: Space Physics, 127, e2022JA030 704, https://doi.org/10.1029/2022JA030704, 2022.

Smith, C. W., L'Heureux, J., Ness, N. F., Acuña, M. H., Burlaga, L. F., and Scheifele, J.: The ACE Magnetic Fields Experiment, Space Science Reviews, 86, 613–632, https://doi.org/10.1023/A:1005092216668, 1998.

Solar Influences Data Analysis Center: Sunspot Index and Long-term Solar Observations: Solar Cycles Min/Max, `https://www.sidc.be/SILSO/cyclesminmax`, 2023.

Spreiter, J. R., Summers, A. L., and Alksne, A. Y.: Hydromagnetic flow around the magnetosphere, Planetary and Space Science, 14, 223–253, https://doi.org/10.1016/0032-0633(66)90124-3, 1966.

Sulaiman, A. H., Masters, A., Dougherty, M. K., Burgess, D., Fujimoto, M., and Hospodarsky, G. B.: Quasiperpendicular High Mach Number Shocks, Phys. Rev. Lett., 115, 125 001, https://doi.org/10.1103/PhysRevLett.115.125001, 2015.

Sundberg, T., Burgess, D., Scholer, M., Masters, A., and Sulaiman, A. H.: The Dynamics of Very High Alfvén Mach Number Shocks in Space Plasmas, The Astrophysical Journal Letters, 836, L4, https://doi.org/10.3847/2041-8213/836/1/L4, 2017.

Suni, J., Palmroth, M., Turc, L., Battarbee, M., Johlander, A., Tarvus, V., Alho, M., Bussov, M., Dubart, M., Ganse, U., Grandin, M., Horaites, K., Manglayev, T., Papadakis, K., Pfau-Kempf, Y., and Zhou, H.: Connection Between Foreshock Structures and the Generation of Magnetosheath Jets: Vlasiator Results, Geophysical Research Letters, 48, e2021GL095 655, https://doi.org/10.1029/2021GL095655, 2021.

Suvorova, A. V., Shue, J.-H., Dmitriev, A. V., Sibeck, D. G., McFadden, J. P., Hasegawa, H., Ackerson, K., Jelínek, K., Šafránková, J., and Němeček, Z.: Magnetopause expansions for quasi-radial interplanetary magnetic field: THEMIS and Geotail observations, Journal of Geophysical Research: Space Physics, 115, https://doi.org/10.1029/2010JA015404, 2010.

Swisdak, M., Rogers, B. N., Drake, J. F., and Shay, M. A.: Diamagnetic suppression of component magnetic reconnection at the magnetopause, Journal of Geophysical Research: Space Physics, 108, https://doi.org/10.1029/2002JA009726, 2003.

Swisdak, M., Opher, M., Drake, J. F., and Bibi, F. A.: The vector direction of the interstellar magnetic field outside the heliosphere, The Astrophysical Journal, 710, 1769, https://doi.org/10.1088/0004-637X/710/2/1769, 2010.

Torbert, R. B., Russell, C. T., Magnes, W., Ergun, R. E., Lindqvist, P.-A., LeContel, O., Vaith, H., Macri, J., Myers, S., Rau, D., Needell, J., King, B., Granoff, M., Chutter, M., Dors, I., Olsson, G., Khotyaintsev, Y. V., Eriksson, A., Kletzing, C. A., Bounds, S., Anderson, B., Baumjohann, W., Steller, M., Bromund, K., Le, G., Nakamura, R., Strangeway, R. J., Leinweber, H. K., Tucker, S., Westfall, J., Fischer, D., Plaschke, F., Porter, J., and Lappalainen, K.: The FIELDS Instrument Suite on MMS: Scientific Objectives, Measurements, and Data Products, Space Science Reviews, 199, 105–135, https://doi.org/10.1007/s11214-014-0109-8, 2016.

Treumann, R. A.: Fundamentals of collisionless shocks for astrophysical application, 1. Nonrelativistic shocks, The Astronomy and Astrophysics Review, 17, 409–535, https://doi.org/10.1007/s00159-009-0024-2, 2009.

Tsurutani, B. T. and Rodriguez, P.: Upstream waves and particles: An overview of ISEE results, Journal of Geophysical Research: Space Physics, 86, 4317–4324, https://doi.org/10.1029/JA086iA06p04317, 1981.

Turc, L., Roberts, O. W., Verscharen, D., Dimmock, A. P., Kajdič, P., Palmroth, M., Pfau-Kempf, Y., Johlander, A., Dubart, M., Kilpua, E. K. J., Soucek, J., Takahashi, K., Takahashi, N., Battarbee, M., and Ganse, U.: Transmission of foreshock waves through Earth's bow shock, Nature Physics, 19, 78–86, https://doi.org/10.1038/s41567-022-01837-z, 2023.

Vainio, R. and Afanasiev, A.: Particle Acceleration Mechanisms, in: Solar Particle Radiation Storms Forecasting and Analysis: The HESPERIA HORIZON 2020 Project and Beyond, edited by Malandraki, O. E. and Crosby, N. B., pp. 45–61, Springer International Publishing, Cham, https://doi.org/10.1007/978-3-319-60051-2_3, 2018.

Verigin, M. I., Tátrallyay, M., Erdős, G., and Kotova, G. A.: Magnetosheath – Interplanetary medium reference frame: Application for a statistical study of mirror type waves in the terrestrial plasma environment, Advances in Space Research, 37, 515–521, https://doi.org/10.1016/j.asr.2005.03.042, 2006.

Vokhmyanin, M. V., Stepanov, N. A., and Sergeev, V. A.: On the Evaluation of Data Quality in the OMNI Interplanetary Magnetic Field Database, Space Weather, 17, 476–486, https://doi.org/10.1029/2018SW002113, 2019.

Vuorinen, L., Hietala, H., and Plaschke, F.: Jets in the magnetosheath: IMF control of where they occur, Annales Geophysicae, 37, 689–697, https://doi.org/10.5194/angeo-37-689-2019, 2019.

Vuorinen, L., Hietala, H., Plaschke, F., and LaMoury, A. T.: Magnetic Field in Magnetosheath Jets: A Statistical Study of BZ Near the Magnetopause, Journal of Geophysical Research: Space Physics, 126, e2021JA029 188, https://doi.org/10.1029/2021JA029188, 2021.

Vuorinen, L., Vainio, R., Hietala, H., and Liu, T. Z.: Monte Carlo Simulations of Electron Acceleration at Bow Waves Driven by Fast Jets in the Earth's Magnetosheath, The Astrophysical Journal, 934, 165, https://doi.org/10.3847/1538-4357/ac7f42, 2022.

Vuorinen, L., Hietala, H., LaMoury, A. T., and Plaschke, F.: Solar Wind Parameters Influencing Magnetosheath Jet Formation: Low and High IMF Cone Angle Regimes, Journal of Geophysical Research: Space Physics, 128, e2023JA031 494, https://doi.org/10.1029/2023JA031494, 2023a.

Vuorinen, L., LaMoury, A. T., Hietala, H., and Koller, F.: Magnetosheath Jets Over Solar Cycle 24: An Empirical Model, Journal of Geophysical Research: Space Physics, 128, e2023JA031 493, https://doi.org/10.1029/2023JA031493, 2023b.

Walsh, B. M., Sibeck, D. G., Nishimura, Y., and Angelopoulos, V.: Statistical analysis of the plasmaspheric plume at the magnetopause, Journal of Geophysical Research: Space Physics, 118, 4844–4851, https://doi.org/10.1002/jgra.50458, 2013.

Walsh, B. M., Phan, T. D., Sibeck, D. G., and Souza, V. M.: The plasmaspheric plume and magnetopause reconnection, Geophysical Research Letters, 41, 223–228, https://doi.org/10.1002/2013GL058802, 2014.

Wang, B., Nishimura, Y., Hietala, H., Lyons, L., Angelopoulos, V., Plaschke, F., Ebihara, Y., and Weatherwax, A.: Impacts of Magnetosheath High-Speed Jets on the Magnetosphere and Ionosphere Measured by Optical Imaging and Satellite Observations, Journal of Geophysical Research: Space Physics, 123, 4879–4894, https://doi.org/10.1029/2017JA024954, 2018.

Wang, B., Nishimura, Y., Hietala, H., and Angelopoulos, V.: Investigating the Role of Magnetosheath High-Speed Jets in Triggering Dayside Ground Magnetic Ultra-Low Frequency Waves, Geophysical Research Letters, 49, https://doi.org/10.1029/2022GL099768, 2022.

Wang, R., Lu, S., Wang, S., Li, X., and Lu, Q.: Recent progress on magnetic reconnection by in situ measurements, Reviews of Modern Plasma Physics, 7, 27, https://doi.org/10.1007/s41614-023-00129-0, 2023.

Webb, G. M., Axford, W. I., and Terasawa, T.: On the drift mechanism for energetic charged particles at shocks, The Astrophysical Journal, 270, 537–553, https://doi.org/10.1086/161146, 1983.

Wilson III, L. B.: Low Frequency Waves at and Upstream of Collisionless Shocks, chap. 16, pp. 269–291, American Geophysical Union (AGU), https://doi.org/10.1002/9781119055006.ch16, 2016.

Wiltberger, M., Lopez, R. E., and Lyon, J. G.: Magnetopause erosion: A global view from MHD simulation, Journal of Geophysical Research: Space Physics, 108, https://doi.org/10.1029/2002JA009564, 2003.

Zhang, T., Zhao, H., Russell, C., Petrinec, S., Schwingenschun, K., and Riedler, W.: Dayside reconnection during IMF northward: A possible foreshock effect, Advances in Space Research, 19, 1943 – 1946, https://doi.org/10.1016/S0273-1177(97)00106-3, proceedings of the D0.4 Symposium of COSPAR Scientific Commission D, 1997.

Zurbuchen, T. H. and Richardson, I. G.: In-Situ Solar Wind and Magnetic Field Signatures of Interplanetary Coronal Mass Ejections, Space Science Reviews, 123, 31–43, https://doi.org/10.1007/s11214-006-9010-4, 2006.

TURUN
YLIOPISTO
UNIVERSITY
OF TURKU

Painosalama, Turku, Finland 2024

ISBN 978-951-29-9777-0 (PRINT)
ISBN 978-951-29-9778-7 (PDF)
ISSN 0082-7002 (Print)
ISSN 2343-3175 (Online)